RHEOLOGICAL AND COMPOSITION ANALYSES OF CO_2 GAS HYDRATES

Gustavo Alonso Barrientos Sandoval

Tese de doutorado apresentada ao Programa de Pós-graduação em Engenharia Mecânica, COPPE, da Universidade Federal do Rio de Janeiro, como parte dos requisitos necessários à obtenção do título de Doutor em Engenharia Mecânica.

Orientadores: Roney Leon Thompson
Edson José Soares

Rio de Janeiro
Março de 2019

RHEOLOGICAL AND COMPOSITION ANALYSES OF CO_2 GAS HYDRATES

Gustavo Alonso Barrientos Sandoval

TESE SUBMETIDA AO CORPO DOCENTE DO INSTITUTO ALBERTO LUIZ COIMBRA DE PÓS-GRADUAÇÃO E PESQUISA DE ENGENHARIA (COPPE) DA UNIVERSIDADE FEDERAL DO RIO DE JANEIRO COMO PARTE DOS REQUISITOS NECESSÁRIOS PARA A OBTENÇÃO DO GRAU DE DOUTOR EM CIÊNCIAS EM EMGENHARIA MECÂNICA.

Examinada por:

Prof. Roney Leon Thompson, D.Sc.

Prof. Edson José Soares, D.Sc.

Prof. Fernando Pereira Duda, Ph.D.

Prof. Daniel Onofre de Almeida Cruz, D.Sc.

Prof. Marcio Nele de Souza, D.Sc.

Prof. Paulo Roberto de Souza Mendes, Ph.D.

RIO DE JANEIRO, RJ - BRASIL
MARÇO DE 2019

Sandoval, Gustavo Alonso Barrientos

Rheological and composition analyses of CO_2 gas hydrates/ Gustavo Alonso Barrientos Sandoval. - Rio de Janeiro: UFRJ/COPPE, 2019.

XV, 96 p.: il.; 29,7 cm.

Orientadores: Roney Leon Thompson

Edson José Soares

Tese (doutorado) - UFRJ/ COPPE/ Programa de Engenharia Mecânica, 2019.

Referências Bibliográficas: p. 88-96.

1. CO_2 gas hydrates. 2. Rheology. 3. Water in oil emulsions. 4. High pressure cell. I. Thompson, Roney Leon *et al.* II. Unversidad Federal do Rio de Janeiro, COPPE, Programa de Engenharia Mecânica. III. Título.

Blessed is the one who finds wisdom, and the one who gets understanding, for the gain from her is better than gain from silver and her profit better than gold. She is more precious than jewels, and nothing you desire can compare with her. Long life is in her right hand; in her left hand are riches and honor. Her ways are ways of pleasantness, and all her paths are peace. She is a tree of life to those who lay hold of her; those who hold her fast are called blessed.

Proverbs 3:13-18.

À Deus e minha família.

Agradecimentos

Agradeço a Deus pela sabiduria e saúde para conducir este estudo. Abençoado e exaltado seja para sempre seu Nome glorioso.

À minha família pelo seu apoio incondicional. São minha maior fonte de inspiração.

Aos professores Roney Thompson e Edson Soares pela orientação e disponibilidade durante istos anos de aprendizagem. Me sinto privilegiado e motivado de trabalhar com eles.

Aos professores Rafhael Milanezi, Rogerio Ramos, Jan Vermant, José Joaquin Santos, Marcio Martins, Renato do Nascimento Siqueira e Ivanor Martins da Silva pela colaboração e conhecimento oferecido durante esta pesquisa.

Aos meus amigos Eddy Chirinos, Lauro Carvalho, Eduardo Pereira e demais colegas da UFES, UFF, UFRJ e ETH-Zürich com quêm tenho tido a oportunidade de compartilhar excelentes experiências. Peço a Deus muito mais sucesso na suas vidas.

À Leidy Johana com quem tenho vivenciado momentos muito agradáveis. Desejo êxitos no seu caminhar.

À Cristina Sad, Laine Pereira, Mayara Silva, Rayane Reinholz e demais colegas do LabPetro pela assistência para a caracterização e preparação das emulsões.

Às instituições: UFES e seus laboratórios LabReo e LabPetro, UFRJ, UFF e ETH-Zürich e seu laboratório de *soft materials* por me permitir desenvolver minha investigação.

Agradeço às funcionárias da secretaria do programa de pós-graduação da UFES e da UFRJ, Andréia Eyng e Vera Lúcia Pinheiro, pela atenção e diligência.

Por fim, agradeço à Coordenação de Aperfeiçoamento de Pessoal de Nível Superior (Capes), à Agência Nacional do Petróleo, Gás Natural e Biocombustíveis (ANP) e à Petrobras pela bolsa de estudos e pelo financiamento dos materiais e serviços necessários para o desenvolvimento deste trabalho.

Resumo da Tese apresentada à COPPE/UFRJ como parte dos requisitos necessários para a obtenção do grau de Doutor em Ciências (D.Sc.)

ANÁLISES REOLÓGICA E COMPOSICIONAL DOS HIDRATOS DE GAS DE CO_2

Gustavo Alonso Barrientos Sandoval

Março/2019

Orientadores: Roney Leon Thompson
Edson José Soares

Programa: Engenharia Mecânica

No presente trabalho é pesquisado o comportamento reológico dos hidratos de CO_2 formados a partir de emulsões de água em óleo, pois grandes concentrações deste gás foram reportados nos poços de petróleo do Pré-sal brasileiro, com grande potencial para formar hidratos. Para investigar este fato, realizou-se uma sequência de testes utilizando uma montagem composta por um reômetro, uma célula de pressão magnética e um sistema de alta pressão, onde foram aplicadas condições de pressão e temperatura similares às encontradas na indústria do petróleo. Os resultados inéditos exibidos em curvas de viscosidade ao longo do tempo são expostos em duas seções principais. Primeiramente, é mostrado o efeito produzido pela taxa de cisalhamento, a fração de volume da água e o impacto do sal nos hidratos de CO_2. Também, é investigado a capacidade de reconstrução dos hidratos de CO_2 e seu efeito de memória. Em segundo lugar, são mostrados alguns resultados que indicam o efeito produzido no tempo de indução da formação de hidratos pela adição de gás condensado e pela adição de pequenas quantidades de asfaltenos em pó nas emulsões de água em óleo. Parece ser que essas partículas ativas interfacialmente atuam como inibidores cinéticos de hidratos.

Abstract of Thesis presented to COPPE/UFRJ as a partial fulfillment of the requirements for the degree of Doctor of Science (D.Sc.)

RHEOLOGICAL AND COMPOSITION ANALYSES OF CO_2 GAS HYDRATES

Gustavo Alonso Barrientos Sandoval

March/2019

Advisors: Roney Leon Thompson
Edson José Soares

Department: Mechanical Engineering

In the present work, it is investigated the rheological behavior of CO_2 hydrates form from water-in-oil emulsions since high concentrations of this gas have been reported in the Brazilian Pre-salt oil wells, with large potential to form hydrates. To investigate this fact, a sequence of tests was conducted using an assembly composed by a rheometer, a magnetic pressure cell, and a high-pressure system, where similar pressure and temperature conditions were applied to those found in the petroleum industry. The novel results displayed in curves of viscosity over time are revealed in two main sections. Firstly, it is shown the effect produced by the shear rate, water volume fraction and salt impact on CO_2 hydrates. It is also investigated the ability of the reconstruction of the CO_2 hydrates and its memory effect. Secondly, results that indicate the effect produced on the induction time of hydrate formation by the addition of gas condensate and by the addition of small amounts of powder asphaltenes in the water-in-oil emulsions are shown. These interfacially active particles seem to act like kinetic hydrate inhibitors.

Contents

List of Figures

Chapter 1

Introduction

1.1 Motivation

Natural gas hydrates are solid compounds that are formed when the water hydrogen bonds (hosts) encage and hold one or more guests molecules (usually low molecular weight gases) at particular thermodynamic conditions of high-pressure and low-temperature (Sloan et al., 2011). The arrangement host-guest molecules forms a cage-like structure in different points of a system, which are surrounded by a thin layer of liquid water that leads to a capillary bridge between hydrate particles, since hydrate surface is hydrophilic (Sun and Firoozabadi, 2015).

Gas hydrates have several applications in different areas, such as: energy recovery, climate change, transportation of gas and flow assurance. Sloan (2003) indicates that even the most conservative current estimates suggest that the amount of energy in hydrates is equivalent to twice that of all other fossil fuels combined. The existence of gas hydrates in nature was proven in the 1960s by Makogon (1965) showing the potential for the exploration of this source of energy. Most of the natural hydrates around the world are composed of living organisms, the guest gas comes from bio-degraded plant and animal matter. They are present both in the universe and in our planet, especially in the polar region and in the ocean bottom as shown in Fig. 1.1. Despite pilot drilling projects to characterization and production of gas hydrates, nowadays its production is too expensive.

Scientists have done significant efforts to investigate the role of hydrates in climate change, but there are controversial opinions. Kennett et al. (2003) reported the so-called “hydrate

Figure 1.1: Hydrates accumulation in cold layers. Figure taken from:www.geotimes.org

gun hypothesis", which suggests that when hydrates dissolve then the methane released to the atmosphere causes an important increase in the temperature. The impact on climate must be carefully analyzed before the production of gas hydrates.

Gudmundsson et al. (1995) suggested that it is economically feasible to transport stranded gas in hydrated form since each volume of hydrates can contain as much as 184 volumes of gas. They proposed to transport natural gas in hydrated form, rather than in liquefied one. The advantages of gas storage in the hydrated form are the lower space occupied and the low necessary pressure to be used. However, nowadays this technique is not applied by the industry.

Due to the solid crystalline structure of gas hydrates, they are substances that do not flow. This situation must be considered when drilling and extracting oil and gas, or during well maintenance when the passage of oil is stopped because of the formation of hydrates plug flow lines, what causes expensive production shutdowns. Figure 1.2 illustrates a hydrate block removed after running a scraper in a gas production pipeline of Petrobras Company.

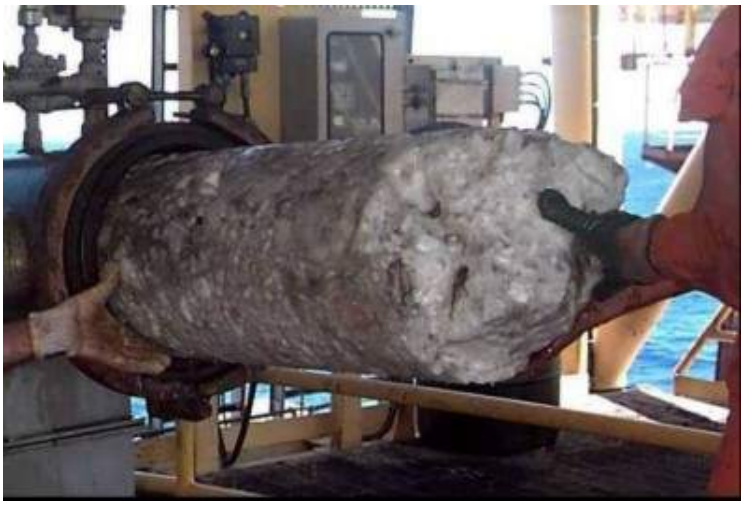

Figure 1.2: Hydrate plug removed from a gas production pipeline. Picture from Petrobras.

As reported, the gas hydrates are and will be an interesting and challenging topic to be explored in the next decades. In fact, different countries have national programs to investigate safe and economical methods to produce energy from hydrates. The hydrates formation have two principal and opposed applications; first, is a large energy resource and second is the main problem present in the oil and gas industry (Sum et al., 2009). This research is primarily concerned with the flow assurance problem, since the thermodynamic conditions of oil and gas production in the Brazilian coast are favorable to the appearance of hydrates in the majority of the cases, because the oil reserves are located in ultra-deepwater (WD) fields where pressure is high and temperature is low (WD $>$ 1500 m), as reported by Camargo et al. (2004). Another important problem reported by Brazilian and international flow assurance engineers is related to wax deposition and heavy and extra-heavy oil production, since a relevant part of recent offshore discoveries involves this type of oil.

Several methods have been utilized by the oil and gas companies to prevent hydrate blockage. Some of them use an appropriate subsea layout combined with insulated flexible flowlines. The insulation is designed to permit enough cooldown time to allow operational procedures to be executed before the well restarts and the flexible flowlines are usually designed to be piggable (see Fig. 1.3).

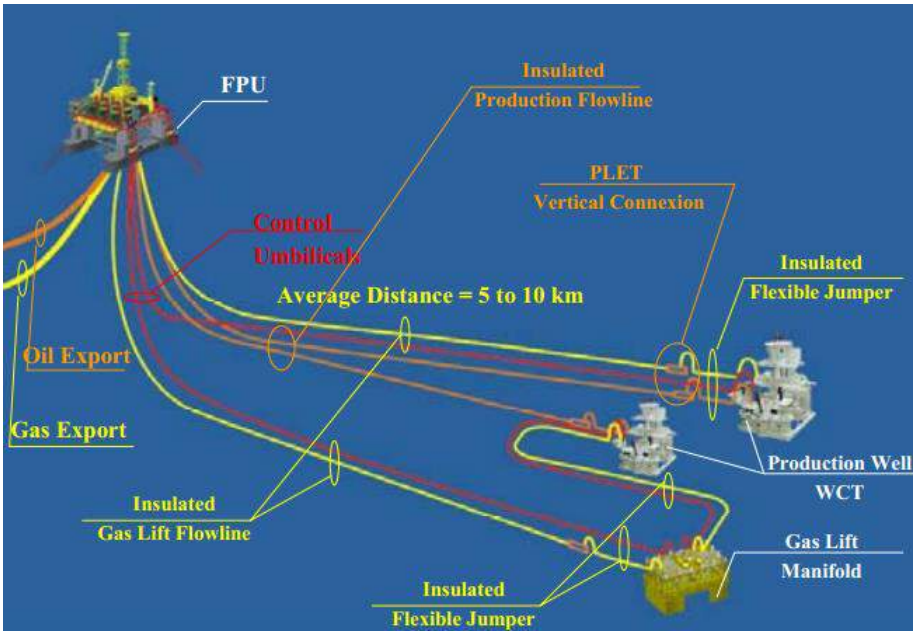

Figure 1.3: Example of a typical subsea development strategy. Figure taken from Camargo et al. (2004).

Due to high heat losses in multiphase flow is necessary to apply corrective techniques for the operational continuity of the well. Cardoso et al. (2003) mentioned the methods that are mostly used by the Brazilian flow assurance engineers, such as, an exothermal chemical reaction, round-trip cleaning pigs and Nitrogen Generating System, (due to the fact that Nitrogen is immiscible with oil and water, it has low density and it supports high pressures, this gas is used to maintain the pressure in the reservoirs and melt down the wax deposits along the flowlines). Nitrogen generating system is sometimes used to warm the tree cap region to melt the hydrates accumulated underneath (Camargo et al., 2004). Surprisingly, despite different preventives and correctives methods, hydrates formation and wax deposition still continue to be responsible for the main flow assurance issues and deserve special consideration. These problems (most of them caused by operational failures) enhance when the well is required to be shut down and, as expected, the costs caused by these events are highly expensive.

This work aims to investigate the rheological behavior of CO_2 hydrates slurries formed from water-in-crude oil emulsions. Viscosity and pressure of the hydrate slurry during its formation and dissociation are measured taking into account different variables, such as: water volume fraction, shear rate, pressure, time-dependency, and memory effect. The influence caused on the induction time of CO_2 hydrate formation by the addition of asphaltenes and gas condensate it is also investigated. The main tests are displayed in terms of viscosity over time. For this purpose a rheometer with a magnetic high-pressure cell is employed, where it is possible to use similar thermodynamic conditions of those utilized in the petroleum industry.

1.2 State of the art

The gas hydrates discovery is attributed to Joseph Priestley in 1778 when he was working with bubbling SO_2 at 0 ^{o}C water and atmospheric pressure. Nevertheless, he did not name the phenomenon observed as “gas hydrates” (Makogon, 2010). Almost 30 years later, in 1811 the British chemist Humphrey Davy observed that a solution of oxymuriatic gas in water freezes more readily than pure water. The author was the first in documenting the natural gas hydrates and is known as the pioneer with respect to this phenomenon. Over the following century, since the notification by Humphrey Davy, the interest for hydrates

was only a scientific curiosity and the researchers in the area have begun to study the compounds that form hydrates and to quantify the number of water molecules per guest molecule. This latter issue is still under investigation because it is very complex to analyze, due to the fact that the hydrate composition varies with pressure and temperature. In 1934, Hammerschmidt found that gas hydrates blocked the flowlines at a temperature above the ice point. This was observed when the results of the inspection of the United States gas pipelines were analyzed. This fact increased significantly the attraction to the topic in both industry and academia. Subsequently, investigators started to analyze the conditions for the hydrate formation and tried to control the water content in natural gas pipelines. Also, the effects of thermodynamic hydrates inhibitors like methanol and monoethylene glycol began to be investigated by Hammerschmidt and others.
Nowadays there are different techniques to prevent hydrates formation, however, the low temperature and the higher demanding pressures to extract oil and gas fit within the hydrate equilibrium curve. Thus, the industry has done significant investment, research and development to implement efficient solutions to mitigate the drawbacks of this phenomenon. The most common initiatives used by the companies in partnership with universities to optimize flow assurance and to reduce hydrate blockage are:

- Programs to simulate hydrate formation and dissociation.
- Experimental flow loops.
- Analysis of rheological properties of water in oil emulsions.

Several companies and universities have commercially available computer programs for the prediction of hydrate properties. Many of these programs are based on the van der Waals and Platteeuw (1995) method. In addition to the accuracy of the method, it allows envisaging properties of mixtures from single hydrate formers using statistical thermodynamics. The method predicts macroscopic properties, such as temperature and pressure using microscopic properties such as intermolecular potentials (Sloan et al., 2011). The computer hydrate prediction programs most common are:

- CSMGem - Colorado School of Mines - Ballard and Sloan Jr (2002).
- DBRHydrate - DBRobinson and Associates Ltd.

- PVTsim - Calsep A/S.
- Multiflash - Infochem Computer Services Ltd.

These programs are generally incorporated into flowsheets programs. Other efforts have been done to study time-dependent properties of hydrates both at macroscopic and at the molecular levels. These studies together with technological aids in the oil and gas industry have allowed the engineers to shift from hydrate avoidance to hydrate risk management. That is, hydrate risk management uses transient methods and corrective techniques to delay hydrate formation or prevent hydrate blockage. On the other hand, hydrate avoidance consists in preventing hydrate formation without going into the hydrate thermodynamic region. Perhaps the most studied technique in the last years was computer simulations. In this approach, an assembly of molecules is simulated to predict macroscopic properties. With computer simulations, it is possible to analyze different steps of hydrate formation as nucleation and dissociation, and it can also be used to explain experimental observations. The simulation techniques most used are Monte Carlo (MC) and Molecular Dynamic Simulation (MD). MD is more commonly used than MC because it can compute time-dependent phenomena and transport properties such as viscosity and thermodynamic characteristics (Sloan et al. (2011)).

Flow loops are another alternative to investigate gas hydrates. Through those pipe configurations are possible to conduct tests with similar conditions to the ones found in field operations (pipe lengths and diameters, flow rates, temperatures, and pressures), therefore, is one of the most reliable ways to predict hydrates formation for a specific oil under certain conditions. Figure 1.4 shows the flow loop at Atalaia, located in Brazil at Campinas State University. The experimental facility operates with compressed air or Nitrogen and water or oil with several viscosities and can generate various phase flow patterns. The experimental procedure usually used to perform the tests in the flow loops is the following: initially, the loop is charged with water, oil, and gas, subsequently, the sample is placed under thermodynamic conditions of hydrate formation and it is confirmed free water in the pipes, and finally, it is observed the behavior of the sample and verify if the hydrate is formed. The experimental procedure explained above is also used to study the effect of chemical additives in the phenomenon.

Figure 1.4: Atalaia flow loop located at the University of Campinas, Brazil.

Other flow loops are reported in the literature as in the Tulsa University, Norwegian University of Science and Technology where a large scale hydrate laboratory was built to evaluate the feasibility of such phenomenon.The experimental equipment is described by Andersson and Gudmundsson (2000), where it was concluded that the frictional pressure drop of the hydrate in water slurries is determined by the properties of the carrying water phase alone. Peytavy et al. (1999) also used a recirculating flow loop to investigate the hydrate formation kinetics and proposed a method to predict the methane hydrate growth rate. Di Lorenzo et al. (2011) explained the CSIRO'S hydrates flow loop designed to simulate the conditions found at Australian offshore in gas dominated pipelines. The main results of this research were presented as pressure drop profiles. In addition, it was reported a type of test referred as "restart test" to investigate transient flow conditions simulating pipeline restart operations after a shut-down period.

In addition to study flow assurance issues, the loops are used to analyze and calibrate some electronic devices such as: pressure transducer, liquid flow meters, and temperature sensors. On the other hand, the disadvantages of this large flow loops are the need of a large amount of sample of oil and gas and inhibitors to be used as well as the high costs for the construction of the system.

A rheological analysis is an important and efficient initiative to prevent hydrate plug formation as well as to understand its properties. A reliable measure of the yield stress at a laboratory scale could provide to the engineers important information to the flow assurance management after a well shutdown. There are mainly two methods to analyze

the hydrate rheological properties based on the pressure value in which they are formed: one method is to use a high-pressure cell in order to provide a pressure level similar to the field, and the other is to use hydrates formers at atmospheric pressure such as cyclopentane (CP) and tetrahydrofuran (THF), both substances are able to form hydrates with readily accessible temperatures (Peixinho et al., 2010; Leopércio et al., 2016). Ahuja et al. (2015) have shown that CP offers advantages over THF since it forms structures of second type hydrates which are commonly encountered in petroleum fields. However, CP is immiscible to water as opposed to THF which is fully miscible. When the material is immiscible to water does not occur mass transfer, as happens in hydrate emulsion systems. The rheological analyzes are usually performed using rheometers. In addition to accuracy, the equipment has the advantage of using a small amount of sample and works at several and controlled temperatures and shear rates. Concerning rheological investigations using high-pressure cells, at the final of this chapter a survey of the literature is made.

1.2.1 Hydrate Crystal Structures

Three different types of crystalline units are known: Structure I, II, and H. The formed structure (shape and size) depends on the guest-molecule repulsion and on the pressure and temperature conditions.

The cubic structures I and II were determined by von Stackelberg and coworkers (1949 -1952) as reported by Sloan Jr and Koh (2008). The presence of the structure H was discovered by Ripmeester in 1987. Structure I is found in natural environments, specially formed with pure methane; cubic structure II is scarce in nature and is formed with a mixture of ethane, propane, and methane. It is usually found in the oil production flowlines in deep and ultradeep water; structure H hydrate is acutely rare in nature and occurs in the presence of two different molecules. It is studied as a scientific curiosity and may occur in either environment, as in the outer space. The characteristics of the mentioned unit crystals are shown in Fig. 1.5, where are depict the structures I and II, which are formed by hydrogen bonds called pentagonal dodecahedra (labeled 5^{12}) because there are composed of 12 faces (superscript number) and each face is formed with 5 equal edges lengths and equal angles. The numbers above the arrows indicate the quantity of crystal units that form each structure.

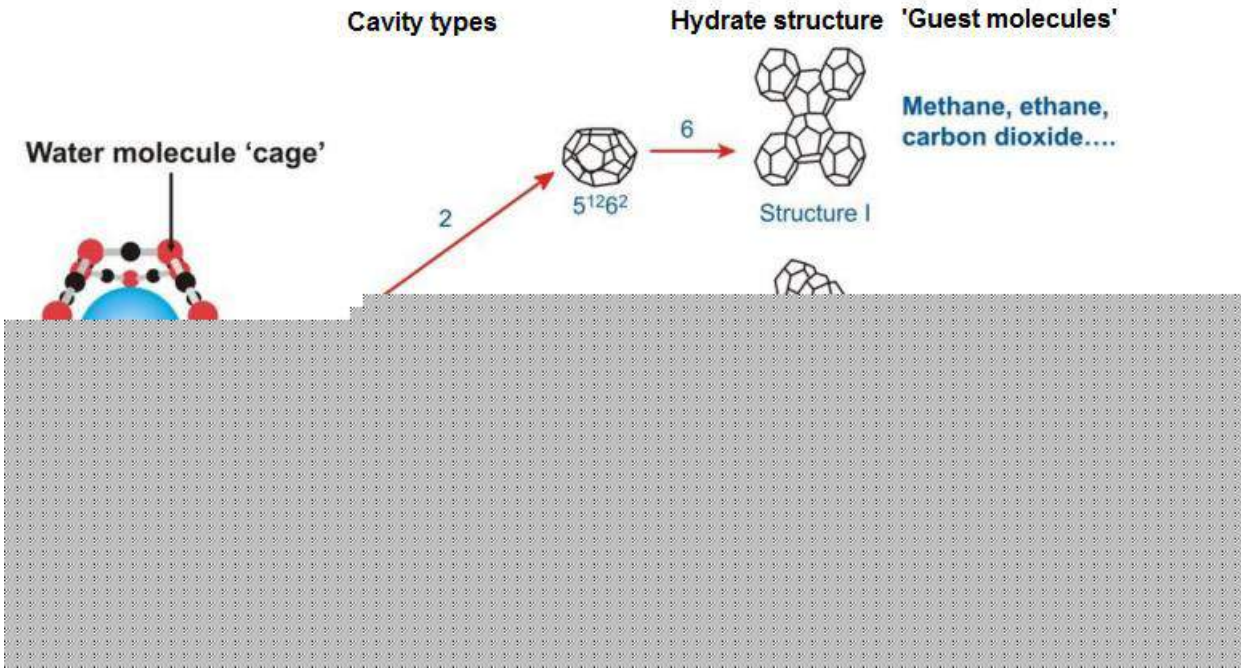

Figure 1.5: Common unit crystals of gas hydrates. Taken from Sloan and Koh 2008.

1.2.2 Nucleation of hydrates

Hydrates are solid compounds, and its formation occurs within a metastable region. There is a pressure-temperature relationship that defines the favorable conditions for hydrate formation or dissociation. Figure 1.6 shows a hydrate-aqueous vapor equilibrium curve for CO_2. At the right side and below the curve, the crystallization is impossible (no-crystal growth), therefore hydrates do not form. However, if this curve is crossed, either through cooling or increase in pressure, nucleation will readily occur (Sloan Jr and Koh, 2008). Another zone (not shown in Fig. 1.6) obtained from a parallel curve shifted from the equilibrium curve, is known as the metastable region. It is a transition between the two regions illustrated in Fig. 1.6 where spontaneous crystallization is improbable. Therefore, if a crystal seed is located in such a region, growth would occur on the seed.

In the industry, as in academia, there are interesting questions about this theme, for example: when hydrates begin to form? How do hydrates get to block the pipelines? Once the line is blocked, it is possible to disaggregate the hydrate?. Figure 1.7 shows a hypothetical case of how hydrate nucleation occurs. The viscosity as a function of time is plotted from experimental data obtained in a high-pressure rheometer and the circles are conceptual images which represent the hydrates clusters.

The theory used to explain the behavior in this case is known as homogeneous nucleation

occurs as a consequence of a sufficiently large number of individual interactions (such as atoms colliding simultaneously).

Excess Gibbs free energy ΔG is a thermodynamic potential that can be used to interpret that behavior of critical cluster size formation and spontaneous growth. This phenomenon behaves as a system that evolves in time in which the free energy is released trying to reach a more stable energetic state. The sum of the surface excess free energy ΔG_S and the volume excess free energy ΔG_V is the total excess free energy ΔG, then:

$$\Delta G = \Delta G_S + \Delta G_V = 4\pi r^2 \sigma + \frac{4}{3}\pi r^3 \Delta g_V \tag{1.1}$$

Where r is the cluster radius, σ is the surface tension between the crystal and liquid interface and Δg_V is the free energy change per unit volume. As can be observed in Fig. 1.8, ΔG_S and ΔG_V are of opposite sign and both are functions of r. Initially, the excess surface free energy is higher than the excess volume free energy, then ΔG slope is positive until it reaches its maximum value known as the free energy barrier, ΔG_{crit}, the corresponding radius at this point is the critical nucleus r_C, or critical cluster size. Therefore, to form a critical nucleus the free energy barrier where clusters grow spontaneously must be overcome.

1.2.3 Hydrate formation in a pipeline

As was previously mentioned, the necessary conditions for the hydrate formation are: free water, the guest molecule, low temperature, and high pressure. All such conditions are satisfied in the production of oil and gas in deep and ultra-deep water. Analyzing the above conditions, the phenomenon of hydrate formation would not be possible without any of them, since the guest molecule is inherent to the process; reservoirs always release free water, especially when increasing its age; and decrease the pressure could be unviable economically.

The oil industry would benefit if production processes were maintained outside the gas hydrate-formation stable range. However, if by one side, this task is facilitated by knowledge of the thermodynamic conditions favorable to the hydrates formation, by the other, the usual temperature conditions in ultra-deep waters, associated with high pressures from the economic production demands, leads to a risky situation; because the thermodynamic conditions are in the hydrate formation region (Sloan, 2003). A strategy that could be

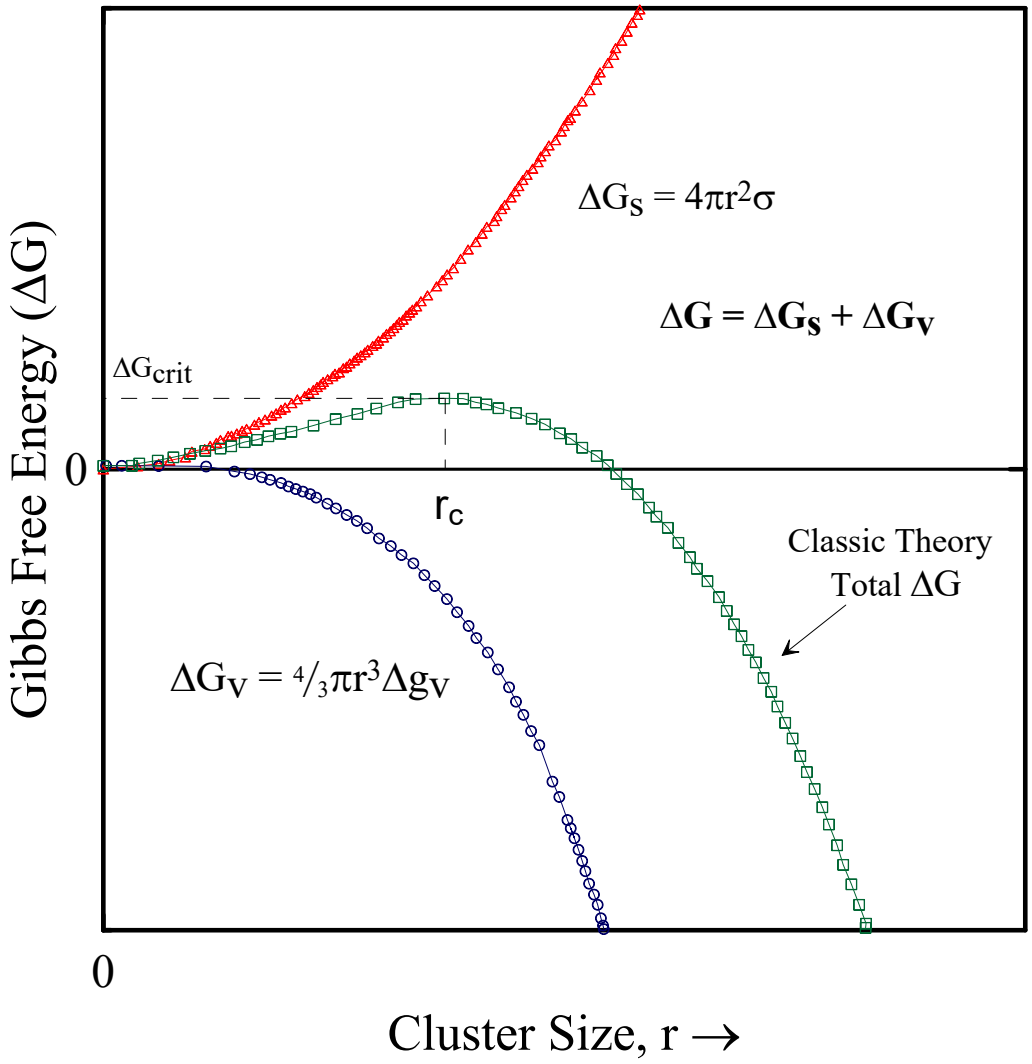

Figure 1.8: Variation of excess Gibb free energy as a function of cluster size. Figure taken from (Sloan Jr and Koh, 2008), edited.

taken by the oil industry is to continue working in the thermodynamic region of hydrate formation. Nevertheless, given the scale of the problem, the introduction of hydrate inhibitors methods are required as reported by Chen et al. (2013). However, Tariq et al. (2014) states that the adoption of these methods of hydrates inhibition can reach 15% of the total production cost. There are different methods to prevent the problem associated with hydrates formation, for example: in dehydration (since water is essential in this process), the free water and vaporized water are removed by separation and drying the remaining gas with molecular sieves or triethylene glycol; a second method is to keep the temperature outside the zone of stable hydrate using insulation or heating, albeit insulation is only useful for oil systems during steady state flow (Camargo et al., 2004). Another

method is using inhibitors, typically alcohols like ethanol and glycols, where much of the free water is hydrogen bonded to the inhibitor. Since, it modifies the thermodynamic conditions of hydrate formation, lower temperatures, and higher pressures are required to form hydrates.

Hydrate nucleation requires emulsified water droplets. The free water extracted in the production process and transported through the pipelines is dispersed and mixed with the crude oil when turbulent mixing conditions are attended, for example in choke valves. These mixtures often form water-in-oil stable emulsions (Paso et al., 2008). Hydrates initially form at the oil-water interface as illustrated in Fig. 1.9.

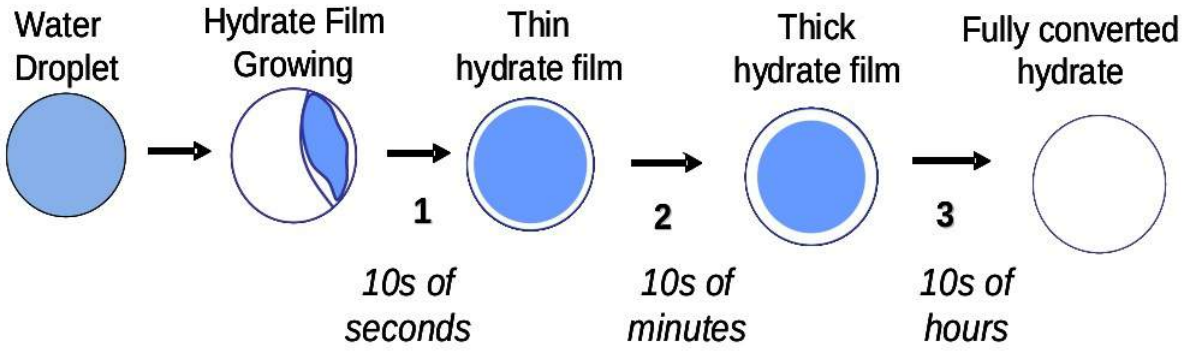

Figure 1.9: Hydrate formation in an emulsified water droplet. Figure taken from Taylor (2006).

The mechanism of hydrate formation in an emulsified water droplet explained below was initially reported by Taylor (2006), and states the following: on the left of the conceptual Fig. 1.9 is shown a water droplet on an oil medium, then a thin hydrate film grows at an oil-water interface from small guest molecules dissolved in the oil (Sloan et al., 2011). This hydrate film thickens over time and forms a shell on a droplet surface that works as a diffusion barrier with two roles, one is to control the subsequent rates of hydrate formation and the other is to separate the oil and water phases. After step 2 the hydrate film begins to grow inward due to the diffusion of the components through the shell. Sloan et al. (2011) indicated that the guest molecules are scarcely soluble in the water droplet that they must come from the external oil phase to convert the water droplet into hydrate. However, Davies et al. (2009) suggest that the water molecules are more mobile than the guest molecules in the hydrate phase, and that the movement of water within the hydrate film controls the hydrate growth. To the right of Fig. 1.9 is depicted as a conceptual

water droplet totally converted to hydrated. The total conversion of the water droplet in a hydrate depends on the size of this droplet. If the diameter of the droplets is less than 40 μm, then they will fully convert to hydrate, otherwise, may only form a hydrate shell (Webb et al., 2012b). After nucleation of water droplets in different parts of the domain, there is a growth of hydrate crystalline structure that is governed by the kinetics of formation of new crystal structures attached to the old. Since this process occurs in several regions, these structures are found and have a tendency to agglomerate and form a plug.

1.2.4 Oil dominated system

These systems have oil, gas, and water, but typically 50% or greater of the domain volume is influenced by the presence of oil (Sloan et al., 2011). In fact, the main assumption in this system is that all of the water is emulsified. Usually, the oil-dominated system with a good heat design to hold the reservoir temperature is less susceptible to hydrate blockage. Figure 1.10 represents a conceptual image of how a series of events lead to jamming in an oil pipeline dominated system.

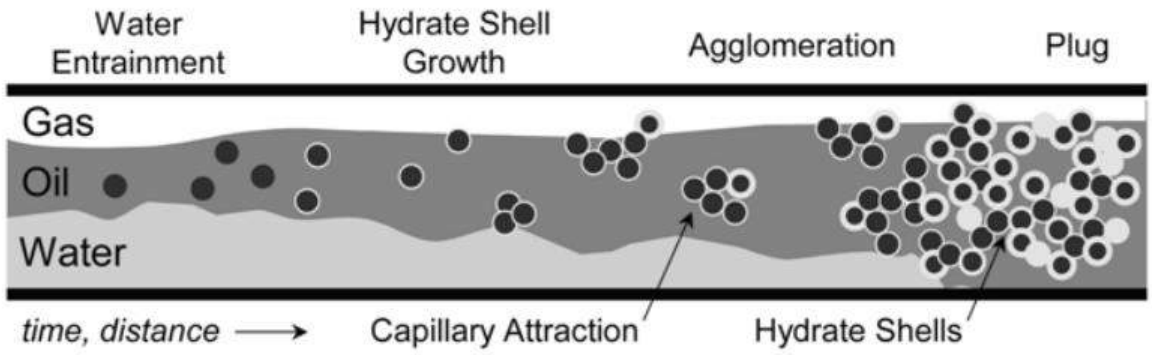

Figure 1.10: Schematic illustration of hydrate formation in oil-dominated systems. Figure taken from Sloan et al. (2011).

In Fig. 1.10 it can be observed gas, oil, and water with small cut volume. In the entrance, the water is dispersing in the oil continuous phase emulsions as droplets. Then, with the distance in the pipe, that is, when a pipe section is found in the region of hydrate formation, a hydrate shell appears around the droplets. The formed film begins to grow as a function of mass transfer of the guest and water through both the oil and the hydrate shell.

Sloan et al. (2011) described that free water may be present which enable strong capillary attractive forces between the hydrates droplets. Hydrates droplets will agglomerate until becomes sufficiently large to increase the pressure drop and plug the streamflow. The plug formed tends to anneal as time elapses and the same becomes more solid-like. This model explained above imply that agglomeration is the factor of the pipe blockage, suggesting that preventing and controlling with anti-agglomerants is a possible strategy for preventing plug formation.

1.2.5 Gas dominated system

The system has a small amount of liquid hydrocarbon and water and the blockage is caused by accumulations of hydrate-incrusted gas bubbles. In this method as well as in the oil-dominated system is necessary water accumulation and subcooling. The subcooling temperature is the difference between the system temperature and the equilibrium temperature for hydrate formation. The schematic Fig. 1.11 depicts a hypothesis of how hydrate is formed for gas dominated systems.

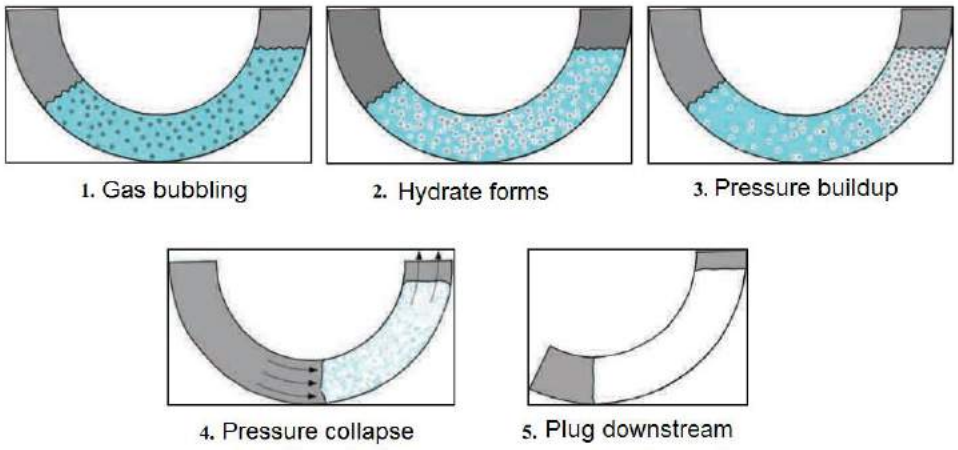

Figure 1.11: Conceptual image of hydrate formation in a gas dominated system. Figure taken from Sloan et al. (2011).

In the first step, it is observed gas bubbles disperse in water (gray) accumulated at the bottom of the pipe. Then, when the subcooling is large enough (below the hydrate formation temperature) the gas bubbles tend to turn into hydrates. Sloan Jr and Koh (2008) suggested that hydrates are generally formed at the wall of the pipe, since the wall is the radial point of lowest temperature, and consequently the site of hydrate deposition

due to the heat transfer with the environment. In step 3 the hydrates gas bubbles begin to aggregate, but the flow pressure leads to a collapse of the hydrate piled up and, subsequently, the block forms downstream of the original water accumulation, after the creation of large amounts of surface area (Sloan Jr and Koh, 2008).

Other models are gas condensate systems and high water cut systems. The former differs from oil dominated systems in that they cannot disperse the water in the oil phase (does not occur stable water-emulsions), due to the absence of surface-active components and hydrocarbon liquid viscosity (Sloan et al., 2011). High water cut systems occur in later reservoir life, since in this case, the well increases the production of water with age. In this system one part of the water phase is not emulsified, then, there is a separated water phase. Unfortunately, these two methods do not have published field data.

1.2.6 Inhibitors

Many mechanical methods to prevent gas hydrates formation (e.g. flowlines insulation, pigs, electrical heating as explain above) are very expensive and can be unsatisfactory under certain conditions. The most common and effective way to prevent and control plugs due to hydrate is through chemical reagents. The main inhibition methods used in the oil and gas industry are thermodynamic inhibitors (TIs) and LDHIs (low-dosage hydrate inhibitors).

1.2.6.1 Thermodynamic inhibitors

TIs such as methanol, glycol, and saline solutions act changing the hydrate equilibrium curve. That is, the equilibrium temperature for hydrate formation is reduced for a certain pressure, shifting the chemical potential of water. Most of them are used in gas dominated systems, from which a large amount of TIs is required for the process to be effective. In fact, Chen et al. (2013) showed that the quantity of TIs used in a specific case often reaches 20 - 50 wt% or more, which is sometimes not cost effective. Another disadvantage is that some of these agents are pollutants, such as methanol (Kelland et al., 2009).

As methanol and ethylene glycol are the thermodynamic inhibitors most used due to its cost and effectiveness, then a brief description of them is made. Figure 1.12(a) shows the structure of the methyl alcohol-CH_3OH. Methanol obtained during a chemical process by mixing carbon monoxide and hydrogen. Some of its properties are: lightness, flammable,

volatile, colorless, and with odor very similar to drinking alcohol (ethanol). At room temperature, it is a polar liquid and is used as antifreeze, solvent, and fuel. Methanol is the simplest alcohol, containing only one methyl group linked to a hydroxyl group, which makes it highly soluble in water. Polar compounds such as alcohols and glycols form hydrogen bonds with the water interfering in the arrangement of the water molecules, decreasing the hydrate formation temperature. Sloan Jr and Koh (2008) referred to the review made by Franks (1973) and Ben Naim (1980), which have shown that the hydrocarbon end of the alcohol molecule causes a clustering effect on water molecules similar to that of hydrate formation.

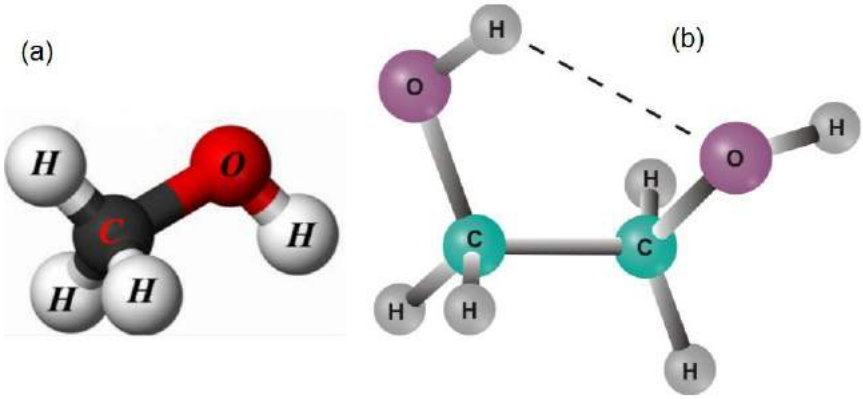

Figure 1.12: Chemical structures of a) Methanol b) Ethylene glycol. Its hydroxyl group renders them highly soluble in water.

In the gas production systems the methanol is injected into the transmission line, and then this agent dissolves in the free water accumulation in order to avoid hydrate formation. The main problem of methanol (besides its toxicity and high flammable point) is how to induce it to make contact with the free water, since methanol evaporates downstream of the injection point due to a factor such as bathymetry, line length, and gas flow. Therefore, glycols are preferred in many of the applications. In addition, the glycols generally have higher molecular weights with lower volatility, so they may be recovered (Sloan Jr and Koh, 2008). Figure 1.12(b) shows the chemical structure of the ethylene glycol, with the formula $(CH_2OH)_2$. It is produced by reacting ethylene oxide with water and it is used in many industrial applications, such as: antifreeze, hydraulic brake fluids, coolant, heat transfer agent, and as a solvent. The physical properties of this organic compound are: colorless, odorless, and high viscosity.

The glycols have more hydrogen bonding opportunity when in contact with water since they have one more hydroxyl group than methanol. Typically, the effectiveness of the TIs is measured through the subcooling, in this case, defined as the difference between the formation temperature for hydrates with and without inhibitor. Salts also are efficient inhibitors; however, its use is limited in some flowlines due to corrosion problems.

1.2.6.2 Low-dosage hydrate inhibitors

Low-dosage hydrate inhibitors are divided in two groups: KHIs (Kinetic hydrate inhibitors) and AAs (anti-agglomerants). KHIs affect the kinetics of the process since they delay the crystal growth and avoid the agglomeration, which makes them time dependent. In practice, the performance of a KHI depends on the composition of the liquid hydrocarbon phase. Other factors such as pressure, salinity, other additives, and mixing also have an effect (Kelland, 2006). Since the LDHIs are time-dependent, the subcooling chart is required to analyze its effectiveness.

1.2.6.2a Kinetic inhibitors

KHIs are polymers of low molecular weight that avoid hydrate formation incrementing the induction time for hydrate nucleation (Chen et al., 2013). Sloan et al. (2011) reported that when these compounds have contact with the hydrate surface, they are absorbed by it, and the hydrate formation rate is reduced as well as the crystal growth. Kvamme et al. (2005) reported that the presence of inhibitor molecules decreases the hydrate-water interactions by increasing hydrate-inhibitor interactions. 'OReilly et al. (2011) were the first authors to validate the efficiency of poly-N-vinylpiperidone (PVPip) and also evidenced that the highest molecular weight polymer was responsible for a longer delay in the growth of gas hydrates crystals. The most common polymers used as KHIs are polyethylene chain attached to a polar group of a cyclic amide (lactam). Figure 1.13 shows some examples of KHIs structures.

Moore et al. (2009) hypothesized that the KHI polymer has anchor points that work by distorting the hydrate structure. This distortion produces and increases the amount of energy needed to form hydrates and thus slows down the reaction kinetics. The author also indicated that Makogon et al. (2002) reported that the polymer induces the crystals to grow around and between the polymer strand and, consequently blocks the diffusion

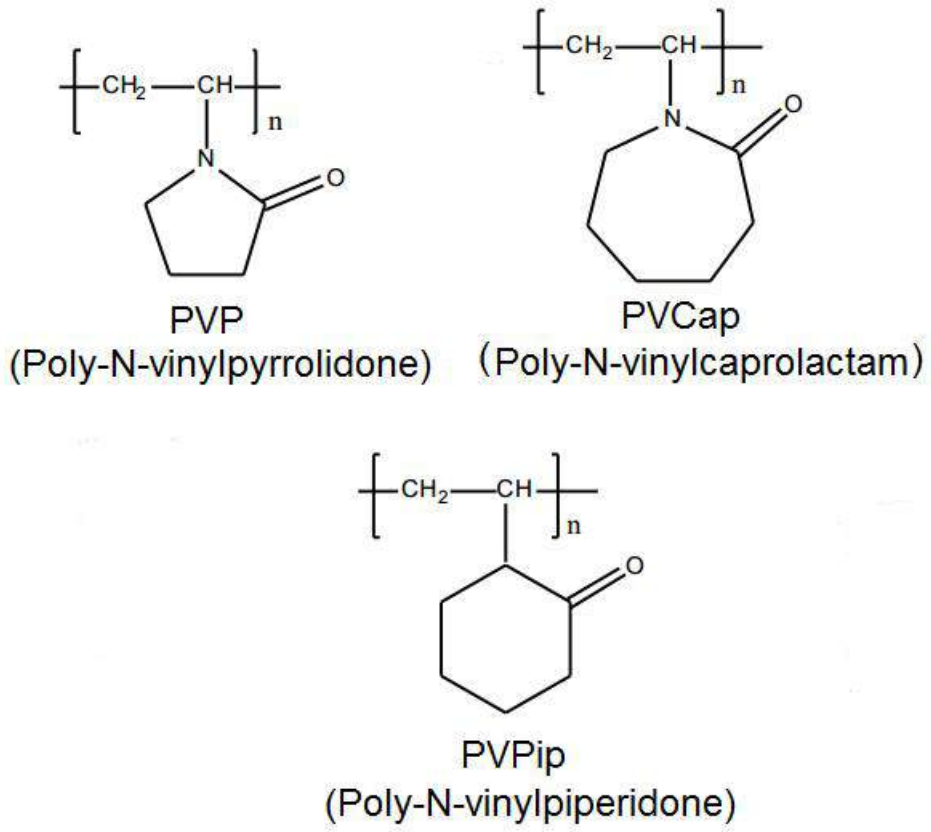

Figure 1.13: Chemical structures of some KHIs. PVP, PVCap, and PVPip containing the 5-ring, 6-ring, and 7-ring lactam respectively.

of gas to the hydrate surface. In fact, there are several theories to explain the interaction between the polymer and the hydrate structure, but the mechanism is still unknown. The understanding of the phenomenon of hydrate formation in the presence of kinetic inhibitors is important to control and prevent hydrates blockages.

KHDIs are usually used in quantities of less than 3% of the produced water, reducing the high expenses (Tohidi et al., 2015). Another advantage of KHIs is the synergism that these reagents have with other substances, as monoethylene glycol. In fact, KHIs can be blended with other chemical products to avoid the occurrence of other problems in the process, such as paraffin deposition or to prevent corrosion on the equipment or the flowlines.

Other inhibitors that are more environmentally friendly than synthetic polymer reagents are biological or green inhibitors. They are natural inhibitors that have been studied during the evolutionary process in the organism over a very long period of time (Daraboina, 2012). There are several known green inhibitors. Two important examples are the an-

tifreeze protein (AFP) and the antifreeze glycoprotein (AFGPs) from ocean fish, which allows certain organisms to survive during winter periods. Al-Adel et al. (2008) studied its effectiveness as kinetic hydrates inhibitors and compared with polymer kinetic hydrate inhibitors at the same pressure, temperature, and weight percentage conditions. The experimental results suggested that AFP inhibits hydrate growth to the same extent as PVP and PVCap at the same weight concentration and for specific thermodynamic conditions.

1.2.6.2b Anti-agglomerants

AAs are surfactants soluble in oil. Quaternary ammonium salts and quaternary phosphonium salts are examples of commonly used substances to this end. AAs allow the hydrate crystal to form and maintain the hydrate particles in the oil phase avoiding their aggregation. The formed hydrate particles are transported by the streamline as a low-viscous liquid and cannot be limited by the subcooling. The evaluation of AAs is usually performed using rocking cells. Chen et al. (2013) examined single and compounded commercial chemical additives to evaluate the ability to prevent gas hydrate from agglomeration. The authors found five kinds of gas hydrate morphologies from water + diesel oil: slush-like, flocculent-like, clumpy-like, powder-like, and slurry-like. The two last morphologies have shown good ability to flow, while the others were considered not suitable in water + oil system.

The asphaltenes and resins that are present in the oil act as natural surfactants (Soares et al., 2013). They can stabilize the water droplets or hydrates particles. Hence, there are crude oils that have the ability to transport hydrate particles as a slurry, and also to delay hydrate formation (Palermo et al., 2004). The AAs decay their efficiency with a certain level of water cut and water salinity.

1.2.7 Rheology

Rheology is the science concerned with the deformation and flow of matter, and with the response of the material to the application of a mechanical force or to a deformation (Lambourne and Strivens, 1999). This subject studies the behavior of different substances that have a complex microstructure, such as: muds, waxy crude oils, additives, polymeric solutions, bodily fluids as well as many others. Depending on the response of the fluid to an applied force, they are classified as Newtonian or non-Newtonian fluids.

To define Newtonian fluids it can be considered a small layer of a fluid confined into two infinite parallel planes, where one of them is fixed as shown in Fig. 1.14. If this fluid is subjected to shear through a force **F**, then after fully developed and steady-state flow conditions are reached, this force is going to be balanced with an opposite and same magnitude frictional force in the fluid. For an incompressible Newtonian fluid and laminar regime the shear stress, τ is equal to the product by the viscosity of the fluid μ with the shear rate, $\dot{\gamma}$.

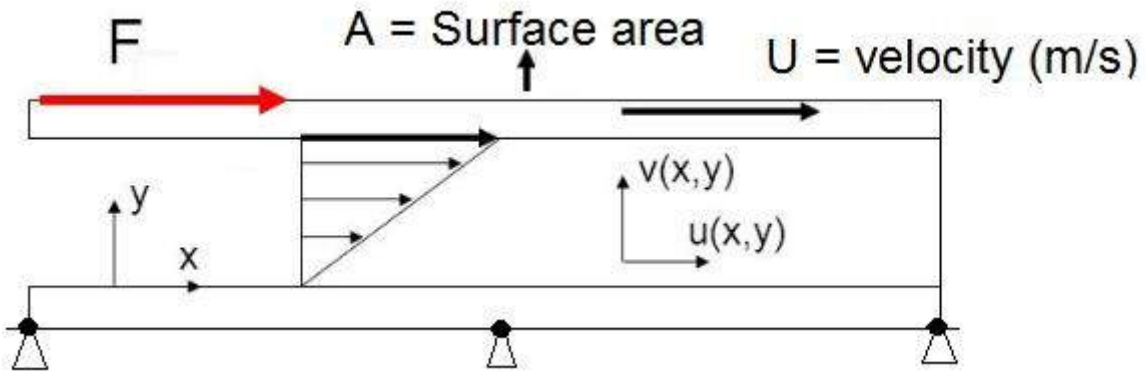

Figure 1.14: A simple shear flow between two parallel infinite plates.

The shear stress is given by:

$$\frac{F}{A} = \tau_{yx} = \mu \frac{dU_x}{dy} = \mu \dot{\gamma}_{yx} \tag{1.2}$$

Where A is the plate area, and the subscript y indicates the direction normal to that of the shear force and the subscript x indicates the direction of the force. The Newtonian fluids are characterized by the viscosity or proportional constant that relates stress and shear rate. The Newtonian viscosity is independent of the shear rate or shear stress and depends only on the material, temperature, and pressure. Some substances that show this behavior at room temperature are: water, honey, air, and ethylene glycol among the others. On the other hand, substances that do not exhibit constant viscosity are non-Newtonian fluids. That is, the result obtained from dividing the shear stress by the shear rate can vary at a given temperature and pressure. These fluids are dependent on other factors such as flow geometry, deformation rate, temperature, history, timescale, etc. This group is composed of a large class of materials such as: dairy products, waxy crude oils,

foodstuff, and drilling muds. Non-Newtonian fluids are distinguished to have at least one of the next characteristics:

1. Viscosity dependence on the shear rate or corresponding shear stress.

2. Shear viscosity is different from elongational viscosity.

3. Presence of a yield stress.

4. Elasticity.

5. Time-dependency.

Chhabra and Richardson (2011) classified the non-Newtonian fluids into three groups:

- Fluids that are time-independent, also known as purely viscous, inelastic or Generalized Newtonian Fluids. In this case, the stress is only function of the deformation rate or vice versa at a given point and instant.

- Time-dependent fluids. In this group, the stress in addition to depend on the deformation rate, is also a function of other parameters as shear history and temperature history.

- Materials showing both viscous and elastic behavior when undergoing deformation. That kind of substances is known of viscoelastic materials.

A simple class of inelastic materials is the so-called Generalized Newtonian Fluids which may be described by the following constitutive Equation:

$$\begin{aligned} \mathbf{T} &= -p\mathbf{I} + \boldsymbol{\tau} \\ \boldsymbol{\tau} &= \eta\dot{\boldsymbol{\gamma}} \end{aligned} \tag{1.3}$$

in which $\mathbf{T}$ is the stress tensor, p is the mechanic pressure, $\mathbf{I}$ is the unit tensor, $\boldsymbol{\tau}$ is the extra stress tensor, $\dot{\boldsymbol{\gamma}}$ is the deformation tensor, and η represents the non-Newtonian viscosity.
The Generalized Newtonian Fluids can be roughly divided in three classes:

a. Shear thinning or pseudoplastic materials.

b. Shear thickening or dilatant materials.

c. Viscoplastic.

Pseudoplastic materials are the most common behavior observed in the group of inelastic fluids. They are characterized by a viscosity decrease when the deformation rate increases. Also, at both very high and very low shear rates, most of the shear thinning materials has a Newtonian plateau. As examples of this class of materials are found: polymer solutions and melts. On the other hand, the viscosity of dilatant materials increases with the increment of the shear rate. To explain this feature is hypothesized that at low shear rates the space between the particles is lubricated by the fluid between them, but at higher shear rates the material expands slightly and is not enough to lubricate this space, permitting the contact between the particles and producing in this way the viscosity increment. Materials such as sand dunes and titanium dioxide may exhibit this kind of behavior.
There are different models to describe dilatant and pseudoplastic materials. Perhaps the most common method used is the Power-law or Ostwald de Waele, given by the expression:

$$\tau = m(\dot{\gamma})^k \tag{1.4}$$

where τ is given by $\tau = \sqrt{\frac{1}{2}tr\boldsymbol{\tau}^2}$ and $\dot{\gamma} = \sqrt{\frac{1}{2}tr\dot{\boldsymbol{\gamma}}^2}$. The viscosity for the Power-law model is given by:

$$\eta = \frac{\tau}{\dot{\gamma}} = m(\dot{\gamma})^{k-1} \tag{1.5}$$

Where k and m are two empirical curve-fitting parameters, named as flow behavior index and fluid consistency coefficient respectively.
For:

$k < 1$, the fluid shows shear thinning behavior.

$k = 1$, the fluid exhibits Newtonian behavior.

$k > 1$, the fluid exhibits shear thickening properties.

For pseudoplastic materials the smaller the values of k, the greater is the degree of shear thinning. For a dilatant fluid, the index k will be greater than unity. Figure 1.15 represents several types of time-independent materials.

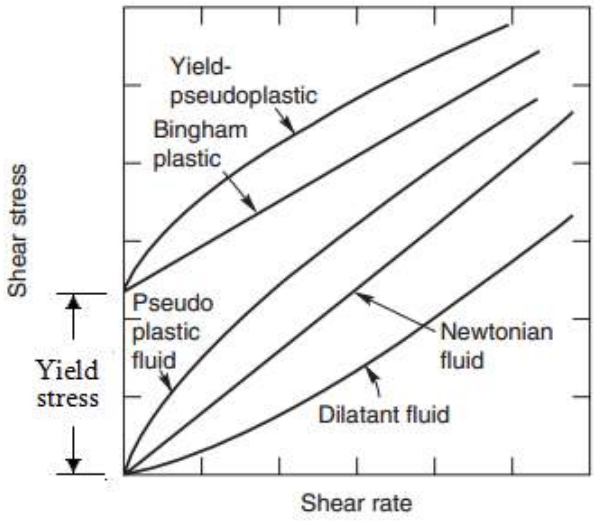

Figure 1.15: Behaviors of purely viscous materials.

1.2.7.1 Viscoplastic materials

This type of material behavior is characterized by the presence of yield stress, τ_0, which must be exceeded before the fluid deforms continuously or flow. If the externally applied stress is smaller than τ_0 the material behaves as a rigid solid, and if the stress is higher than τ_0, then it behaves as a shear-thinning liquid (de Souza Mendes and Dutra, 2004). This kind of material is such that at rest it has a structure of sufficient rigidity to resist any external stress below τ_0, and for stress levels greater than τ_0, the structure breaks down and the substance behaves as a viscous material. Despite the fact that the existence of τ_0 is not proven, from the practical point of view it is a convenient assumption because there are materials that have approximately such behavior. Common examples of viscoplastic fluid behavior are foodstuff, emulsions, drilling fluids, and blood.

Bingham (1916) proposed the simplest model for materials of this kind of behavior; the mathematical equation in one-dimensional steady shearing motion is given by:

$$\begin{aligned} \tau &= \tau_0 + \mu\dot{\gamma}, \qquad && \tau \geq \tau_0 \\ \dot{\gamma} &= 0, && \tau < \tau_0 \end{aligned} \tag{1.6}$$

where μ is called plastic viscosity. The Bingham plastic function predicts a rigid body behavior when $\tau < \tau_0$, otherwise, the material flows with a constant slope in the stress-shear rate relation. In this model, the viscosity tends to infinity at low shear rates and decreases when the shear rate increases.

Herschel and Bulkley (1926) proposed a generalization of the Power-law and Bingham models, with the objective to capture the non-linearity of the flow curve when $\tau > \tau_0$. The Herschel-Bulkley model incorporates three characteristic parameters as described in the next equation:

$$\begin{aligned} \tau &= \tau_0 + m\dot{\gamma}^k, \quad && \text{if} \quad |\tau| \geq |\tau_0| \\ \dot{\gamma} &= 0, && \text{if} \quad |\tau| < |\tau_0| \end{aligned} \tag{1.7}$$

The physical meaning of m and k is similar to that in the Power-law equation. This model is widely used in both industry and research due to the good fitting to the flow curve obtained with this kind of materials.

Several models of viscoplastic materials were proposed in the literature such as the Casson model and the Cross model. The Casson fluid model describes very well the behavior of many foodstuffs and biological materials (Chhabra and Richardson, 2011). On the other hand, the Cross model has the advantage of permit working in a wide range of shear rates. de Souza Mendes and Dutra (2004) proposed a viscosity function for apparent yield stress fluids, i.e materials that flows continuously for any stress level but exhibit a transition from a high viscosity behavior to a low viscosity one at critical stress (called apparent yield stress). That function is continuous and fits with accuracy the different regions of the flow curve generated by this type of fluid behavior. At low shear rates it presents a viscosity plateau, followed by a sharp viscosity drop when the apparent yield stress value is reached, and after that, a power-law region.

Bonnecaze and Brady (1992) referenced a model (initially presented by Kraynik (1990)) with three shear stresses that has gained good acceptance by the rheology community. The three critical shear stresses that characterize the rheological behavior are the elastic, the static, and the dynamic yield stresses as shown in Fig. 1.16.

The elastic limit yield stress is most commonly used in solid mechanics and represents

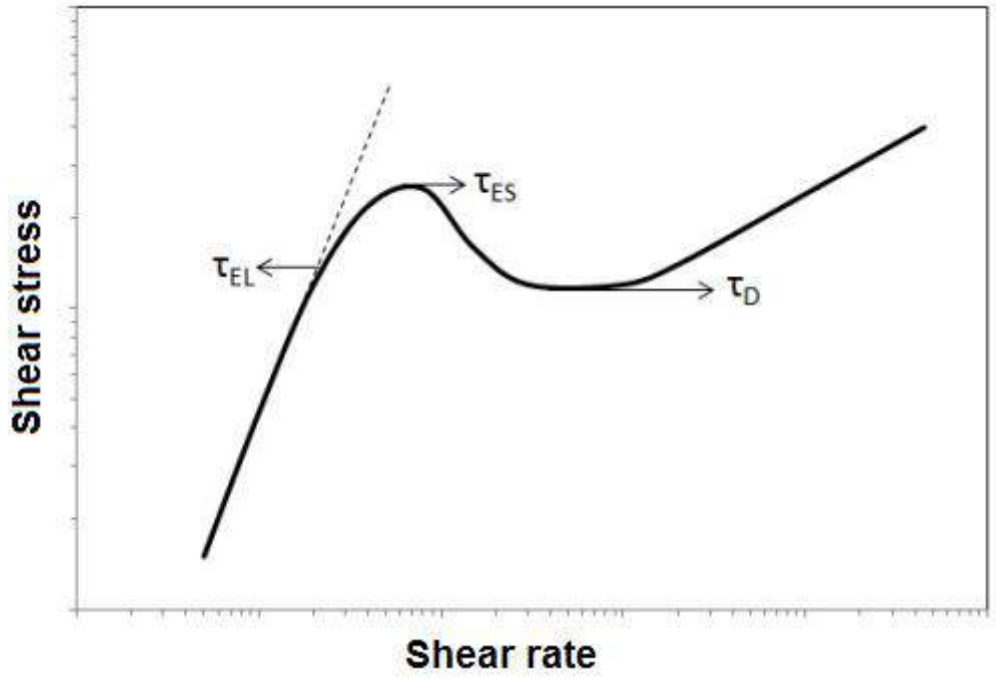

Figure 1.16: Flow curve model with three shear stress proposed by Kraynik (1990).

the transition between elastic and plastic deformations. Bonnecaze and Brady (1992) explained that the elastic-limit yield stress is not the limit of linear behavior, but rather, is the limit of reversibility for the material. As the authors indicate, the loss of linear behavior generally occurs before the elastic limit. The static yield stress is the minimum stress necessary for the material to deform continuously. This value is very important to practical applications. The dynamic yield stress resembles the Bingham concept and represents the minimum value to maintain the material flowing.

1.2.7.2 Time-dependent materials

It is difficult to obtain a good measure of a yield stress when a viscoplastic model exhibits thixotropic behavior. Thixotropic materials are a subclass of time-dependent materials that are characterized by two additional features. They exhibit a destruction rate which increases with the stress level and a one-to-one correspondence between the stress and the structure. In fact, the thixotropic behavior of many industrial substances cannot be described by simple equations.

The time scales involved can range from many minutes in the case of breakdown until many hours in rebuilding (Barnes, 1997). Many fluids such as food, cosmetics, and paints have this kind of behavior.

The microstructure of the fluid usually tends to a stable configuration when is submitted to a constant shear rate or shear stress during a long time. de Souza Mendes and Thompson (2012) interpreted the flow curve as the set of attractor points of the structure dynamics and elected the interception between the constant stress line and the flow curve as the equilibrium point associated with the current non-equilibrium state. The structural level is generally modeled by a kinetic equation, where competition between a build-up and break down terms are present. Time-dependent fluids are divided in reversible and irreversible. Reversible may be further sub-divided in thixotropic and rheopectic or negative thixotropic. In opposition with thixotropic materials, the rheopectic is characterized by the increases in its apparent viscosity whit time of shearing. In a rheopectic fluid, the structure builds up by shear and breaks down when the material is at rest. There are few known materials with this behavior; some of them are colloidal suspensions and protein solutions.

1.2.7.3 Viscoelastic materials

A viscoelastic material shows both viscous and elastic characteristics under appropriate circumstances. Many fluids of practical interest such as soap solutions and synovial substances exhibit viscoelastic behavior. These materials have the ability to store and to recover energy. However, the response of a material depends not only on its structure level, but also on the conditions to which it is subjected. In other words, the material can behave like a viscous fluid in one situation and like an elastic solid in another.
Viscoelasticity and thixotropy have similarities related to time-dependency. Viscoelastic systems sheared in their linear region show time-dependency because the microstructure takes time to respond to the stress. At short times the structure cannot respond quickly and is observed an elastic reaction, while given time, the system can adjust itself continuously showing viscous effects (Barnes, 1997). This process shows linearity between the shear stress and shear rate and does not present break down of the structure, that is, the material recovers after the suspension of the external force. On the other hand, in thixotropy, the structure retards in demonstrating a response to shear, but the corresponding deformations are stronger and have slow recoveries. Thus, the time-dependency occurs differently in the two behaviors, making the structure recovery the main difference between the viscoelasticity and thixotropy. These characteristics could be present in the

same material, which probably happen with the gas hydrates.

1.2.8 Rheology of gas hydrates

There are several goals with respect to the rheological analysis of gas hydrates. Firstly, through this approach, it is possible to get a better understanding of the phenomenon, as well as to explain some behaviors, as time-dependency and memory effect, which are more complex to explain with other approaches. Secondly, if the experiments are conducted in rheometers, some rheological properties of the non-Newtonian character of the flow such as viscosity, shear rate or shear stress are easier to measure than *in situ*, where the thermodynamic conditions and other factors such as time and oil composition at certain point and instant make the measures difficult. In fact, a good measure of yield stress could be helpful in restart problems as well as in the selection of the pumping system. The efficiency of thermodynamic as well as kinetic inhibitors can be analyzed using small amounts of samples. In this case, commercially available inhibitors, as well as new ones, can be studied. Perhaps, from the practical point of view, the most important contribution of these experiments on a small scale is to conceive an idea if the hydrate will form for certain field operating conditions and, in this way, to help its prediction and prevention. In devices such as pressure cells, where it is possible to work with live crude oil, that is, in presence of light hydrocarbons, it is also possible to analyze the sample at different temperatures, pressures, and water cuts. However, the majority of rheology studies concerned with hydrate slurries has been realized with liquid hydrate formers such as cyclopentane and tetrahydrofuran at atmospheric conditions, see (Leopércio et al. (2016); Ahuja et al. (2015); Peixinho et al. (2010)). This allows the study of hydrate formation processes without the experimental difficulties of dealing with elevated pressure. Measuring the rheological properties with high-pressure devices is complex. However, through this apparatus, it is possible to perform experiments with live crude oil, simulating the conditions for hydrate formation in a similar way to that of the real operations. One factor that imposes difficulties on the investigations in a pressure cell is that these devices cannot create enough interfacial area between the water and the gas, a condition that is required to facilitate the hydrate formation. One way to mitigate this drawback is through rheometric geometries as the one analyzed by Barnes and Carnali (1990) and Yoshimura et al. (1987).

1.2.8.1 Rheology of emulsions

The hydrates slurries studied in this work are formed from water in oil emulsions. However, when the hydrates particles begin to form they are dispersed in a hydrocarbon liquid phase, leading to a suspension. Webb (2014) showed that this transition is not complete, because not all the water droplets are converted to hydrate. Subsequently, the final sample is one part emulsion and the other part suspension. Camargo et al. (2000) suggested that some natural surfactants contained in the crude oil such as asphaltenes and resins can exert a dispersing effect and create hydrate crystals in an oil phase. Then, this mixture would be transportable as a suspension without utilizing further inhibitors.

The emulsion is composed of a liquid continuous phase together with a disperse phase of a liquid or, at least, of deformable drops. In water-in-oil emulsions, the water droplets are injected into the oil by turbulence or wave actions. These droplets can be stabilized by the oil viscosity and on a longer-term basis by resins and then asphaltenes (Fingas, 2014). Barnes (1994) indicated that the interface between the drops is the source of stability of the unstable systems. The author reported that the basic parameters which influence in the emulsion rheology are: first, the continuous phase rheology; second, the nature of the particles, i.e. size distribution, deformability, internal viscosity, and concentration; and third, the nature of the particle-particle interactions. The continuous phase is important because it interferes in the motion of the droplet. Particles size is relevant since smaller particles are less deformable and should lead to higher viscosity and particle-particle interactions are most pronounced in emulsions when there are attractions between the particles, with the potential to form aggregates.

Derkach (2009) suggested that the analysis of rheological properties of suspensions can be treated as the limited case of emulsions when the viscosity of dispersed droplets becomes unlimitedly high. In addition, some models have been developed to predict the rheological behavior of emulsions. Derkach (2009) indicated the Einstein law (Einstein, 1906) as the pioneering work where is proposed the following equation:

$$\frac{\eta}{\eta_0} = 1 + \frac{5}{2}\phi \tag{1.8}$$

Where η is the suspension viscosity, η_0 is the continuous phase viscosity and ϕ is the dispersed phase volume fraction. Einstein's equation is valid in the limiting case of very

low concentrations where the interactions between the dispersed particles are absent. The viscosity of dilute emulsions is also described by Taylor (1932) equation, which is given by:

$$\eta = \eta_0 \left[1 + \frac{2 + 5\lambda}{2(1 + \lambda)}\phi\right] \tag{1.9}$$

The above expression uses the same parameters as the Einstein equation besides a new one, λ, which represents the ratio of the dispersed phase viscosity to the continuous phase viscosity.

Different experimental studies have been performed with emulsions, see for example de Oliveira et al. (2009) and Barnes (1994). De Oliveira studied the rheological behavior of three Brazilian waxy crude oils. These crude oils were mixed with a 5 wt% of synthetic brine and different water volume fractions to prepare the emulsions. The results have shown that the viscosity of the emulsion increases with the water content and with the shear rate. Also, it was demonstrated that the emulsion has a shear-thinning behavior below the temperature where the first paraffin crystals appear, the so-called Wax Appearance Temperature (WAT). In different cases, the viscosity of the emulsion is greater than the crude oil viscosity and de Oliveira et al. (2009) suggested that the main contribution of viscoelastic behavior is provided by the dispersed phase.

1.2.9 Studies of hydrates rheology

There are a limited number of investigations concerned with the rheological characters of the hydrates until now. Andersson and Gudmundsson (2000) presented what is probably the first work about hydrate rheology. These researchers from the Norwegian University of Science and Technology (NTNU) built a hydrate rig to investigate the flow properties of such processes. The experimental setup has a reactor, where the hydrates are produced when the guest molecule and the liquid water are brought into contact under hydrate forming conditions. The measured values are obtained with a high-pressure tube viscometer in which the flow properties of the sample can be studied under laminar and turbulent pipe flow conditions. In that study, the authors assumed that the continuum equations governing single-phase are also valid for water-hydrate slurries. Then, to determine the viscosity, the wall shear stress (through a force balance on the pipe wall) and the

wall shear rate were computed (deriving the local velocity profile) for a Newtonian flow in a laminar regime. The viscosities for the non-Newtonian behavior were estimated using the Rabinowitch technique. For the flows in the turbulent regime, it was employed the hydraulic gradient concept. In that work, it was concluded that the apparent viscosity of the hydrate-in-water slurries increases whit increasing hydrate concentration, the viscosity of the structure I (pure methane) have quite similar values to that of structure II (92% methane, 5% ethane, and 3% propane) and in the turbulent regime, the frictional pressure drop of the hydrate-in-water slurries is determined by the properties of the carrying water phase alone. So, hydrates did not affect the rheology of the system in the turbulent flow regime. Camargo et al. (2000) analyzed the rheological behavior of water-in-oil emulsions before and after the crystallization process. For this purpose, it was used as a pioneer rheological cell that has been adapted to allow the evaluation of the rheological character of the emulsions and suspensions. The device was calibrated with Newtonian as well as non-Newtonian fluids. Several important results were obtained in this work. Firstly, it was observed that the viscosity increased and the pressure decreased for closed systems when the hydrate is formed, probably the first author to report this fact. Secondly, the hydrate suspension viscosity was greater than the emulsion viscosity measured after and before the crystallization respectively as illustrated in Fig. 1.17. Thirdly, both, suspension and emulsion viscosities increased with water volume fractions and fourthly, hydrates suspensions showed a shear thinning behavior that is more pronounced in more concentrated suspensions.

Sinquin et al. (2004) studied the rheological properties of hydrate suspensions in the laminar as well as in the turbulent regime. The experiments were conducted in a multiphase flow loop that permits to study the oil and gas flow at a large scale. The equations used to determine the apparent viscosity were the same used by Andersson and Gudmundsson (2000). In this work, two different oils were studied and the viscosities were measured in the laminar flow regime showing Newtonian behavior. Also, it was observed that the viscosities of the suspensions increase with the volume fraction of hydrate and the authors argued that shear thinning behavior can be observed in the suspensions when the interparticle forces are high enough. In the turbulent flow regime, the friction factor increases with the water cut.

Rensing et al. (2008) studied rheologically the behavior of methane hydrate slurries over

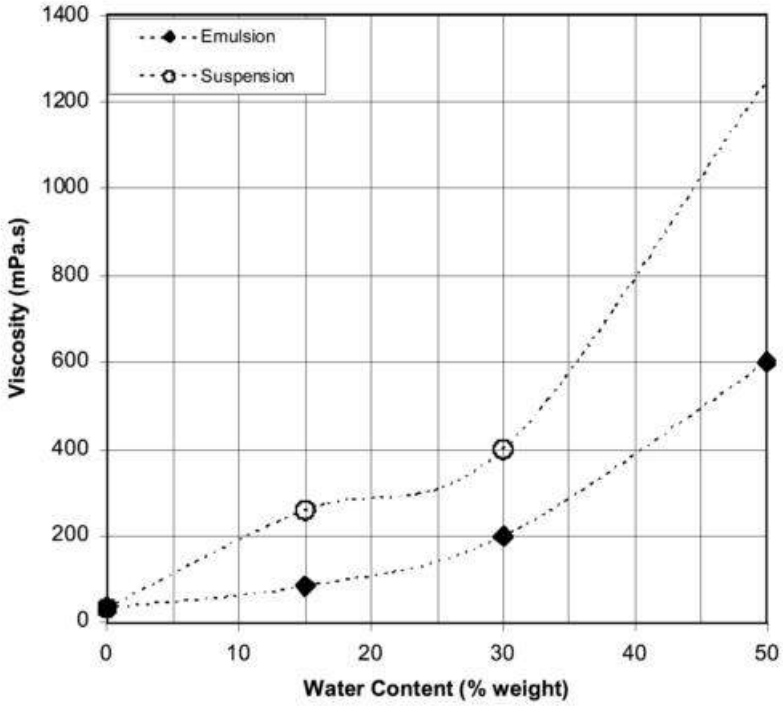

Figure 1.17: Comparison between emulsion and hydrate suspensions viscosities at different water contents. T=280.65 K, P=8 MPa. Figure taken from Camargo et al. (2000).

time. To this end, it employed a pressure cell with a concentric cylinder geometry. The authors analyzed the sample through both constant shear rate and oscillatory tests. First, it was shown during a shear time sweep how the viscosity and the pressure drop increase when the nucleation occurred. Second, the oscillatory test showed that after nucleation the elastic properties of the sample enhance, that is, the sample is annealing over time. Clathrate hydrate dissociation was associated to drop in loss modulus G'', suggesting that the sample has a more solid-like behavior upon dissociation. Rensing et al. (2011) conducted experiments on ice slurries formed in water-in-oil emulsions with brine and fresh water at different water volume fraction. Unlike the work reported in 2008, the emulsion was cooled until -10 °C and held until ice nucleation occurred, in this case, 0.05 g of silica gel was added to the bottom of the cell in order to facilitate ice nucleation without influence in the rheological measurements, according to the authors. The results of this investigation are summarized next:

- The apparent viscosity of the slurries increases with the water volume fractions.

- Three different regimes were identified to analyze the yield stress of emulsions of fresh water. Each of these regimes depends on the water content, see Fig. 1.18a. For water volume fractions below 0.25, the material showed little to no yield stress. It was argued that the water content is so low that does not allow the particles to aggregate and they remained dispersed in the slurry. For water content between 0.25 and 0.55 the sample showed an yield stress of approximately 300 Pa. In this case, was hypothesized aggregation of the ice particles formed large networks. For water volume fractions of 0.60 and greater, the yield stress was substantially increased due to the large agglomerates formed, in some cases sufficient to jam the rheometric geometry.

- Yield stresses for the emulsions prepared with brine were smaller than for the emulsions prepared with fresh water at comparable volume fractions as shown in Fig. 1.18b. A possible explanation is that the salt weakened the aggregate structures.

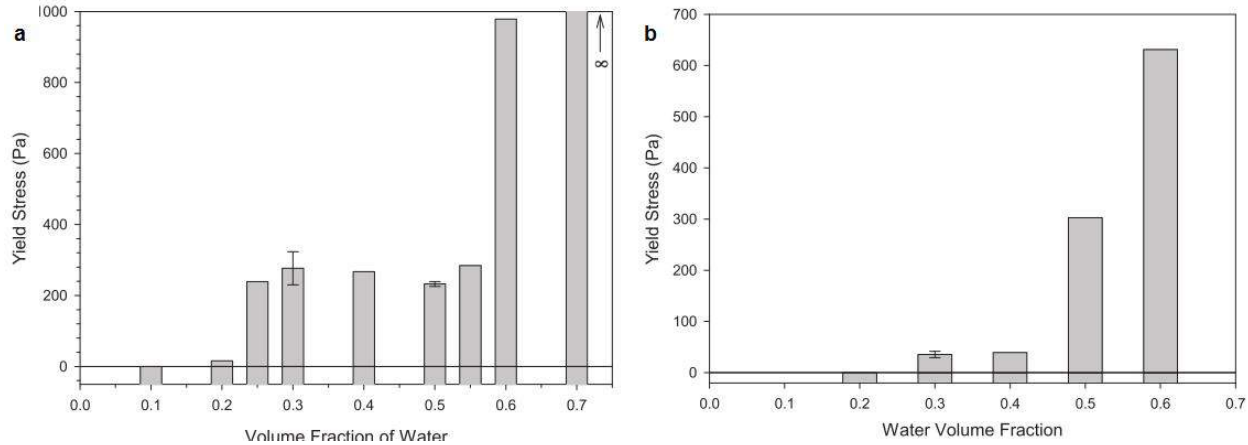

Figure 1.18: Yield stress of a) ice suspensions and b) brine as a function of water volume fractions. Figure taken from Rensing et al. (2011).

- At the end of the test, the sample was sheared at 500 s^{-1} for 60 min in order to dissociate the aggregate structures. The apparent viscosity of the ice slurry increased over that of the emulsion.

- The complex viscosity for the emulsion of fresh water showed a rapid increase in the magnitude after nucleation occurred, then decreased until reach a plateau where remained relatively constant as shown in Fig. 1.19a. For the brine system, the

complex viscosity increased in the first hours and then augmented slowly for the rest of the teste as illustrated in Fig. 1.19b.

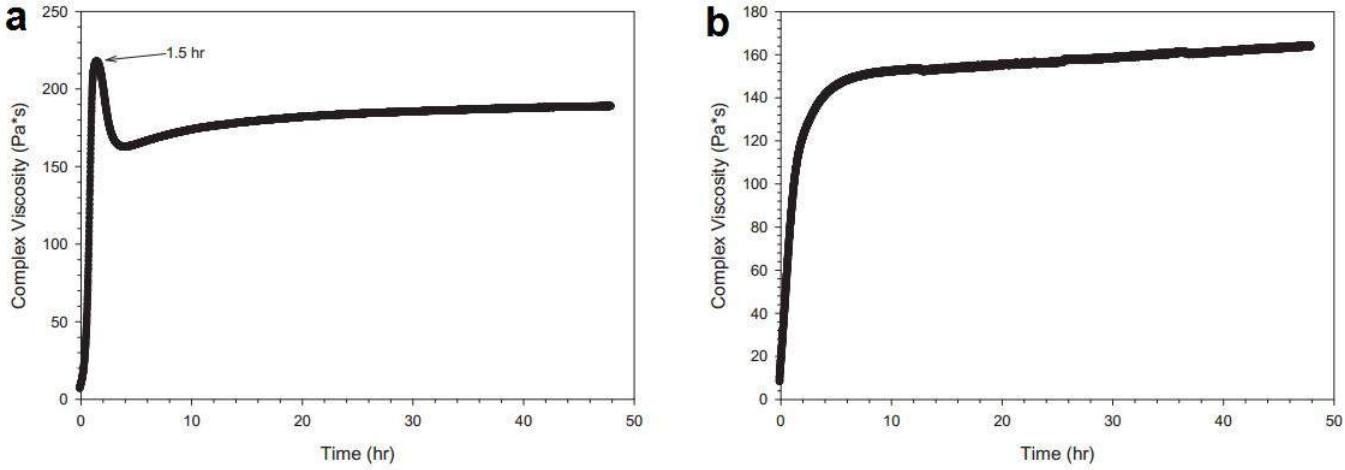

Figure 1.19: The behaviour of complex viscosity over time for: a) Freshwater and b) brine. An emulsion of 30% at -10 °C. Figure taken from Rensing et al. (2011).

Rheological properties of water-in-oil emulsions as hydrate-in-oil slurries were studied by Peixinho et al. (2010) with cyclopentane as a hydrate former. The experiments were realized in a rheometer with Couette cup and vane geometries. The drop size distributions, as well as the shear viscosity of the emulsions, were measured. In some cases, the values obtained exhibited large standard deviations. The authors observed that the dynamic storage modulus G', increases until reaches a plateau indicating that the sample is solid-like in 1 °C (see Fig. 1.20), and then, when the temperature was increased, G' also increased until 20 °C, temperature where most of the experiment time was maintained, and finally G' decreases dramatically due to the dissociation of the block.
The previous result is quite curious because even passing through the dissociation temperature (5 °C in agreement with literature values) G' still continues to increase.

Perhaps the most recent articles that explored the hydrate rheological characterization in a high-pressure cell were made by a Center for Hydrate Research group, at Colorado School of Mines. The group used an apparatus with an external high-pressure mixing cell to saturate water-in-oil emulsions with methane gas. The mixing cell is composed of a stirrer that generates a high contact area between the guest molecules and the liquid phases facilitating the emulsion saturation. After the mixing, the emulsion is moved to

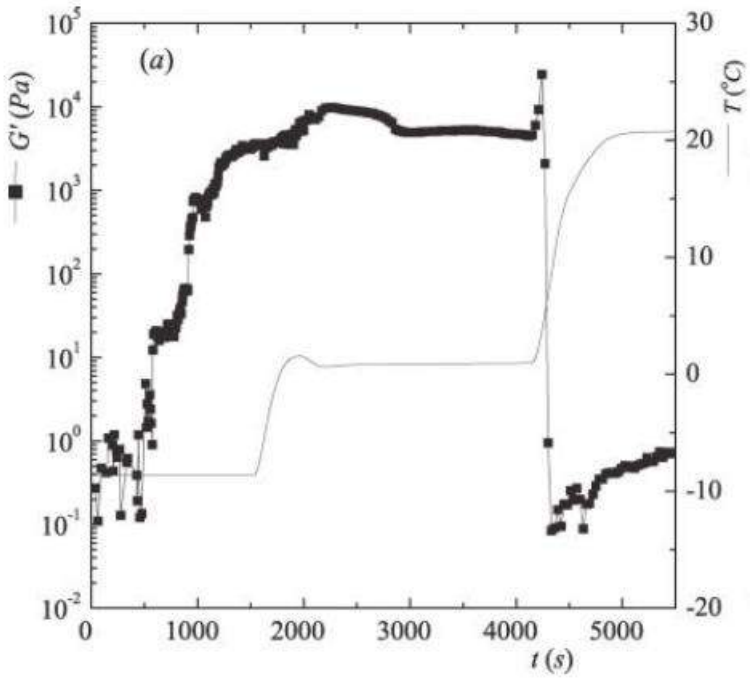

Figure 1.20: G' versus time for a CP emulsion undergoing the quench. Taken from Peixinho et al. (2010).

the rheometer cell that uses concentric cylinders to measure the rheological characteristics of the sample. Mixing and measurement occur in different vessels and under high-pressure throughout the process. A full description of the apparatus is found in Webb et al. (2012a). In a subsequent work (Webb et al., 2012b), it was once more verified that the viscosity increases with the increment of the water volume fraction, see Fig. 1.21.

It is argued that the spike in viscosity upon hydrate formation is due to three reasons. First, solids are created from the emulsified liquid water droplets. Second, particles aggregate. Third, depletion of the methane from the oil phase to the hydrate phase takes place. On the other hand, it is presumed that the decrease in viscosity after a maximum value is reached due to break down and rearrangement of hydrate aggregates since the interstitial liquid is released what decreases the effective volume fraction of particles and consequently the viscosity. Figure 1.21 shows that the spikes in the viscosity are formed at different times because hydrate formation is a stochastic process. The authors suggested that the erratic viscosity behavior observed at higher water volume fractions is due to jam and slip of large aggregate particles between the cup-and-bob geometry. Perhaps another not mentioned reason for this fact is that this behavior could be related to the destabilization of the emulsion.

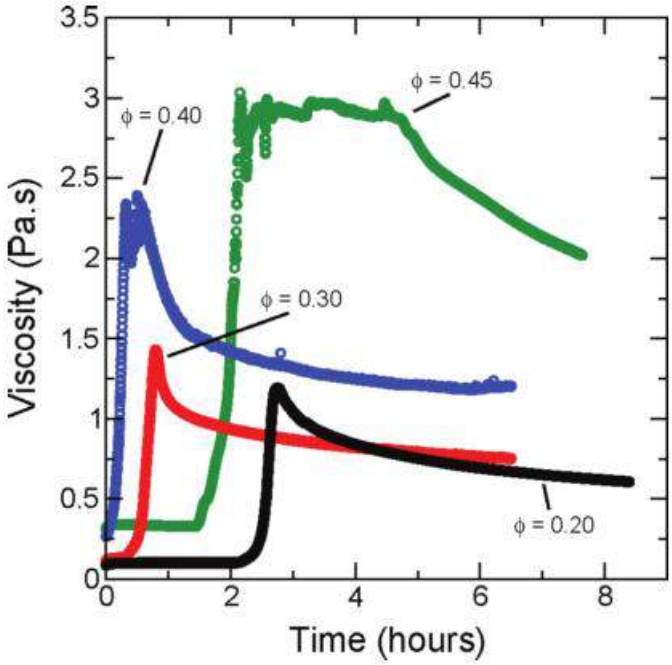

Figure 1.21: Hydrate slurry viscosity as a function of the time for different water volume fractions. Figure taken from Webb et al. (2012b).

Another interesting result obtained in this work is illustrated in Fig. 1.22. The yield stress of the formed hydrate was measured as a function of the time, simulating a shut-in in field conditions. For less than 8 h of annealing the yield stress increases, after this time the yield stress reached a plateau, indicating that the flowline should be fixed as soon as possible. In field applications, the time for attaining the asymptotic value may be less than in the rheometer due to the high heat transfer from the environment. Rheological measurements for hydrate slurries at three different set point temperatures were also studied, as depicted in Fig. 1.23. The relative viscosity is defined as the suspension viscosity divided by the emulsion viscosity. Figure 1.23 shows that the relative viscosity decreases with the increment of temperature. This probably occurs because the driving force for hydrates formation increases as the temperature decreases. It is important to note that, for example at 2 °C, the slurry viscosity seems to remain relatively constant after the initial viscosity peak what suggests a constant aggregate size. In fact, the authors indicate that a possible explanation can be related to the competitive forces between shear forces (break down the aggregates) and cohesion forces (causing the aggregation). Finally, a few experiments using 3.5 wt% NaCl water instead of deionized water were conducted. The results did not show significant differences. For an emulsion with salt water the yield

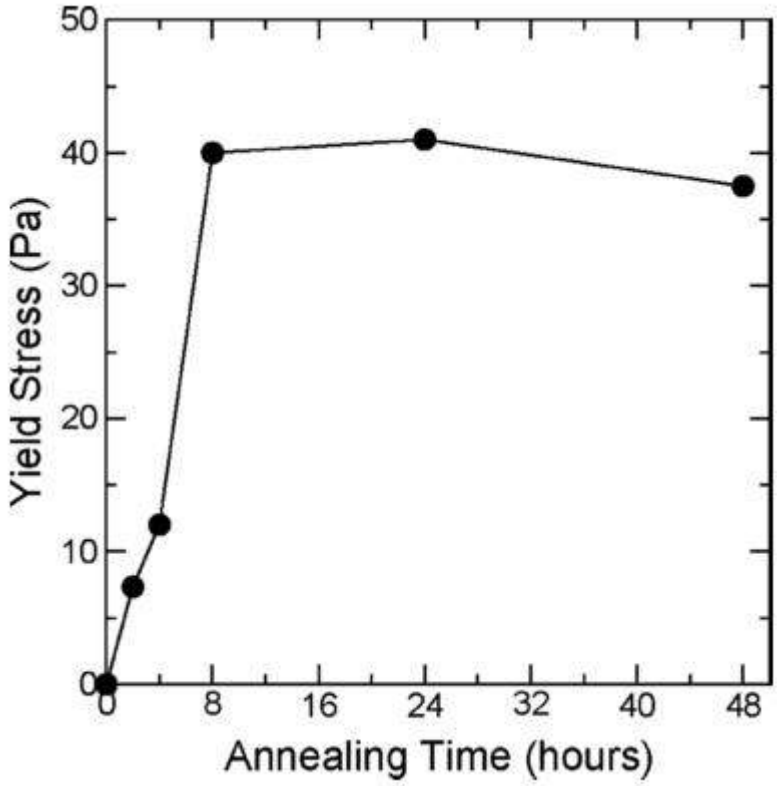

Figure 1.22: Yield stress as a function of the annealing time for a hydrate slurry at 0 °C and 0.4 water volume fraction. Figure taken from Webb et al. (2012b).

stress increases, and for other emulsions at different water volume fraction, the yield stress decreases. This effect needs to be further explored.

1.2.10 CO_2 Studies

Carbon dioxide is a vital gas to live and is characterized to be colorless, odorless, and inert. It is soluble in water and produced in different ways especially during the processes of decay of organic materials. It is known that when CO_2 molecules are trapped by the hydrogen bonds structure I hydrate is formed. Its application in hydrate formation was initially reported as a method for disposal and for sequestration of CO_2 in the deep ocean in order to reduce the atmospheric concentration of this greenhouse gas (Saji et al., 1992). Hydrate formation of natural venting of CO_2-rich fluids was also observed by (Sakai et al., 1990) in the deep ocean. Another important application is in the refrigeration industry since CO_2 hydrates can be used as a secondary refrigerant fluid (Delahaye et al. (2008); Delahaye et al. (2011); Jerbi et al. (2013); Oignet et al. (2017)).

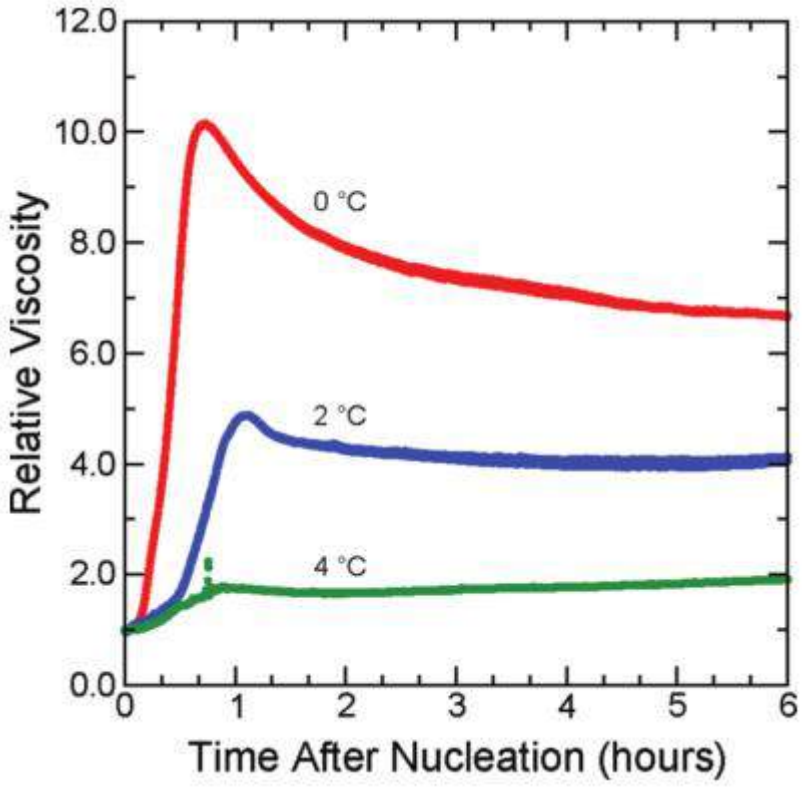

Figure 1.23: Relative viscosity of hydrate slurries at different temperatures. The samples contained 0.3 water content in oil emulsions. Figure taken from Webb et al. (2012b).

Formation of CO_2 hydrate is stable at the conditions of pressure greater than 4 MPa and temperature less than 10 °C (Bozzo et al., 1975), that is, when CO_2 is in a liquid state as shown in the phase diagram Fig. 1.24. In other words, if CO_2 in a liquid state is discharged at that thermodynamic conditions of pressure and temperature within the range of $P > 4$ MPa and $T < 10$ °C, hydrate would form on the surface of the CO_2 droplets (Teng et al., 1995). Shindo et al. (1993) proposed a kinetic mechanism model of CO_2 hydrate formation. The authors assumed that the water dissolves into liquid CO_2 at the interface and reacts to the formed CO_2 hydrates. In this case, the cession of the formation occurs when CO_2 hydrate blocks the mass transfer between water and the liquid CO_2. Also is indicated that the constant reaction rate for formation of the crystals and solubility of liquid increase with the increase of the pressure. The CO_2 hydrate formation occurs instantly and its thickness is very thin. Teng et al. (1995) argued that the assumptions made by Shindo et al. (1993) were challenging because the solubility of CO_2 in water is much larger than that of water in CO_2. Besides that, CO_2 molecules are subjected to weak Van der Wall forces, thus, CO_2 molecules have greater freedom and can migrate into

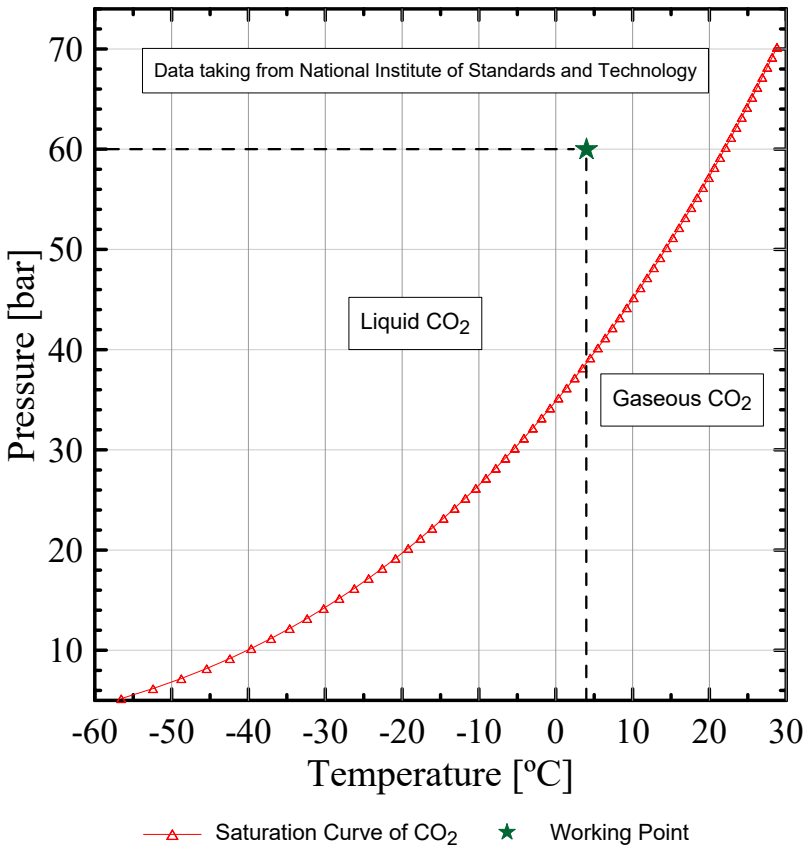

Figure 1.24: Saturation curve of CO_2.

and out of hydrates easier, then it's more likely that CO_2 molecules are guests in hydrate cavities. In that study it was proposed that hydrate clusters (nucleation) form primarily in the water phase; and for CO_2 droplets in high pressure and low water temperature, the concentration of hydrate clusters (crystallization) is highest at the CO_2 water interface, since hydrate crystals first form on the surface of the CO_2 droplet. The authors argued that when hydrate crystals form on the surface of CO_2 droplet, the CO_2 molecules migration is difficulty until it ceases the growth of the hydrate crystal, since molecular diffusion in solids is slower than in liquids. Therefore, only a thin hydrate layer forms on the surface of the CO_2 droplet.

A kinetic model of gas hydrates based on the crystallization theory was proposed by Englezos et al. (1987). Chun and Lee (1996) adopted this model to experimentally analyze the carbon dioxide hydrate formation. The experimental kinetic data of carbon dioxide hydrate formation were obtained from measuring directly the volumetric flow rate of a hydrate-forming gas at several temperatures and pressure conditions. It was observed that the molecules of CO_2 per unit volume of water increase whit the enhance of the

amount of water and it was noted that the CO_2 hydrate formation is not restricted to a thin layer close to the gas-liquid interface but can occur everywhere in the liquid water if supersaturation is achieved as a result of the dissolution process.

Rheological studies of hydrates formed from CO_2 molecules are common in the field of refrigeration since this technology leads to a reduction in the application of classic refrigerants with high global warming potential. In fact, hydrate technology allows cooling the refrigerants by exchanging heat with the help of secondary circuits (Darbouret et al., 2005). Delahaye et al. (2008) used an experimental loop to produce CO_2 hydrate slurry by gaseous CO_2 injection in pre-cooled water. In that study, it was shown how the volume fraction in solid particles influenced the behavior of the material. Indeed, for volume fractions higher than 10% of the fluid, it can be characterized as a Herschel-Bulkley material. However, this behavior can vary with the addition of surfactants as reported by the same research group (Delahaye et al., 2011). The authors reported that CO_2 hydrate slurry in the presence of a specific additive can be represented by a Newtonian model which flows more easily. Nevertheless, according to their results, the apparent viscosity of CO_2 hydrate slurries with the additive is higher than that without additives. Jerbi et al. (2013) also studied the characterization of CO_2 hydrate slurries flowing in a dynamic loop. In that research, it was used a new system (stirred tank + reactor) for the slurry homogenization, which allows obtaining viscosity values lower than that generated in a simple loop for volumes of hydrate fractions less than 20%. The results revealed how the apparent viscosity increases with the solid fraction increase, but decreases with the shear rate increase, that is, the material exhibits shear thinning behavior. The same behavior was observed by Oignet et al. (2017) who studied the CO_2 hydrate slurry in the presence of Sodium Dodecyl Sulfate in a dynamic flow loop. In that research, it was also noted that the use of the additive at concentrations of 1500 and 2000 ppm decreases the agglomeration and reduces the viscosity of the CO_2-hydrate slurry.

1.3 Objectives

The main objective of this research is to analyze the rheology of CO_2 gas hydrates through rheometric geometry in a rotational rheometer. For this purpose, the hydrate will be formed by targeting the same pressure and temperature conditions used in the industry.

Other objectives are described below:

- Evaluate the pressure cell as a rheometric geometry, identifying the range of viscosity and shear rate measurements, as well as the residual friction calibration and rotor stabilization time.
- Investigate several parameters that influence on hydrate formation, such as: variation of initial temperature and pressure, cooling rates, shear rate, sub-cooling, and CO_2 as a guest molecule, among others.
- Analyze the influence of the oil compounds on CO_2 gas hydrates.
- Study the behavior and efficiency of inhibitors in the process of hydrate formation.

Chapter 2

Experimental Procedure

2.1 Equipments

2.1.1 High-pressure system

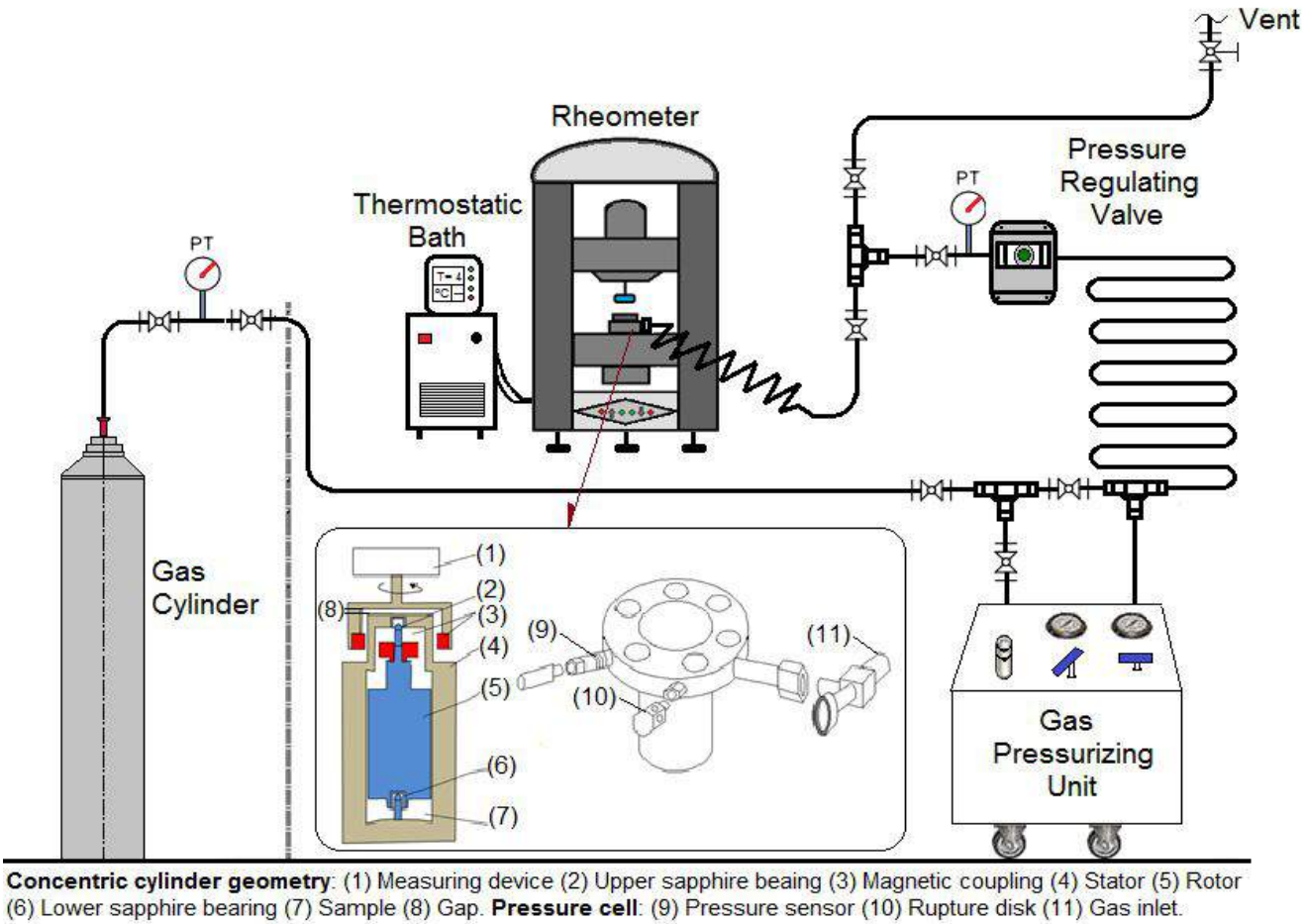

Figure 2.1: High-pressure system employed to conduct the experiments.

As was mentioned in the preview chapter, it is necessary considerably high pressures for hydrate formation. Then, it is required a setup to provide the gas volume and pressure for hydrate analysis in the measured cell. In order to satisfy the conditions mentioned above, it was designed and built a high-pressure system to conduct the experiments, as shown in Fig. 2.1. The system is composed by the gas storage cylinder where pressurized CO_2 or CH_4 is driven until a booster, equipment that allows increasing above 400 bar the initial pressure established in the cylinders. Depending on the experimental pressure applied, the booster is not required. After that, the pressurized gas is conducted to a serpentine pipe configuration to guarantee a constant rate of gas volume in the pressure cell. The maximum volume provides is 300 ml. The experimental pressure is controlled and set up by a regulating valve located at the entrance of the cell. The diameter of stainless steel pipes is of 6.35 mm (1/4 in). Once the experiments are finished, the gas inlet valve of the pressure cell and the regulating valve are closed and the remaining gas in the duct is released through a relief valve.

2.1.2 Rheometer

A shear stress-controlled rheometer Haake Mars II (Thermo Fisher Scientific) is used to perform the experiments. This instrument allows measuring both small and high rotational speeds in the range of $10^{-8} - 4500$ rpm. The device with its main parts is illustrated in Fig. 2.2. The rheometer is connected to a Thermo Haake Phoenix II thermostatic bath, model P1-C50P, also provided by Thermo Scientific, to ensure accurate temperature control during the experiments. The thermostatic bath attains temperatures from -20 to 150 °C, with a maximum cooling rate of 0.6 °C/min and ± 0.2 °C temperature precision. The process of heating/cooling is realized through the heat change between the measuring cup of the pressure cell and the jacket located at the base of the rheometer. The jacket is supplied with a conductive fluid that is a mixture of water and ethylene glycol. The rheometer rotor is driven by a compressed air, which is provided by an oil-free dental compressor CHIAPERINI, model MC 6 BPV RV 60L. After the compressor, the air passes through a Bel Air adsorption filtering and drying system. All experiments are automatically controlled by a computer and the results are extracted with the RheoWin HAAKE program.

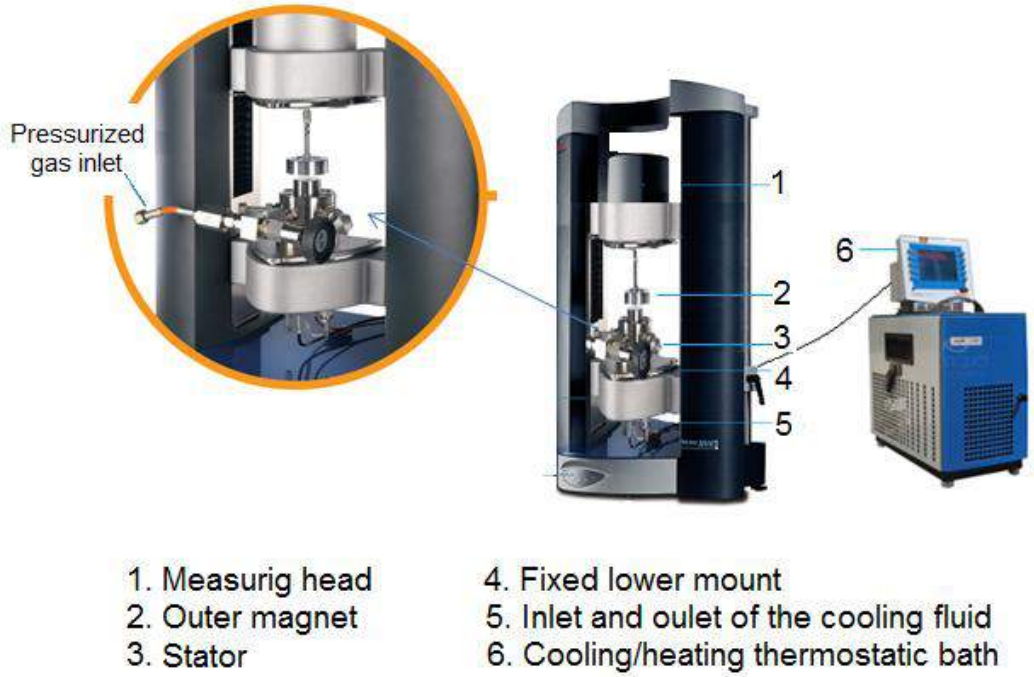

Figure 2.2: Pressure cell, rheometer and thermostatic bath used to do the experiments. Figure taken from the manual of the rheometer of Thermo Scientific (adapted).

2.1.3 Pressure Cell

A pressure cell D400/300 was designed (also by Thermo Scientific) especially to use in conjunction with the Haake rheometer. The device comprises a rotor (measuring geometry) and the stator (cup). The stator consists of a measuring cup with three connections: the rupture disc with 440 bar limit at 300 °C, the attachment for a pressure sensor, and the inlet valve, as shown in Fig. 2.1. The stator is covered with a cap with 6 screws with a clamping torque of 70 Nm permitting a maximum operating pressure for the cell of 400 bar. The rotor that is used in this research is a concentric cylinder which fits into the cup forming a cup-and-bob assembly. Two sapphire bearings located at the bottom and at the cap of the stator are utilized to support and guide the rotor into the stator, see Fig. 2.3. The torque acting on the rotor is transmitted from the drive of the rheometer by means of a magnetic clutch. The magnetic field is generated by two magnets, indicated in red in Fig. 2.3. The inner magnet that is located at the top of the measuring geometry and the outer magnet that is attached to the shaft of the rheometer measuring head. It is important to note, that the torque applied by the rheometer measuring head is not directly transmitted to the rotor, as explained, it is conveyed with a non-contact,

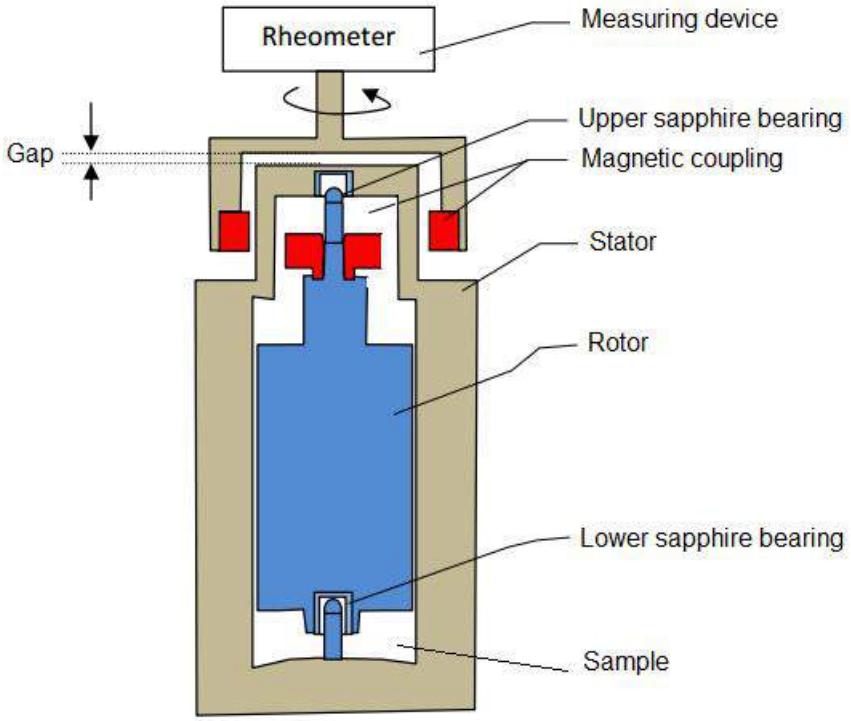

Figure 2.3: Components of the pressure cell. The four pole magnets are highlighted in red. Figure taken from the manual of the pressure cell of Thermo Scientific (adapted).

concentric, magnetic coupling. Therefore, it is necessary to support the rotor in the sapphire bearings. Unfortunately, these mechanical elements have some friction between the connected parts making the rheometer motor to apply an additional torque which is not applied to the sample. Thus the additional torque needs to be corrected, especially when measuring low viscous samples. The torque correction is computed after several tests that are explained below.

2.2 Test to calibrate the pressure cell

The first step to calibrate de geometry and pressure cell used in the experiments is to determine the optimal gap between the outer magnet and the cover of the stator. Then, the torque is analyzed as a function of the angular velocity for standard Newtonian fluids as well as for a stable water-in-oil emulsion of 30%, a water volume fraction typically used in the hydrate formation tests in this study. The results are shown in Fig. 2.4 for a concentric cylinders geometry. As it can be observed, the measured points for the soybean oil (Newtonian fluid) are very similar for the different gaps studied. The same occurs for

the emulsion. The torque obtained for the emulsion is higher than the other oils due to its high viscosity, measured at 4 °C, the temperature at which hydrates are formed. An intermediary gap of 2.9 mm was selected to realize the experiments since this gap helps to levitate the rotor between the sapphire bearings. If the gap is greater than 5 mm, the magnetic field is weakened and the outer magnet does not manage to drive the rotor. On the other hand, if the gap is very small, there can be some interference among the pieces, caused by condensed water droplets, for example.

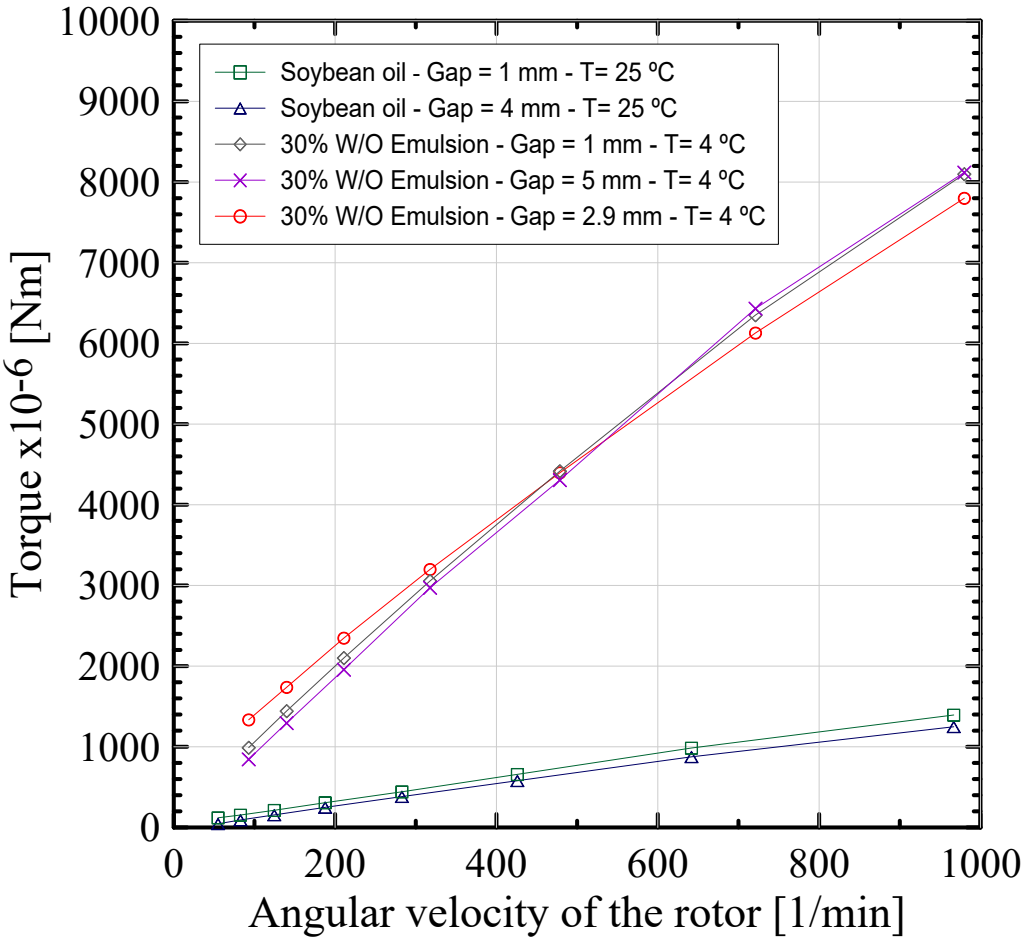

Figure 2.4: Influence of the gap in the measurement torque.

Once the optimal gap is determined by means of the previous test, see Fig. 2.4, the same curve is used to compute the friction correction parameters. This is realized using a linear curve fit model in the Rheowin data program. From the fitting model are obtained three parameters which must be manually filled in the geometry dialog box. By means of these parameters, the program discounts from the originally measured torque the value of the friction fraction between the sapphire bearings and the rotor.

This calibration is carefully performed following the instruction manual of the pressure cell given by the provider company. In the present research, the calibration is realized frequently for each material studied at the test temperature. Figure 2.5 shows the viscosity function measured in the rheometer for the soybean oil with and without friction factor calibration and compared with a referential value obtained in a Cannon-Fenske viscometer. We can notice that the results obtained when the friction factor correction is applied are closer to the values measured by the Cannon-Fenske viscometer, what justifies the importance of the calibration. Another important result is to analyze the time required

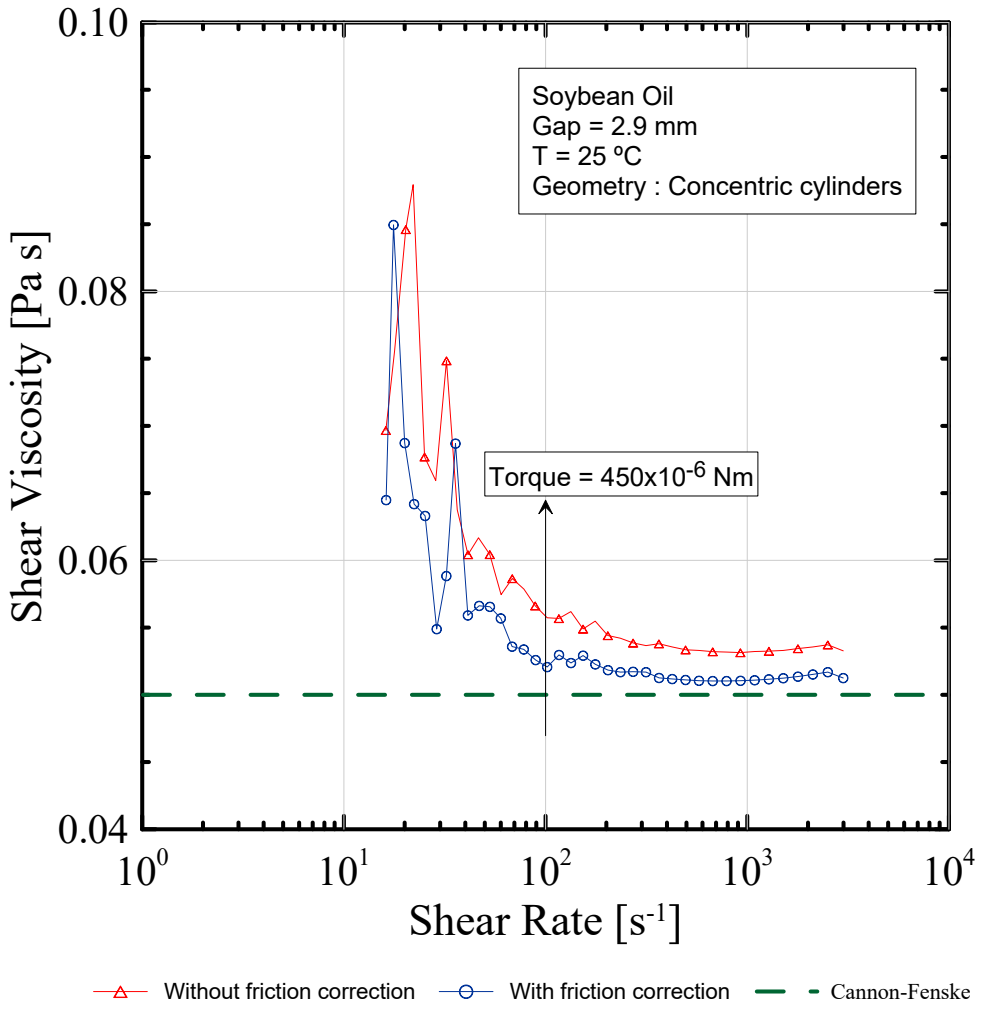

Figure 2.5: Comparison between viscosity values of soybean oil obtained in the rheometer with and without friction correction and with Cannon-Fenske viscometer.

for the rotor to overcome the inertial forces when an experiment is going to start. Then, experiments with the three levels of shear rate most used during the present investigation were performed with the same emulsion of 30% as represented in Fig. 2.6. As shown in Fig.

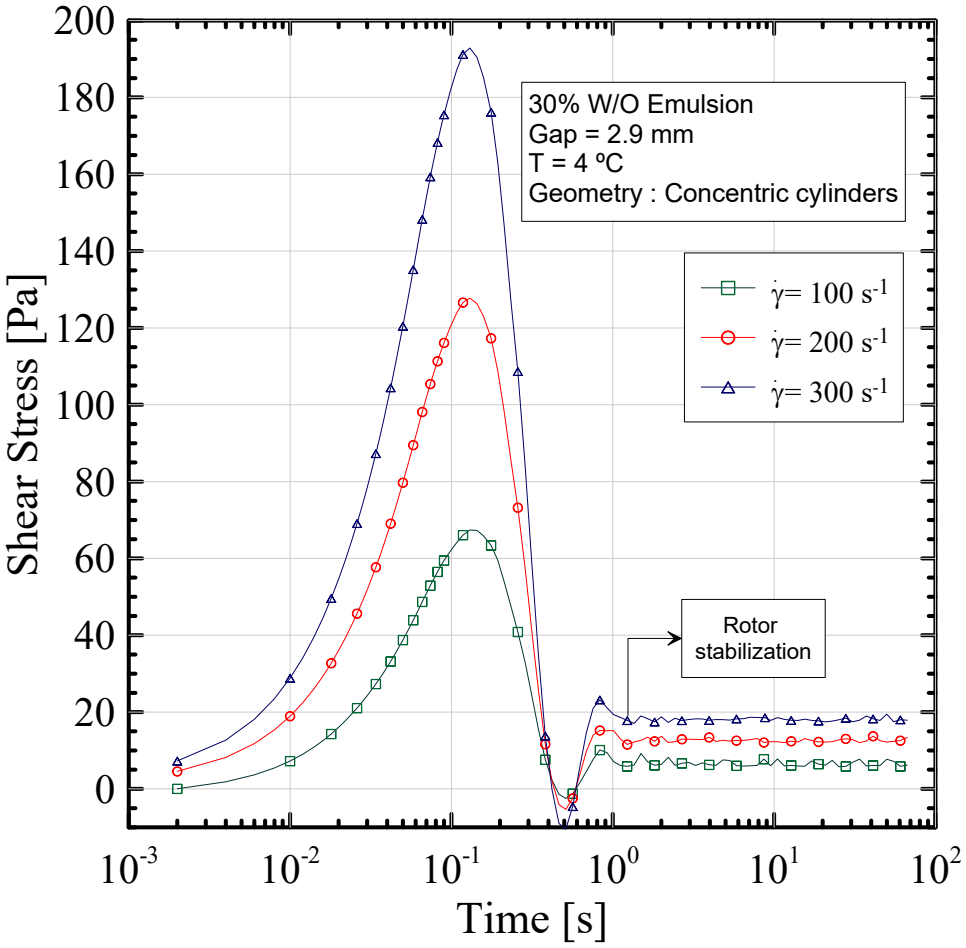

Figure 2.6: Rotor stabilization time.

2.6, after three seconds approximately the shear stress values achieved the steady state. The spike obtained for the shear rate of 300 1/s is the highest because the applied torque is also the highest one needed to overcome the same inertial forces. The results obtained before the first 3 seconds of the experiment had to be omitted since the stabilization of the rotor was taking place.

Finally, two experiments were conducted in different geometries in order to assess the range and reliability of the pressure cell measurements. Then, it was made a test with the plate-plate geometry and another with the concentric cylinders geometry in the cell (without pressure) with different samples of the same dry oil. At the beginning of the experiments, the samples were subjected to a temperature of 50 °C for 20 minutes to delete the temperature and shear histories of the oil. After this time, the temperature was reduced at a constant cooling rate of 0.6 °C/min until 4 °C, the test temperature. The experiment is performed by controlling the shear stress with the aim of capturing

the yield stress of the paraffinic oil. The results are presented in a flow curve as shown in Fig. 2.7, which shows the good agreement of the results for shear rates higher than 1 s^{-1}. Therefore, the value of the yield stress in this specific experiment was difficult to measure with accuracy (data not shown) in the pressure cell. These values are outside of the measuring range of the cell. However, when the hydrate has formed the values of the shear stress increases considerably due to the agglomeration of the hydrate particles. This fact could enable the measurements of these values by the pressure cell with the type of geometry employed.

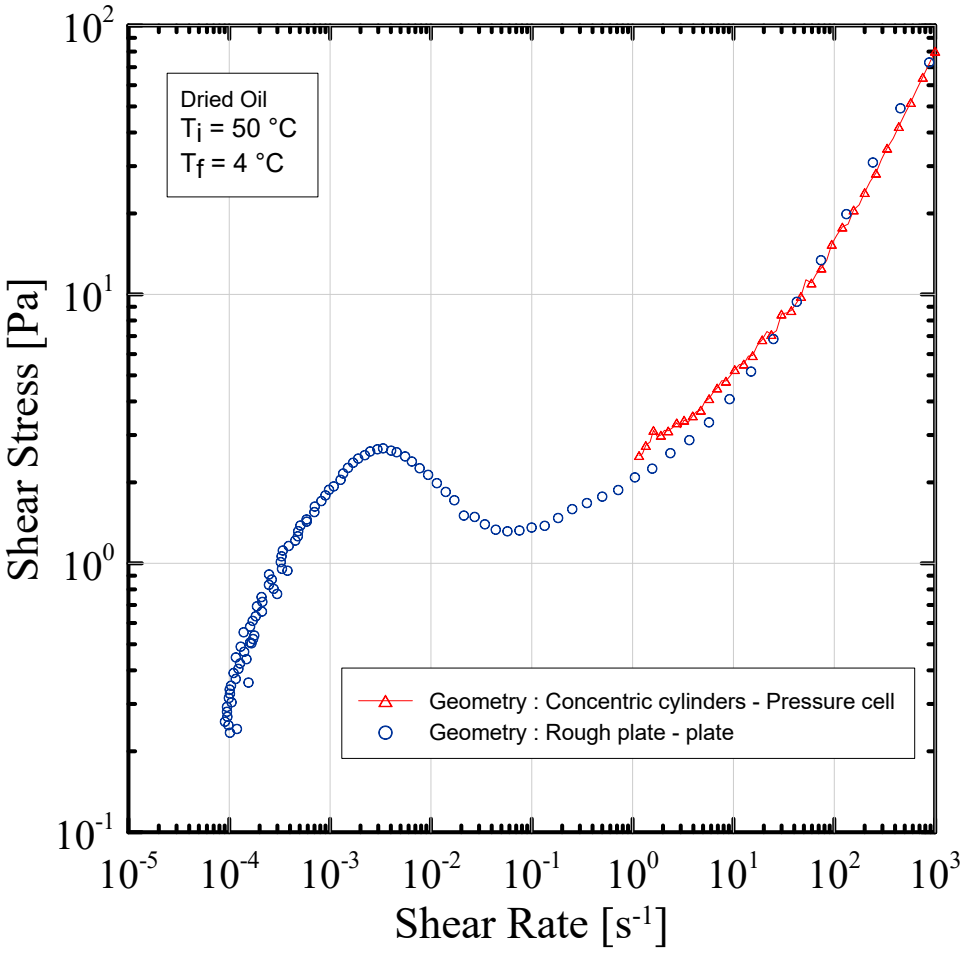

Figure 2.7: Comparison between two different geometries.

2.3 Procedure

Our waxy crude oil extracted from the pre-salt well was provided by the Brazilian Oil Company Petrobras, with 58.10 wt% of saturates, 19.83 wt% of aromatics, 21.43 wt%

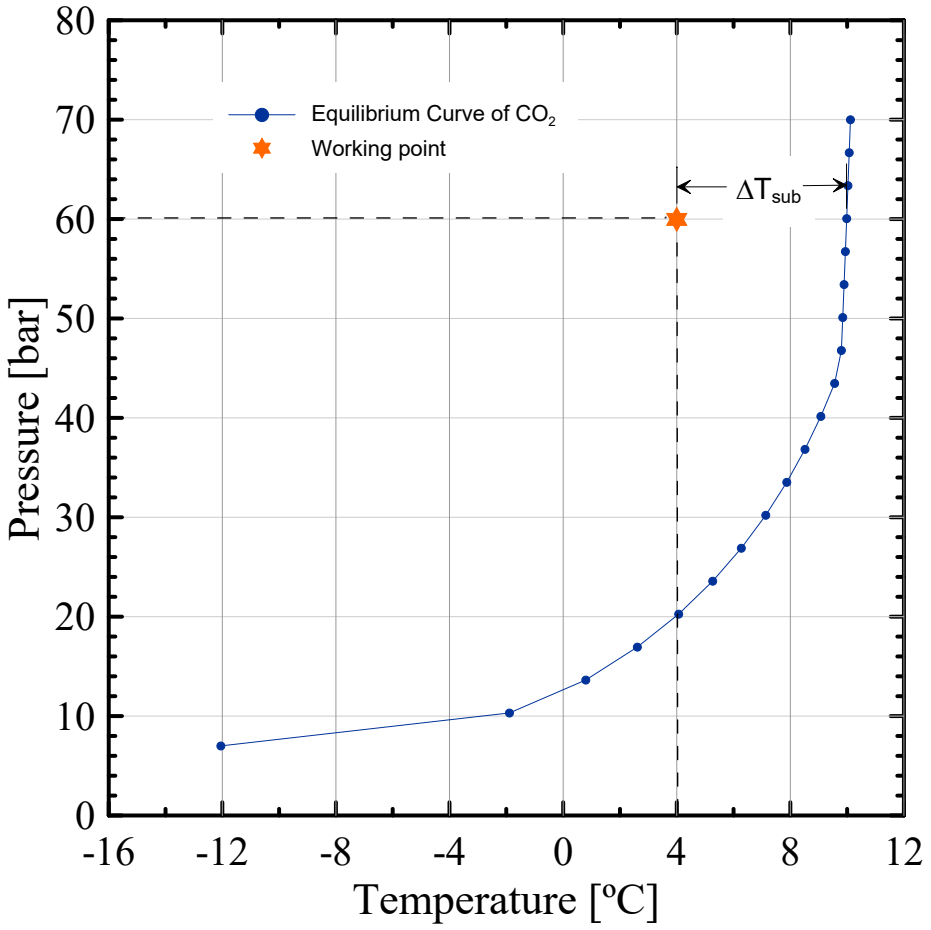

Figure 2.8: CO_2 equilibrium curve with the supercooling grade of the experiments.

of resins and 0.64 wt% of asphaltenes (for more detailed of its chemical analysis see Table 3.1 in the results section). Initially, with 10% of water, it was dehydrated by the gravitational method of the volumetric flask. The residual water content was then measured by Karl Fischer titration technique indicating a volume of 0.3%. This dry oil is used as a reference for all our experiments. The amount of sample used for each test is 53 ml, which is deposited between the rotor and the inner wall of the pressure cell. The emulsions were prepared rigorously following the procedure described next. Initially, the oil and the deionized water were heated at 80 °C in closed bottles for 1h. Next, the desired volume of deionized water is added to the cooled crude oil sample while mixing at 10000 rpm for 3 min in a CAT X360 homogenizer. The emulsions stabilization was measured through gravitational action. Phase separation was not observed in at least two months, except to the 40% water-in-oil emulsion, which remained stable only for two weeks. Before depositing the prepared sample in the geometry of the pressure cell, it was stirred again manually for 3 minutes. The emulsion was pressurized with CO_2

using the high-pressure system explained above. In an attempt to fully saturate the oil phase with CO_2, the pressure cell was heated up to 80 °C. This temperature was retained for 8 h, keeping the rotor of the pressure cell at a constant angular velocity. Next, the pressure cell was cooled until 4 °C, the working temperature. The great majority of the tests was conducted at a constant temperature, pressure, and rotor angular velocity. Specifically, the pressure and temperature were, respectively, fixed at 60 bar and 4 °C. Such a work point is marked in the equilibrium curve in Fig. 2.8 (orange star), from where is possible to deduce the supercooling, $\Delta T_{sub} = 6$ °C. It is important to note that CO_2 is in the liquid state, according to its phase diagram (marked by the green star in Fig. 1.24). This thermodynamic condition corresponds to the condition commonly found in real applications.

Chapter 3

Results and discussion

This chapter is divided in two main sections. The first shows the results obtained to characterize rheologically CO_2 gas hydrates. In the second section, we display several results with the objective of assessing the effect caused by the oil compounds on gas hydrates formation. Moreover, we studied the effect of the addition of the small amounts of asphaltene powders on the hydrate kinetic. To obtain confidence (trueness) in our experiments, the equipments used during the tests like: pressure cell, thermostatic bath, pressure transducer, rheometer, and others were calibrated and validated whit frequency. Also, repeatability tests were made whit different samples and in different days.

3.1 Rheology of hydrates

3.1.1 Viscosity profile of the CO_2 hydrates

Figure 3.1 shows two typical tests where the viscosity of an emulsion with water volume fraction of 30% is displayed over time at a shear rate fixed in 200 s^{-1}. In both tests, the evolution of viscosity over time is very similar (green balls and blues triangles), which suggests a high grade of repeatability. Two different solubilization temperatures were used for each test. The emulsion related to the test, represented by the green balls, was heated up to 40 ^{o}C and the other one was heated up to 80 ^{o}C. Since the results were quite similar, is concluded that heating up to 40 ^{o}C was sufficient to fully saturate the CO_2 but, to be sure of the complete gas solubilization, it was used 80 ^{o}C as highest temperature. The period of solubilization was at least 8 h, when the values of viscosity were below 0.01 Pa.s and rather dispersed, because the torque required to keep the shear rate at 200 s^{-1} at

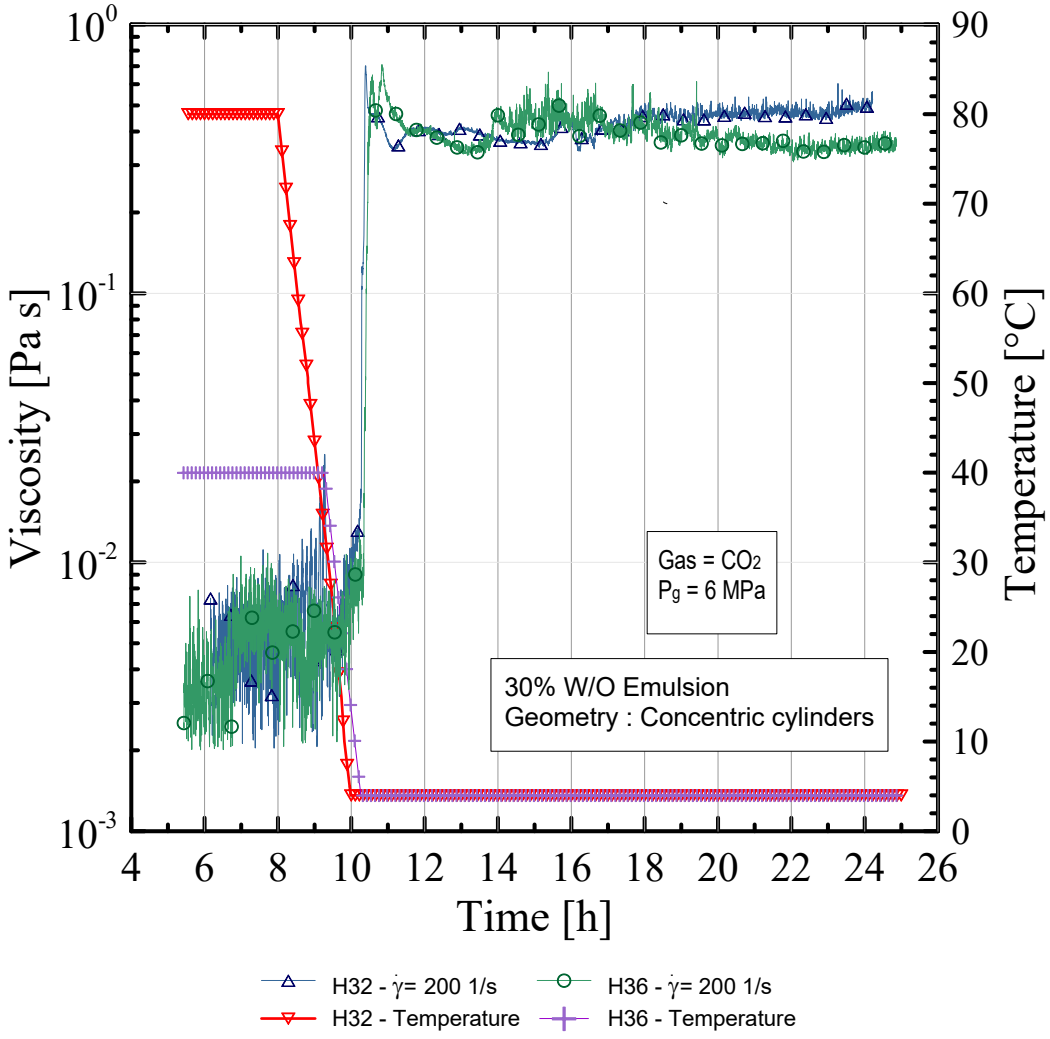

Figure 3.1: Two curves of viscosity (green and blue symbols) over time for an emulsion with 30% of water. Each curve corresponds to a single solubilization temperature (red and purple symbols).

this level of viscosity is close to the lower accuracy limit of our equipment. The viscosity does not change during the cooling process until it reaches the equilibrium temperature, where it increases a little, but it jumps very fast when the temperature reaches 4 ^{o}C, after 10 hours of the test. The exact time of jumping is clearly seen in Fig. 3.2. It was around 20 min past 10 h in both tests. The viscosity changed by almost two orders, from below 0.01 to close to 0.5 Pa.s. The viscosity jump clearly marks the time of CO_2 hydrate formation. The spike in viscosity is due to the aggregation of hydrate crystals, forming a strong structure which is kept by the reconstruction forces.

Experiments with closed valve also show the gas consumption, which is represented by the decrease of the pressure in the cell, also indicating hydrate formation. This result is depicted in Fig. 3.13. It is not possible to observe the hydrate formation by the temperature increment, as reported by Sloan Jr and Koh (2008), because, as described previously, the temperature is measured in the jacket located at the base of the rheometer, instead of in the fluid, and the jacket temperature remains constant by the thermostatic bath.

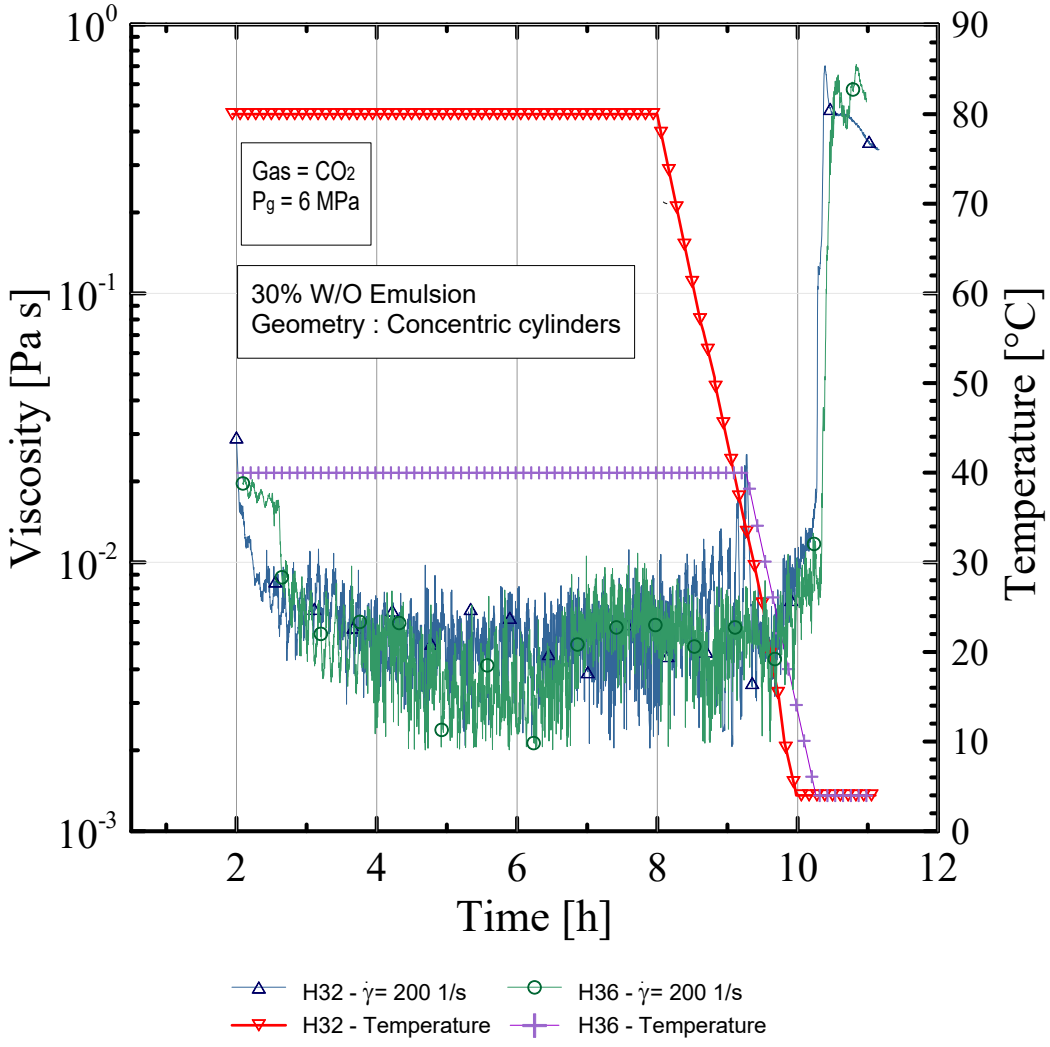

Figure 3.2: Two curves of viscosity (green and blue symbols) over time for an emulsion with 30% of water (close attention on the induction time). Each curve corresponds to a single solubilization temperature (red and purple symbols).

3.1.2 Effect of water volume fraction in CO_2 hydrates

In the next three figures (Fig. 3.3, Fig. 3.4 and Fig. 3.5) is displayed the analysis of water fraction in the emulsion. The tests were carried out at a constant shear rate ($\dot{\gamma} = 200s^{-1}$) for four different water fractions, emulsions with 10%, 20%, 30% and 40% of water in oil. Figure 3.3 shows the beginning of the test when the gas is fully solubilized at constant pressure and temperature for 8 h. The temperature is read on the right side of the figure

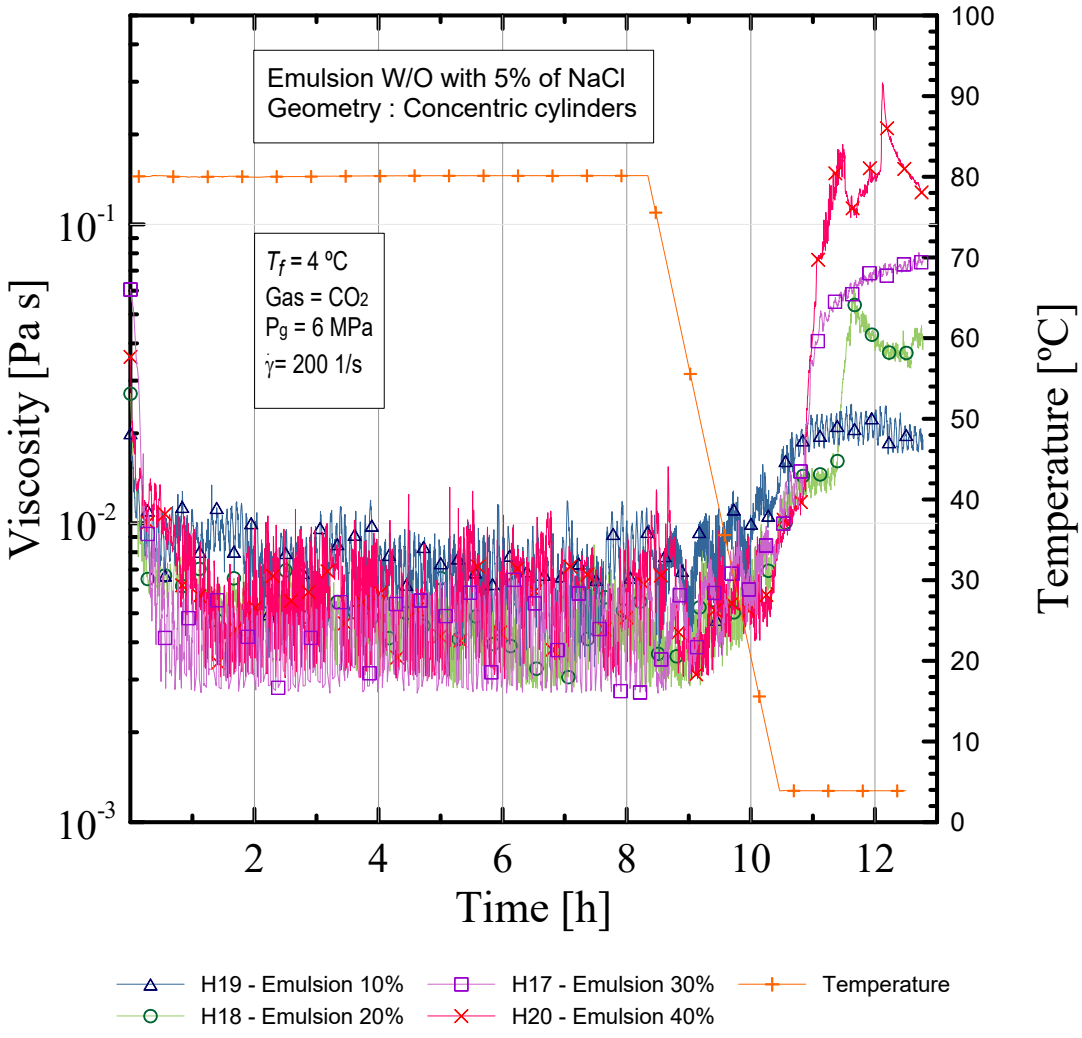

Figure 3.3: Viscosity over time for different water fractions at a fixed shear rate: a close on the gas diffusion.

by the orange crosses. In such temperature, over the period of solubilization, the measured viscosity of all emulsions was below 0.01 Pa.s. The cooling started after 8 h and two hours later the temperature was around 20 ^{o}C, but the viscosity was yet below 0.01 Pa.s. The test temperature of 4 ^{o}C was reached in 10 h and 20 min and, less than 30 min later, the

viscosity jumped in the emulsions of 30% and 40%. For the emulsion of 20%, the jump took more time, around 30 min. It occurred close to 11 h after the test beginning. It seems that the hydrate was not formed in the emulsion with 10% of water in oil and the increasing viscosity was only related to the decrease in temperature.

The induction time is clearly seen in Fig. 3.4, where is showed only the data for the period between 10 and 16 h. The jump of viscosity for the emulsion with 20% of water in oil is shifted to the right, i.e., the induction time is higher for this emulsion. The induction time does not follow a pattern, but this behavior should be expected since hydrates formation is a stochastic event. Webb et al. (2012b) also observed a similar tendency for their water-in-oil emulsions.

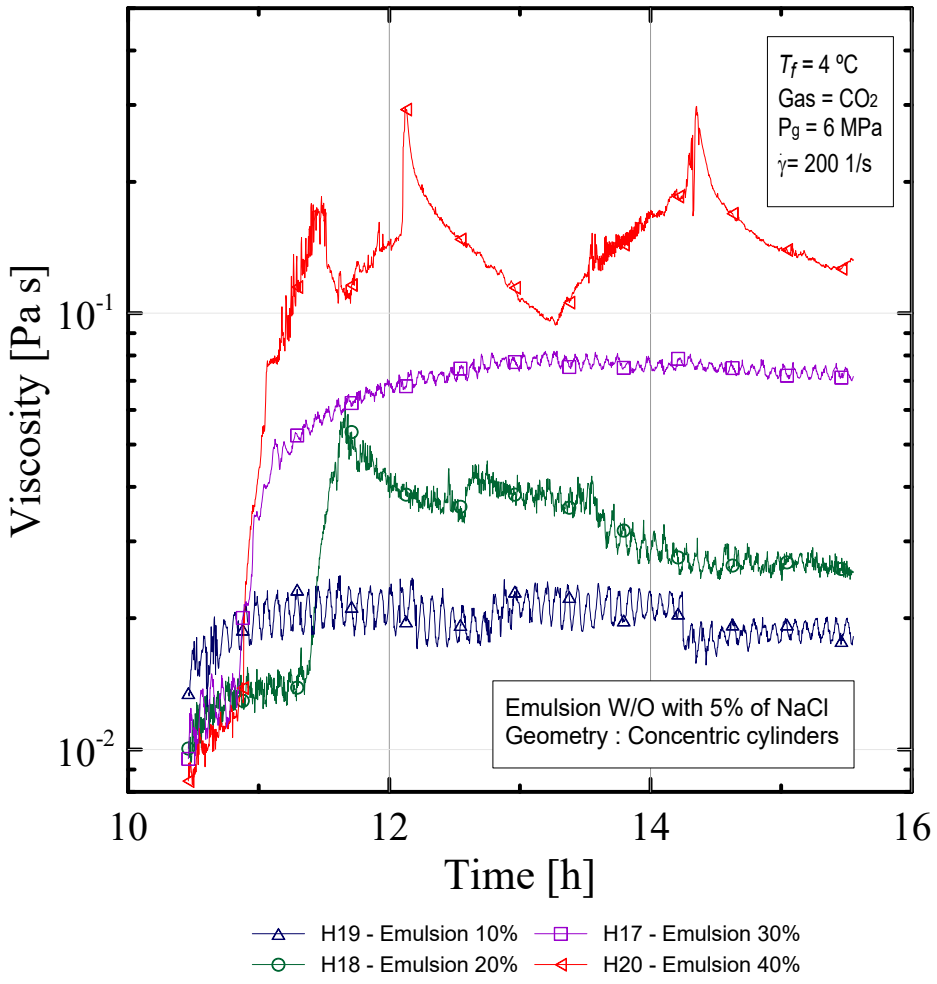

Figure 3.4: Viscosity over time for different water fractions at a fixed shear rate: a close on the induction time.

The complete test is shown in Fig. 3.5. After a time long enough, the viscosity reaches a

steady state, when the shear forces are in equilibrium with hydrate reconstruction forces. Such a balance between these forces is typical of thixotropic materials. It will be discussed a little later. It is believed that the formation of hydrates increases with the water volume fraction because more CO_2 can be captured by the hydrogen bonds. Consequently, the viscosity increment is due to more aggregation between the hydrate particles. Webb (2014) suggested that the viscosity also increases due to the capillary bridges formed by the water between hydrate particles.

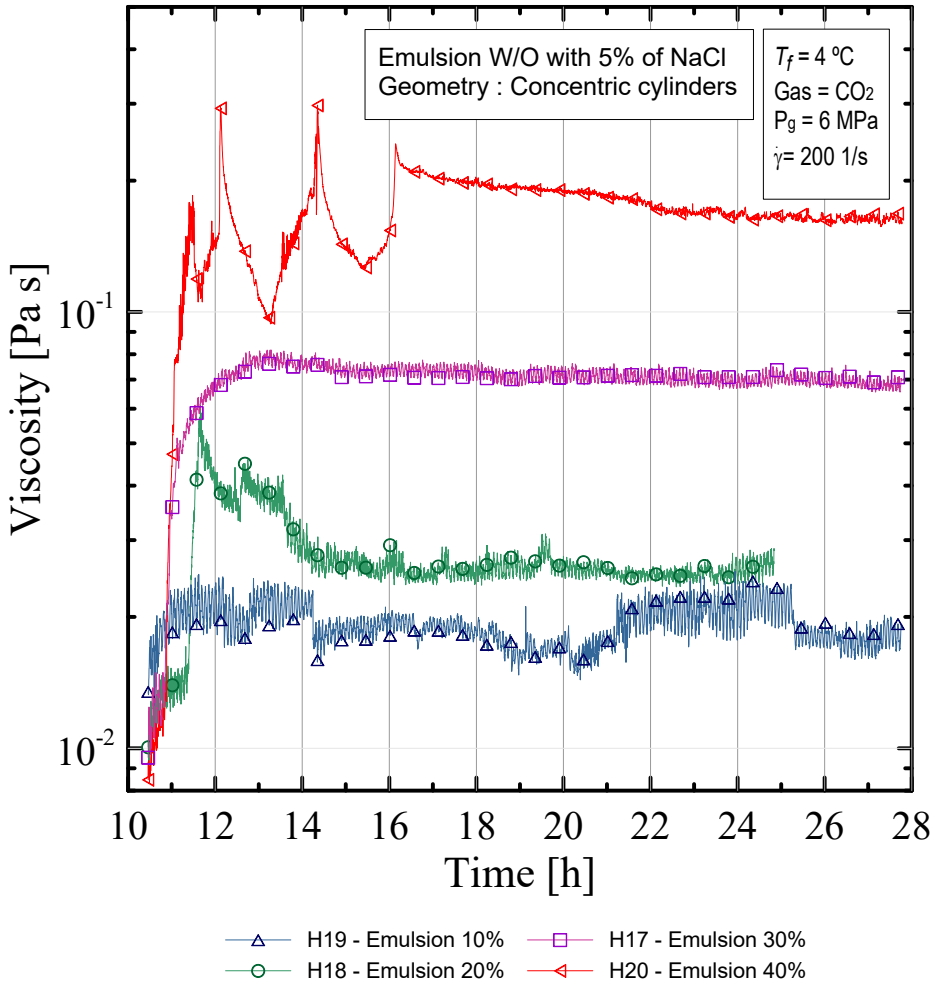

Figure 3.5: Viscosity over time for different water fractions at a fixed shear rate: the complete test.

It is also important to note the instabilities at the initial stage after the hydrate induction for the emulsion of 40% of water in oil. It seems that such instabilities are an increasing function of water fraction. In fact, the emulsions with water fractions above 30% were unstable, which means that the mean drop diameter was above the upper limit in which

an emulsion is stable at rest. Most of the tests were carried out with a water fraction below 30% of water in oil.

These viscosity instabilities, shown for the emulsion of 40% of water in oil after the hydrate formation, were also noted by Webb et al. (2012b). They suggested that this behavior is caused by the size of the aggregates, which jam and slip between the concentric cylinders gap. But if this happens, it should be likely that the viscosity values measured during that slip should be almost zero.

3.1.3 Effect of shear rate on induction time

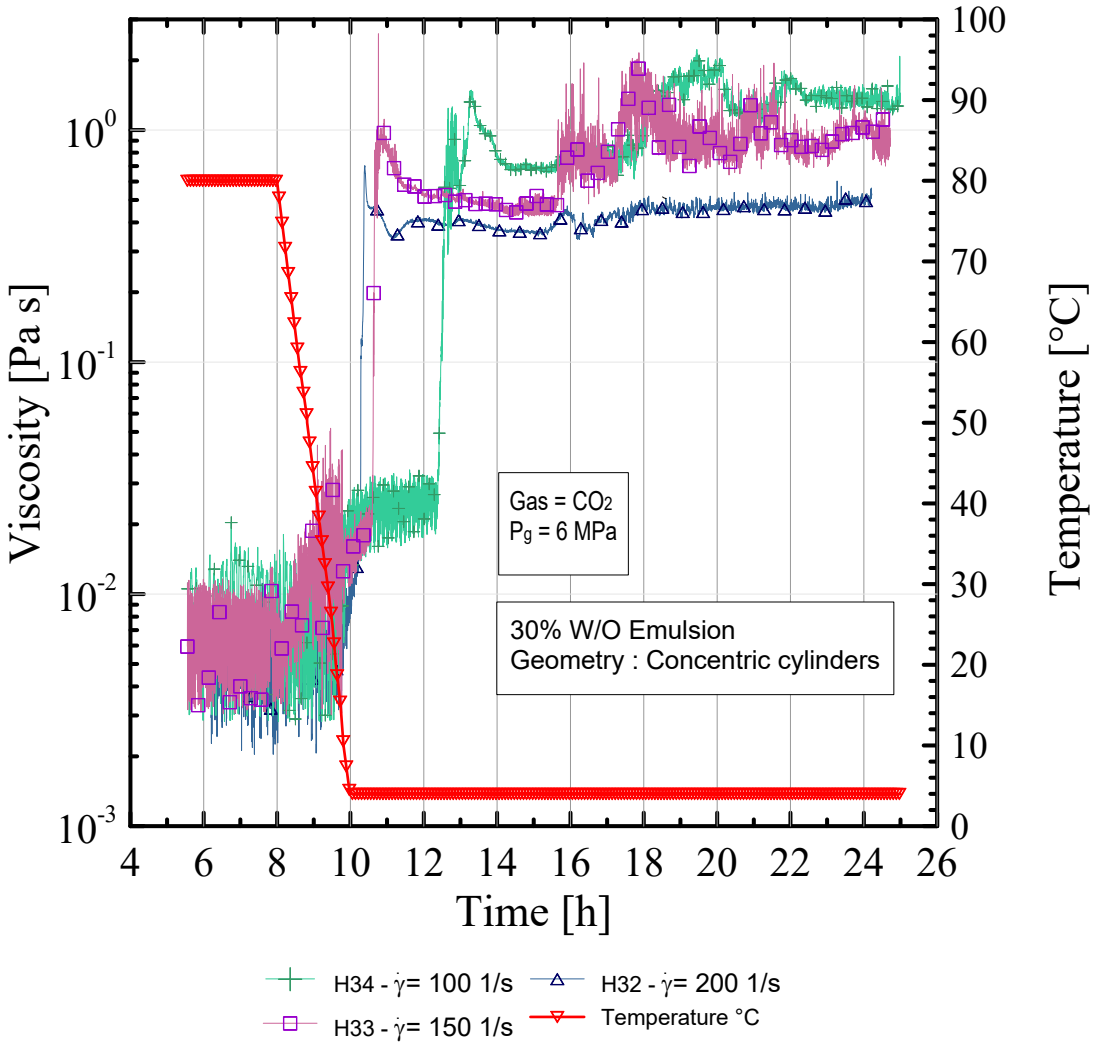

Figure 3.6: Viscosity over time for different shear rates at a fixed water fraction: the complete test.

In the next two figures is shown the effect of shear rate on induction time. Figure 3.7

clearly shows that the induction time increases with a decreasing shear rate.

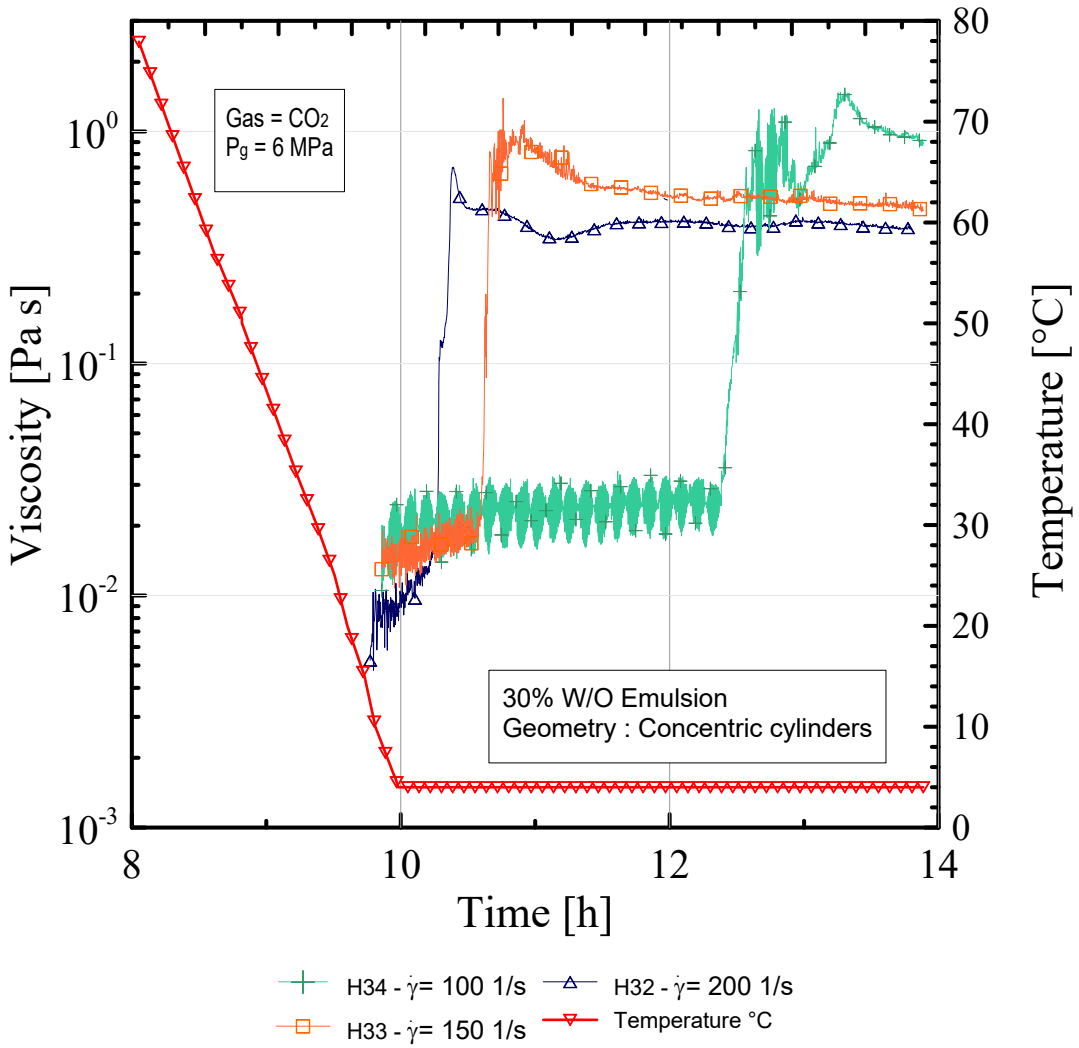

Figure 3.7: Viscosity over time for different shear rates at a fixed water fraction, with a close up on the induction time.

For $\dot{\gamma} = 200$ s^{-1} the jump of viscosity is very fast, just 20 minutes after 4 °C is reached (blue triangles), but it takes more than two hours to occur when the shear rate is 100 s^{-1} (green crosses). Such an effect was expected since the contact area between the two fluids (water and liquid CO_2 droplets) increases with the shear rate. Hence, gas-hydration is facilitated by a higher shear rate. After hydrate formation, the viscosity is also influenced by the shear rate. Perhaps, the high shear rates cause the hydrate aggregation to break up.

The complete tests are shown in Fig. 3.6. It is noted that the viscosity reaches an asymptotic value after 22 h of the test. The asymptotic viscosity η_∞ falls with $\dot{\gamma}$, which shows

that the gas hydrates in crude oil have a shear-thinning behavior. In fact, some tests were carried out for a longer period of time, to certify that the level of viscosity was really asymptotic, as in the case displayed in Fig. 3.8, which shows a test of 72 h for $\dot{\gamma} = 150$ s^{-1}.

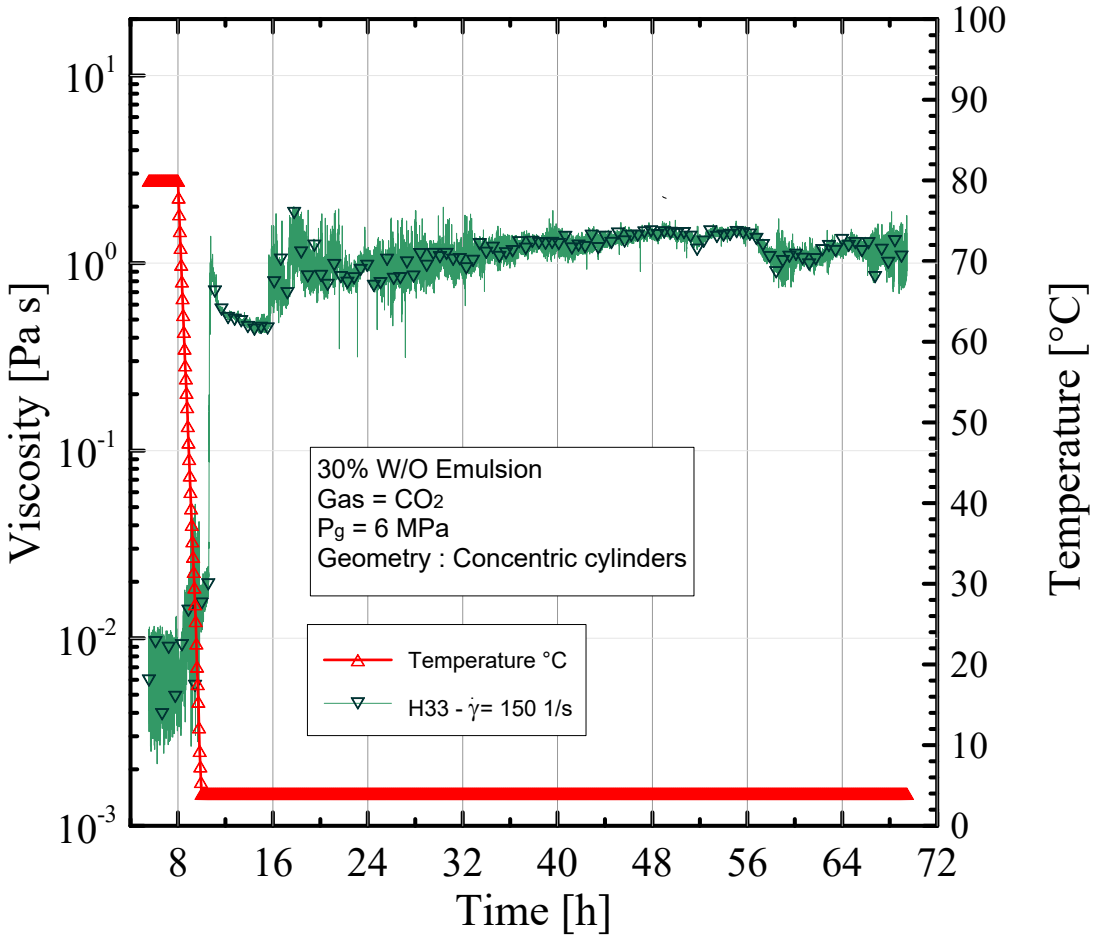

Figure 3.8: Viscosity over time for different shear rates at a fixed water fraction: three-day test.

3.1.4 Salt effect on CO_2 hydrates slurries

Figure 3.9 depicts a quite practical result, which shows how the presence of salt prevents the hydrate formation. In this case, was used emulsions with two water fractions and the tests were carried out with the shear rate fixed at 200 s^{-1}. For the solutions with 30% of water in oil (purple squares and green crosses), η_∞ changed from 0.07 Pa.s, in the emulsion with 5% of salt (purple squares), to 0.4 Pa.s, in the absence of it (green crosses). The asymptotic viscosity increased almost 6 times. Such an increase was even

more pronounced in the emulsions with 20% of water (brown circles and blue triangles), in which η_∞ raised from 0.025 Pa.s (emulsion with salt) to 0.25 Pa.s (emulsion without salt), an order of magnitude. Hence, it seems that salt is a very effective hydrate inhibitor. The induction time was also sensible to the presence of salt. 5% of salt delayed the hydrate formation in around 1 h for the emulsion with 20% of water. However, the delay was larger in the absence of salt in the emulsion with 30% of water. For this emulsion is observed two jumps of viscosity. The first one occurred almost at the same time that in the salty emulsion, but the second was around 2 h later. The effect of salt on the induction time deserves more study, but it seems, from a general point of view, that the salt delays the beginning of hydrate formation, because it reduces the driving forces for hydrate formation.

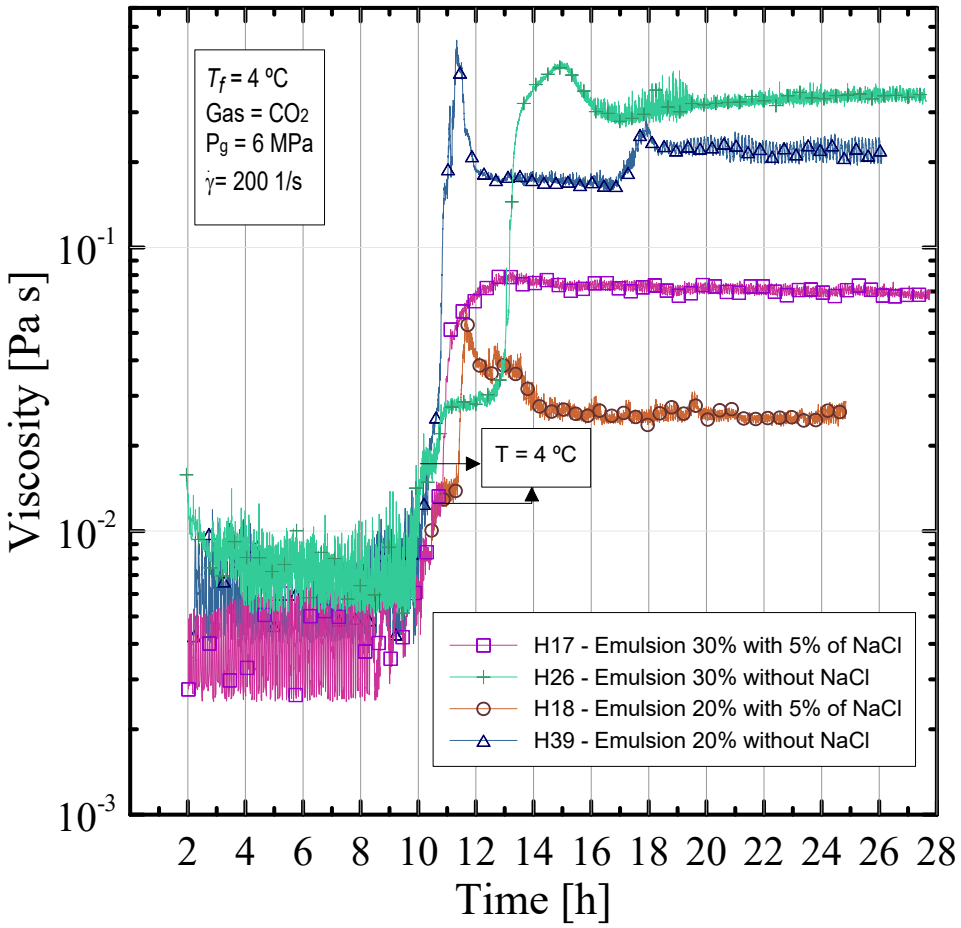

Figure 3.9: Viscosity over time for emulsions with 30% of water. The tests were conducted in an attempt to take into account the effect of salt.

Was also tried to compare emulsions with larger water fractions, with and without salt.

Figure 3.10 was an attempt to measure η_∞ for an emulsion with 40% of water in oil, but the jump of viscosity was too high and our rheometer was blocked up. When this happens, a block of hydrate (as illustrated in Fig. 3.10) forms in the lower and upper space between the cup-and-bob geometry. The viscosity reached around 3 Pa.s, a value more than 15 times the one measured with 5% of salt (see the red triangles in Fig. 3.5). The data measured after hydrate formation were discarded since the hydrate that was formed blocked the rotor movement and the external magnet kept rotating alone.

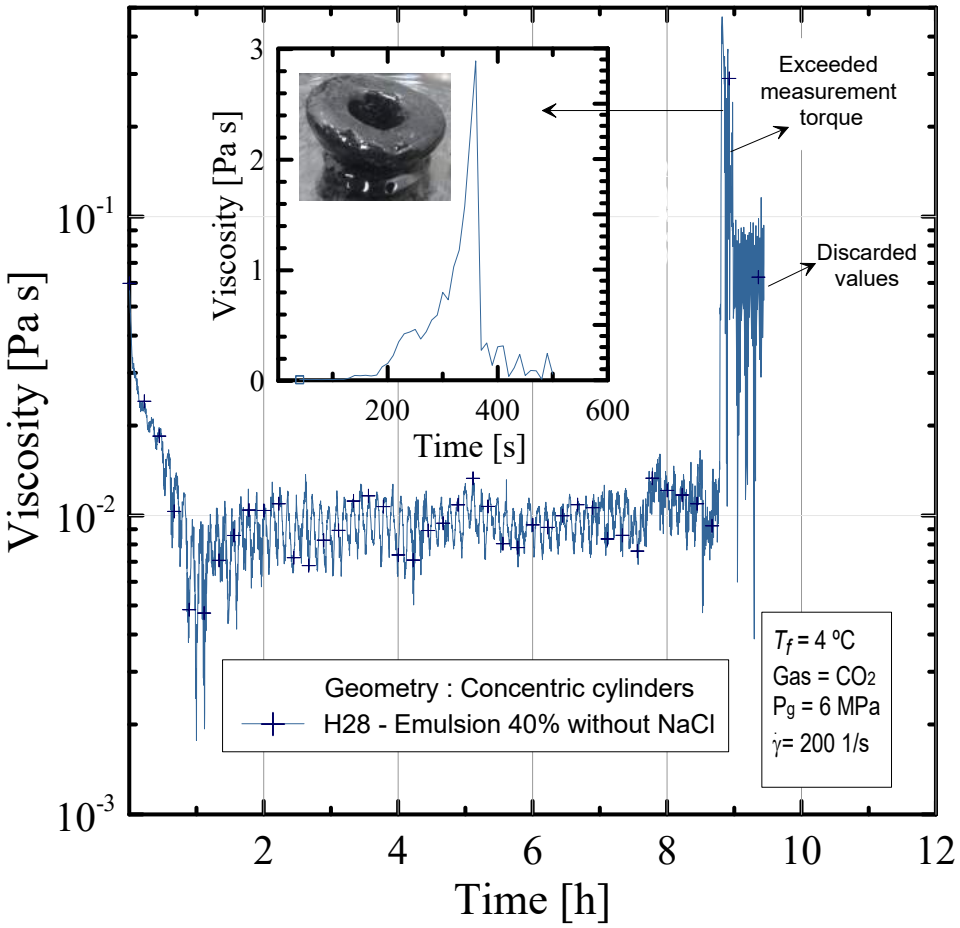

Figure 3.10: Viscosity over time for 40% water fraction emulsion with the absence of salt. The necessary torque to keep the shear rate fixed is above the upper limit of the equipment: the rotor was blocked.

3.1.5 Thixotropic behavior of CO_2 hydrates

The data are shown in Fig. 3.11 is an attempt to see the ability of reconstruction of CO_2 hydrates in crude oils. The tests were conducted for two water fractions with the shear

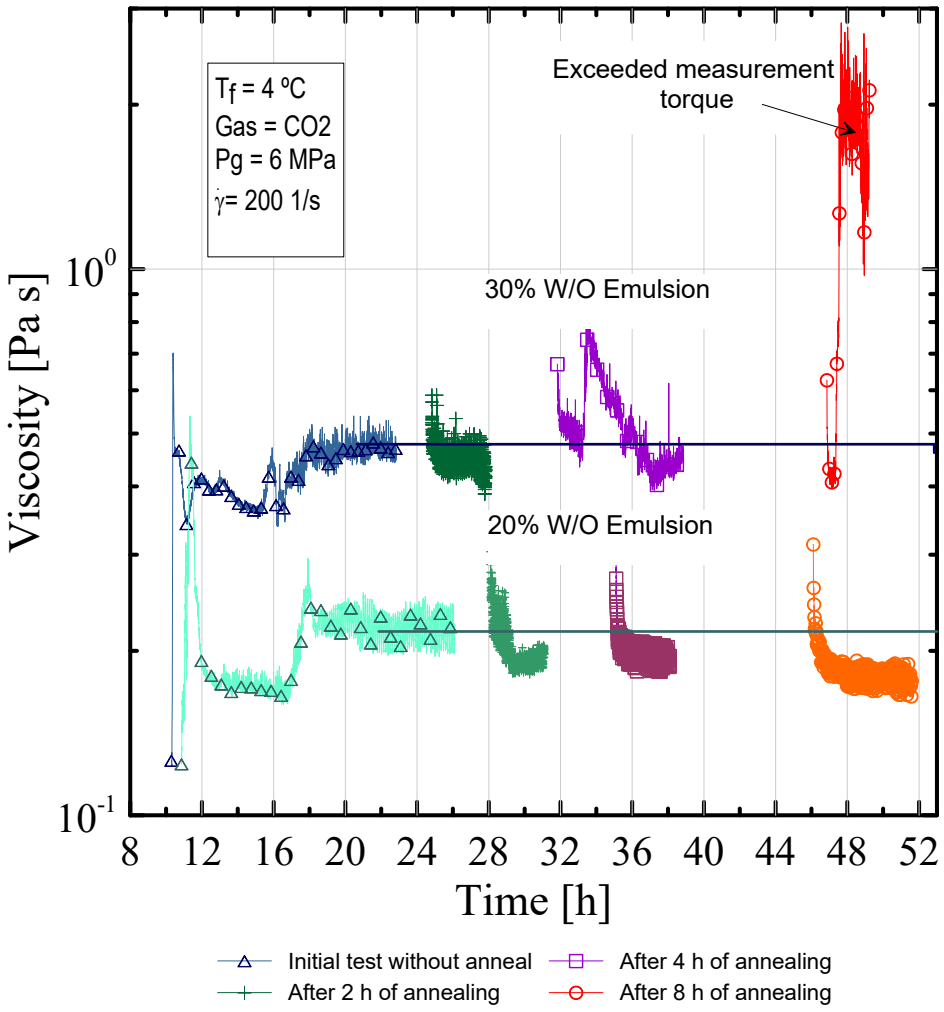

Figure 3.11: Viscosity over time at a fix shear rate for two water fractions. The tests were conducted to evaluate the hydrate structure regeneration.

rate fixed at 200 s^{-1}. A sequence of tests was carried out for each emulsion. After the end of the standard test, in which the viscosity is evaluated at fixed pressure and shear rate until its steady state, the emulsion, now with gas hydrates, is left at rest for a period of time. For the emulsion with 30% of water, the asymptotic viscosity is between 0.4 and 0.5 Pa.s. In the sequence, the emulsion rested for 2 h before the test restarted at the same shear rate and it is observed, in the beginning, a peak of viscosity close to 0.6 Pa.s, before it reaches the same asymptotic value. In the next step, the emulsion rested 4 h. The peak of viscosity is more pronounced, above 0.7 Pa.s, and, again, after a long enough time, the same final value of viscosity is reached. Finally, the emulsion is left for 8 h before the restart of the test and the reconstruction of hydrates is so intense that the rotor was blocked up. The peak of viscosity was above 3 Pa.s. This is a clear thixotropic

behavior. As the mechanical forces are brought to end, the inter-crystals forces work in the sense to build up the gas hydrates structure. The same occurred in the emulsion with 20% of water in oil, but with a smaller intensity. For such an emulsion, the rotor was not blocked after 8 h at rest. The reconstruction ability of the CO_2 hydrates seems to be dramatic and deserves attention for the flow assurance point of view.

3.1.6 Memory effect of CO_2 hydrates

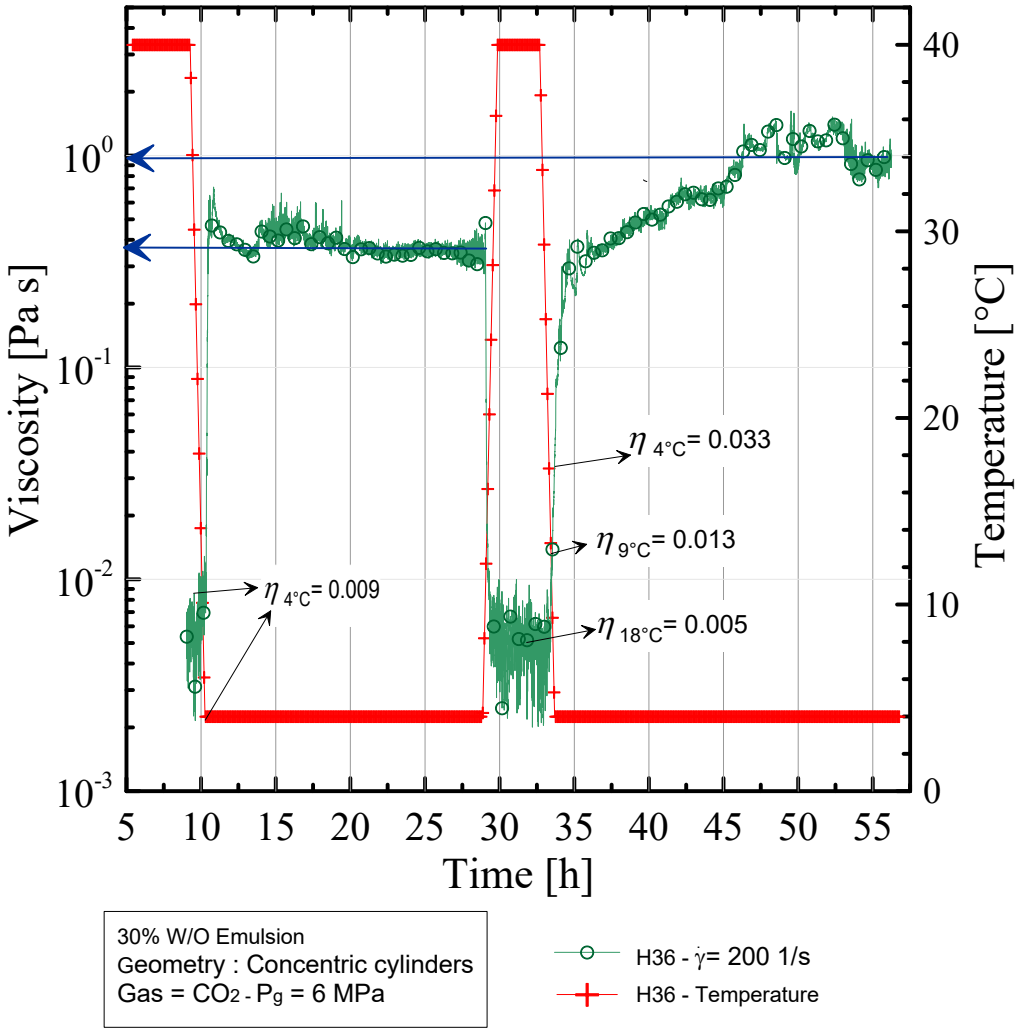

Figure 3.12: Viscosity over time at a fixed shear rate. The tests were conducted to evaluate the memory effect of the hydrate. In this case, the valve kept totally open.

A remarkable phenomenon related to gas hydrates is the so-called *memory effect*. Supposedly, once the gas hydrates are trigged, by a cooling process under high pressure for example, if the emulsion is heated again, some crystals remain and they will work as a

catalyst if another cooling is processed. Hence, if the memory really exists, the induction time should be reduced. Figure 3.12 is an attempt to investigate the memory effect of CO_2 hydrates.

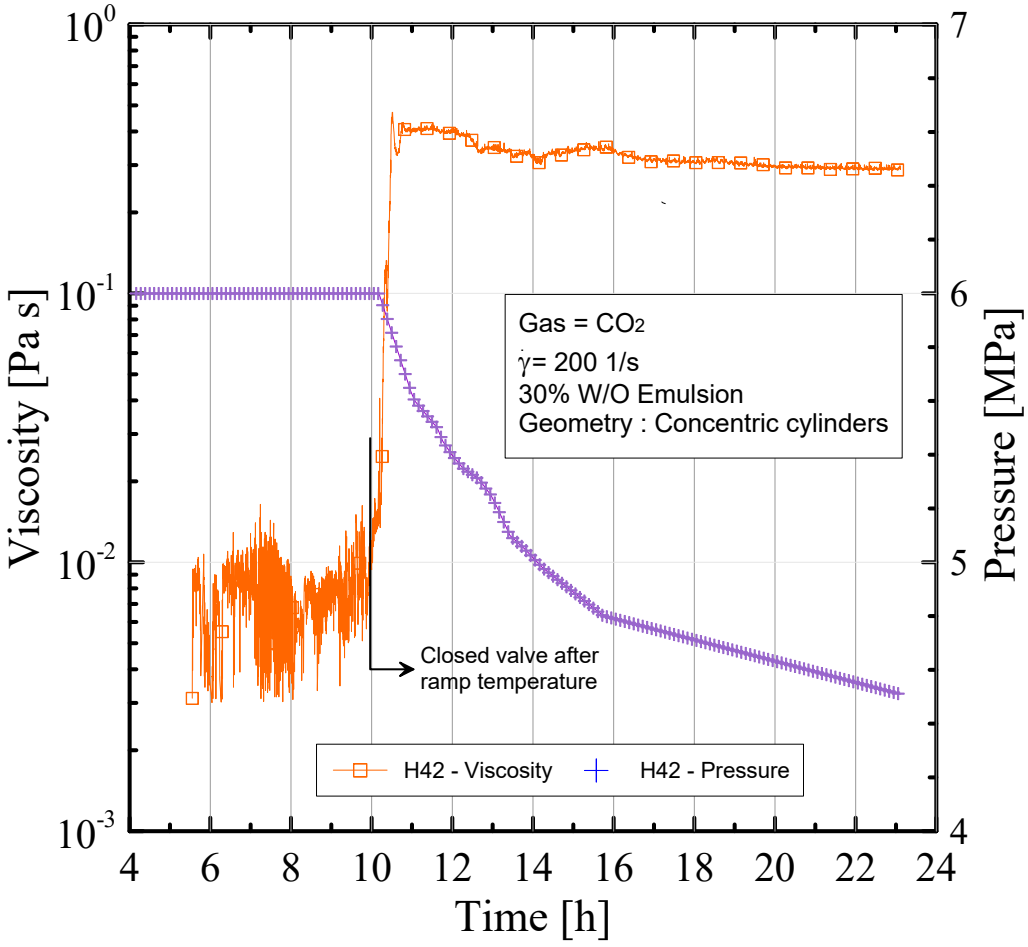

Figure 3.13: Viscosity over time at a fixed shear rate. Gas consumption of CO_2 gas hydrates.

Was conducted a test with two cycles of heating and cooling. The sample was firstly heated up to 80 ^{o}C and cooled to the test temperature of 4 ^{o}C. At the end of the first cycle, in which $\eta_\infty \approx 0.4$ Pa.s, the sample was heated again up to 80 ^{o}C and cooled to 4 ^{o}C. The asymptotic viscosity at the end of the second cycle was much larger, $\eta_\infty \approx 1$ Pa.s. This test was conducted under constant pressure. It means that the valve was kept open during the test. Moreover, CO_2 was injected into the sample to keep the pressure constant since gas is consumed when the hydrate is formed. Thus, the amount of gas was larger in the second cycle and this could be the reason for the increase of hydrates.

In order to verify if the larger amount of gas is playing a role in the second cycle in

Fig. 3.12, were conducted some tests with the valve closed. The first test is displayed in Fig. 3.13. The sample was saturated with gas at the fixed pressure of 6 MPa and 80 ^{o}C

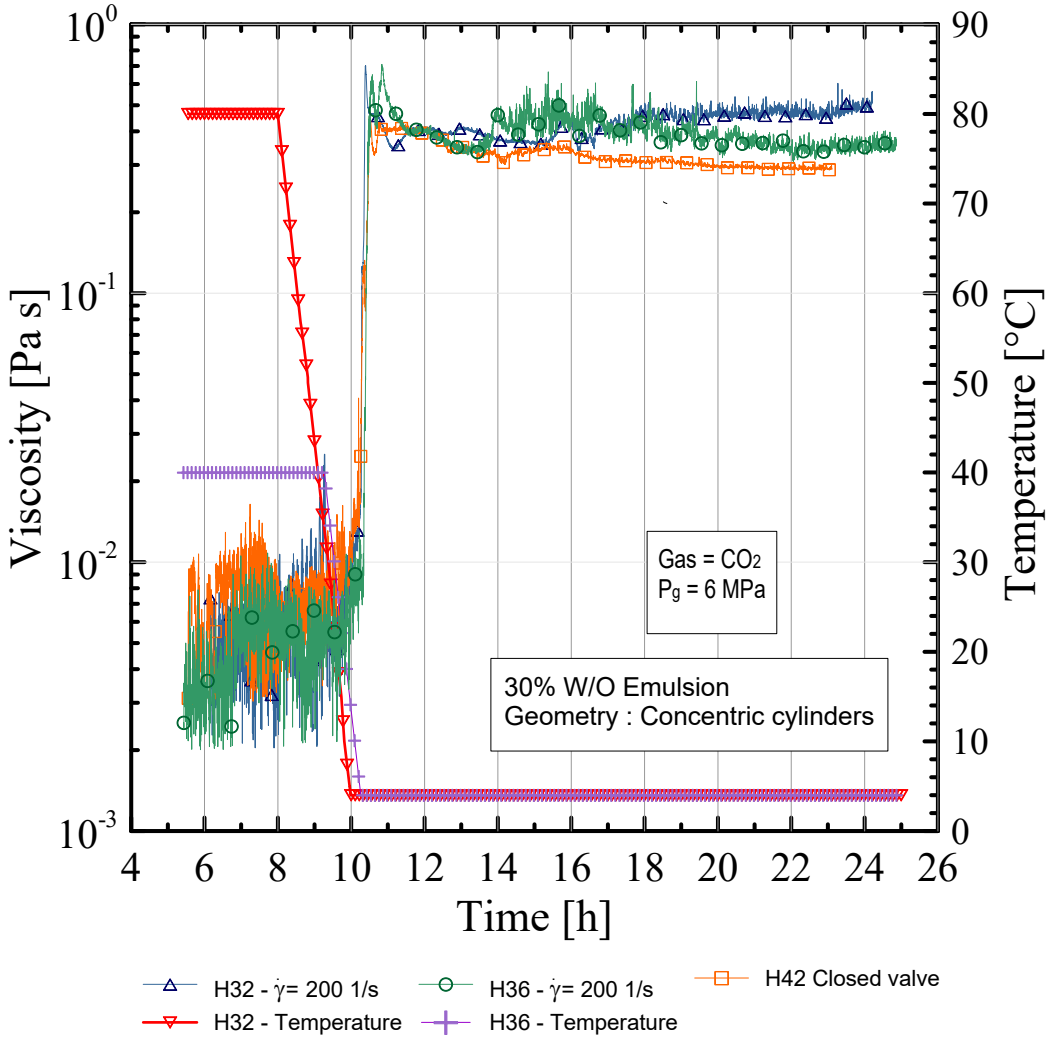

Figure 3.14: Viscosity comparison with open and closed valve.

temperature. As in the previous tests, the cooling begins after 8 h, at a constant rate of 0.6 ^{o}C/min. When the temperature reaches 4 ^{o}C, the valve is closed. Hence, the hydrates start to form at a pressure equal to 6 MPa, which decreases abruptly at the beginning and tends to an asymptotic value after a long enough time. As observed in Fig. 3.14 the peaks of viscosity at the beginning and their asymptotic values are not very different from the cases in which the valve was opened, which suggest that the complement of gas during the process, to keep the pressure constant, is not so important. In other words, it seems that the difference in the amount of gas between the two tests is not relevant in

terms of the final amount of hydrates. Finally, were conducted a sequence of four heating

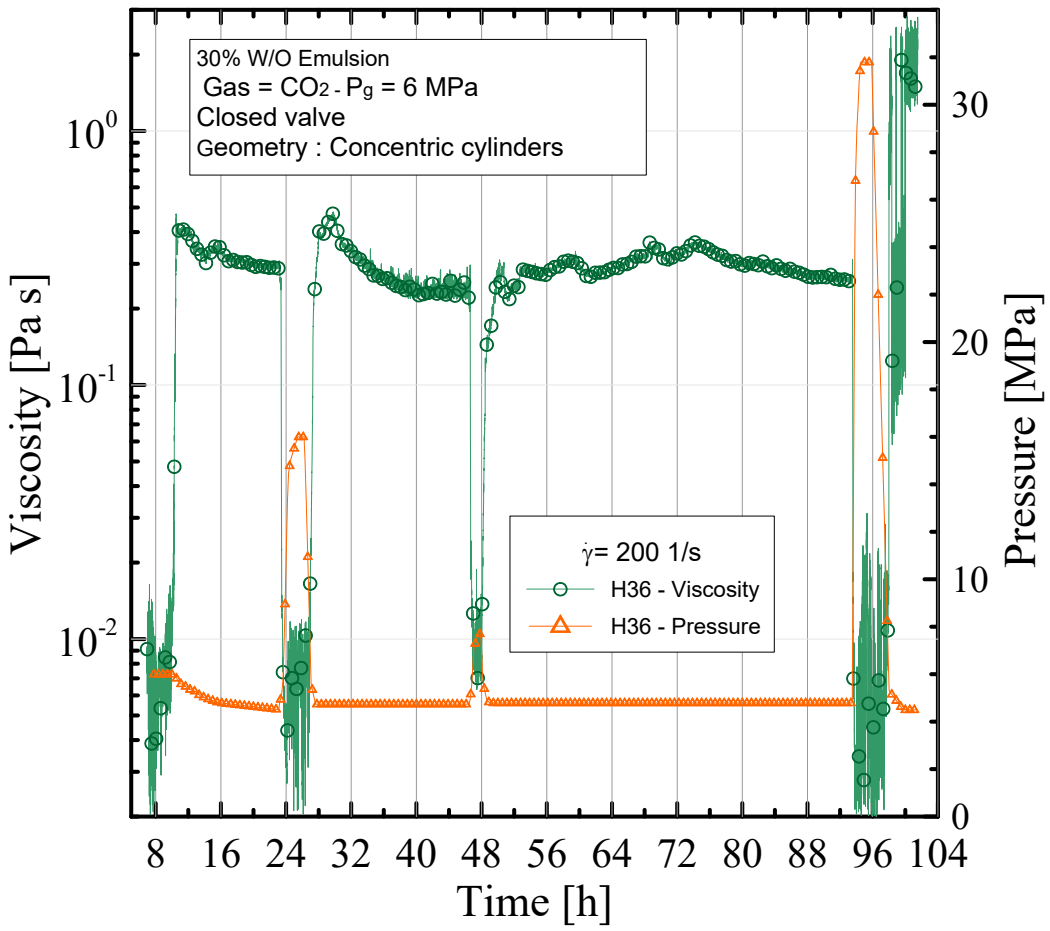

Figure 3.15: Analysis of memory effect with closed valve. The valve was closed when the temperature of 4 °C was achieved, before the first cycle of hydrate formation.

and cooling cycles with the valve closed, which is displayed in Fig. 3.15. The first cycle was conducted in exactly the same way as the other tests, in which the top temperature was 80 ^{o}C. In the second, the top temperature was reduced to 40 ^{o}C and to 20 ^{o}C, in the third cycle. Interestingly, the three first cycles were quite similar in terms of the peak of viscosity and its final value, but in the fourth cycle, when the sample was heated up again to 80 ^{o}C, the increase in the peak of viscosity was dramatic. It was close to 2 Pa.s, 5 times that of the previous cycles. It is possible that the hydrate formation was favored by the temperature of heating. It is worth noting that there was no more gas injected in the fourth cycle since the valve was closed. Maybe, this is kind of a memory effect and one reason for that is the fact that the peak occurred when the sample was heated up to 80 ^{o}C and not less, but such phenomenon really deserves more investigation. The

literature says that the memory decreases when the heating temperature increases, but here it is observed the opposite trend. Another explanation could be due to the emulsion destabilization or the change in the gas hydrate morphology that could be caused when the temperature is incremented.

3.2 Influence of asphaltenes and saturates on gas hydrates formation

There is an intriguing question in the industry as well as in academia: How the crude oils properties influence on hydrate formation? Consider that two different oils with the same water content are submitted at the same thermodynamic conditions of hydrate formation, which of the oils would have a higher tendency to remain more in the unstable region (supersaturated) without hydrate formation?. Those concerns have been raised up when some oil wells are shut down, for unplanned production downtime, for example. Then, there is a limited time to repair and initialize the operations of the well without the risk of hydrate formation. Maybe, this critical period is influenced by the chemical compounds of the crude oils. Indeed, Palermo et al. (2004) stated that the oil extracted from the Brazilian oil well of Campos Basin has some natural surfactants that may explain why no hydrate plugging occurs in the flowlines, even during shutdowns and restart processes. It is known that the main differences among the crude oils are the relative amount of hydrocarbon classes present on it: saturates, aromatics, resins and, asphaltenes, and its stabilization dependents of the molecular relationship between its constituents. One of the petroleum fractions, the asphaltenes, has gained importance in recent years due to the increasing demand for heavy oil extraction. Asphaltenes are generally defined as insoluble in normal alkanes (e.g., n-pentane or in n-heptane) but soluble in aromatics (e.g., toluene). They are the most polarizable fraction of the oil and its amount present in the oil depends on the source of the crude oil. Asphaltenes are important stabilizer of water-in-oil emulsions (Fingas, 2014) and are natural interface-active components, that reduce the surface tension and inhibit drops coalescence (Zhang et al., 2016; Samaniuk et al., 2015). These phenomena are attributed to the steric interaction forces between the chains of interfacial asphaltenes molecules. In the following, we present a series of results with the aim of evaluating the influence of the crude oil properties in hydrate formation.

To this purpose, we used gas condensate (GC) and asphaltenes to vary the amount of light and heavy hydrocarbons respectively.

3.2.1 Oils employed and characterization

Two different oils are employed to conduct the experiments, nominated here as oil A and C. The heavy oil A was extracted from the post-salt well and the oil C from the pre-salt layer and is classified as a medium oil. The oils were provided by Petrobras and were extracted at the Espírito Santo Basins, off the Brazilian coast. The same heavy oil has been investigated by Neto et al. (2018). The medium oil was the same used to obtain the results explained in part 3.1 of this document (for more detailed see (Sandoval et al., 2018)), and the condensate gas was also studied by Bassane et al. (2016). In that case, the condensate was used to reduce the viscosity of the heavy crude oils. The physicochemical properties of each oil and condensate gas are shown in Table 3.1.

Table 3.1: Properties of the dehydrated oils and condensate gas

Properties	Oil A	Oil C	Gas condensated	Standard Method
water content (% v/v)	0.42 (0.01)	< 0.01	0.050 (0.002)	ASTM D4377
Density at 20 ^{0}C (g cm^{-3})	0.931 (0.003)	0.880 (0.002)	0.6734 (0.005)	ASTM D5002
API Gravity at 60 ^{0}F	19.9^0	28.3^0		ISO 12185
TAN in mg of KOHg^{-1}	0.40 (0.02)	0.119 (0.008)	< 0.010	ASTM D664
SARA content				
Saturates (wt%)	41.0 (0.05)	58.10 (0.09)	88.7 (0.04)	ASTM D2549
Aromatics (wt%)	31.5 (0.05)	19.83 (1.21)	11.1 (0.02)	ASTM D2549
Resins (wt%)	19.0 (0.03)	21.43 (1.30)	0.10 (0.010)	ASTM D2549
Asphaltenes (wt%)	8.5 (0.07)	0.64 (0.06)	< 0.05	ASTM D6560

Each oil was treated and conditioning for testing according to the procedure ASTM Standard D 5854 (2005). After removing the free water, the amount of emulsified water was determined using a Methrom KF Titrator, following the procedure indicated by ASTM Standard D 4377 (2011). When the representative samples of each oil showed a water-cut below than 0.5% v/v (dehydrated oil), then, they were utilized to make their characterization as well as to prepare the emulsions to conduct the main experiments. The oils densities were measured in agreement with the ISO 12185 (1996). The total acid number

was determined in accordance with the ASTM Standard D664 (2011) and the SARA content of each oil was estimated by chromatographic analysis under the ASTM Standard D 2549 (2012). The asphaltenes precipitation was attained with heptane in according to the procedure explained in the ASTM Standard D 6560 (2012). The gas condensate characterization was carried out through a chromatographic assessment, and the list of its compounds are published in Bassane et al. (2016).

3.2.2 Emulsification

The procedure to prepare the water-in-oil emulsions was slightly different the one explained in section 2.3 of this document, since it was used a different homogenizer and it was necessary to implement a way to add the gas condensate and the powder asphaltenes into the oil. Then, a similar procedure to the one described by da Silva et al. (2018) was adopted. The procedure consists of the following steps: Firstly, for the desired emulsion, the corresponding dehydrated oil/deionized water proportion was weighted and deposited in separate glass bottles. Secondly, the oil specimen was heated for 30 min at 60 ^{0}C to its homogenization. Thirdly, the deionized water was mixed with the oil and the sample was submitted to a mechanical stirrer in a Turrax homogenizer (model IKA T25, rotor 18G) applying an angular velocity of 7500 rpm for 3 min. When it was necessary to add asphaltenes to the oil, this was realized before step 2. Whenever condensate gas was added, this was done before the mechanical stirrer, since the condensate gas is highly volatile. The powder asphaltenes were added directly to the crude oil as well as the gas condensate, that at room conditions remains at a liquid state. An amount of 60 ml of sample was always prepared for each of the experiments. One part was used to conduct the experiments, another representative small part was taken to measure the drop size and the remaining part was deposited in a thin closed tube to monitor its phase separation by gravitational action.

The droplet size distribution of the 30% water-in-oil emulsions was measured in a Nikon optical polarized light microscope (LV100POL model) with LV100's CFI LU Plan Fluor EPI P 5 X , 10 X , 20 X and, 50 X and DS-Fi1 digital cameras. The droplet diameter size distribution of each sample was quantified by the program NIS-Elements D version 3.2. Representative pictures of the emulsion obtained with the oils A and C are shown in Figs. 3.16, 3.17 and 3.18. Figure 3.16 depicts the mean droplet diameter (MDD) as a func-

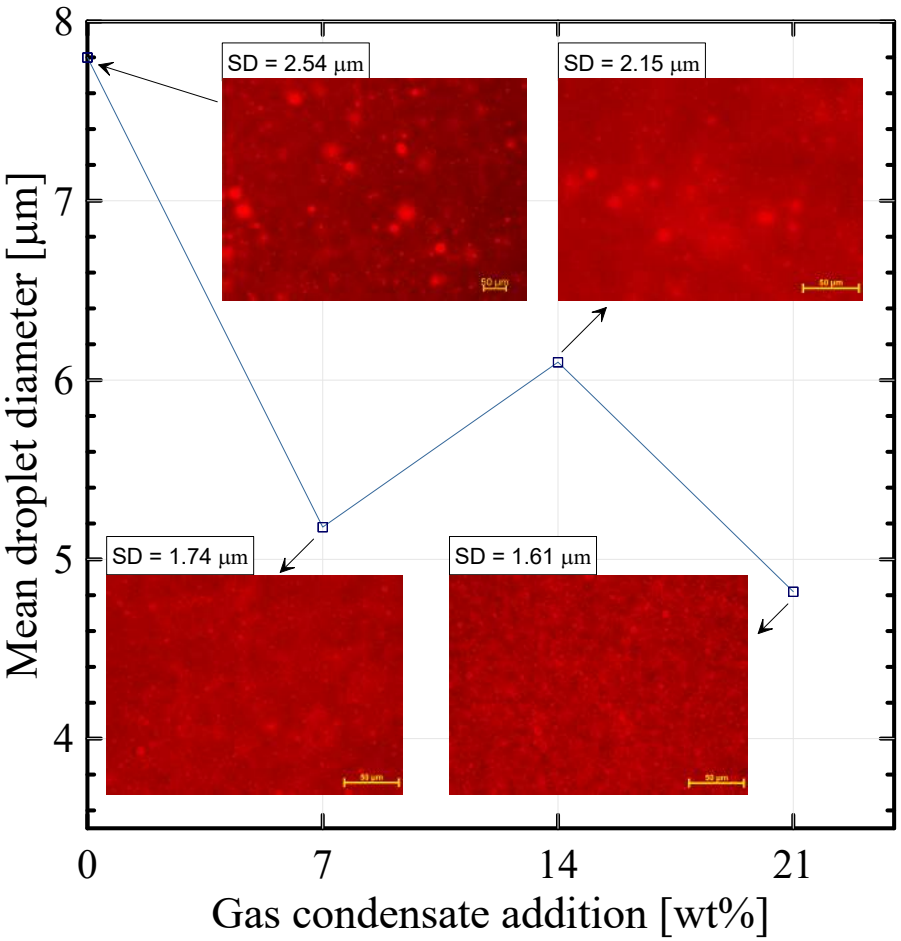

Figure 3.16: Mean droplet diameter as a function of the amount of gas condensate added (in wt%) to the emulsion prepared with the oil A.

tion of the amount of gas condensate added (in wt%) to the emulsion prepared with the oil A. The MDD of the pure emulsion without gas condensate addition is approximately 8 μm with a standard deviation (SD) of 2.54 μm. Indeed, when it was added 7 wt%, 14 wt% and 21 wt% of gas condensate to the emulsion the MDD did not change significantly, and no asphaltenes precipitation was observed in our samples, as it can occur when the gas condensate is added (Shigemoto et al., 2006; Speight, 2004).

Figures 3.17 and 3.18 display the MDD with the respective standard deviation (SD) as a function of the amount of asphaltenes added to the emulsions prepared with the oil A and C. The dark spots observed in both representative pictures, shown in Figs. 3.17 and 3.18 are the asphaltenes particles. The asphaltenes seem to be dispersed in the representative samples of each emulsion, with an exception of the sample of 2.8 wt% of

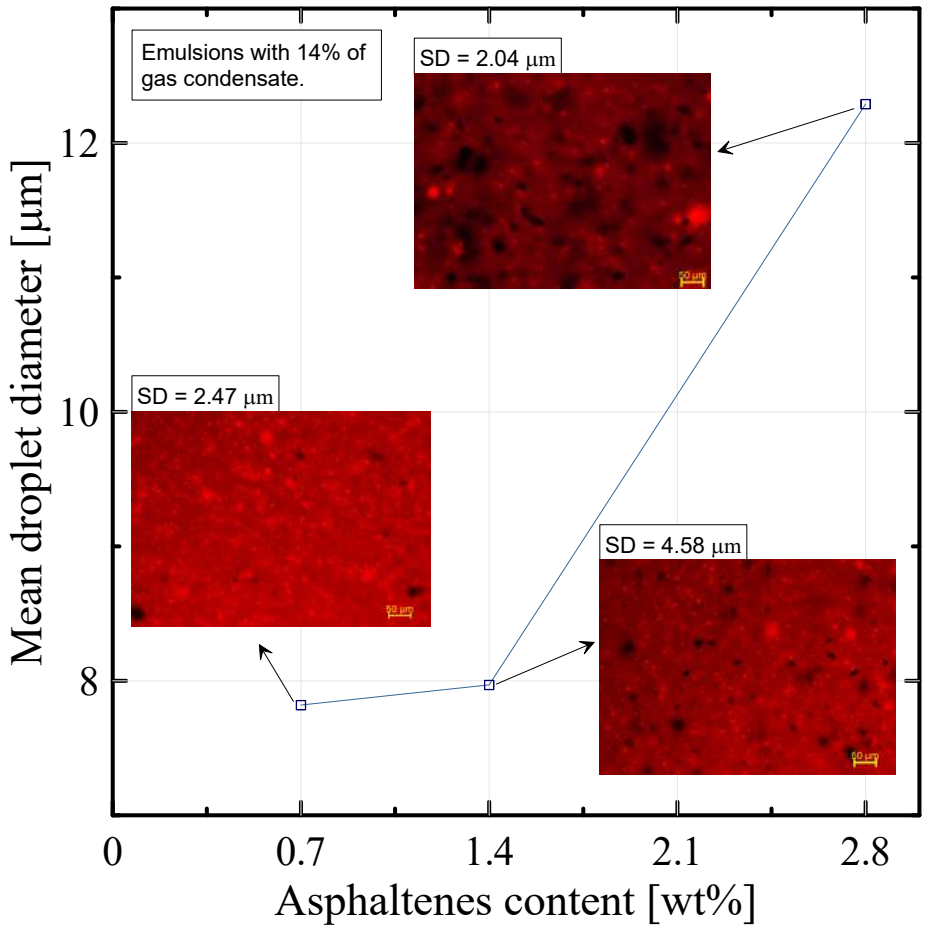

Figure 3.17: Mean droplet diameter as a function of the asphaltenes content added (in wt%) to the emulsion prepared with the oil A.

asphaltenes shown in Fig. 3.17. Note that the MDD does not differ a lot in comparison with the pure emulsions of both oils (the pure emulsion prepared with the oil C is shown in Fig. 3.18 with 0 wt% asphaltenes content). A possible explanation is that the small droplets of the pure emulsion have a highly stabilizing effect on the system. It seems that for these pure emulsions with small droplets the addition of asphaltenes and GC do not affect considerably its final MDD what in turn seems to be a crucial aspect for hydrate formation. In fact, Boxall et al. (2008) demonstrated that for droplet size distribution less than 15 μm the hydrates formation rate is very similar, but it varies for larger droplets between 20-150 μm.

The experiments for the analysis of the samples were conducted in the same equipment and high-pressure system explained in section 2.1. Also, the thermodynamic conditions of

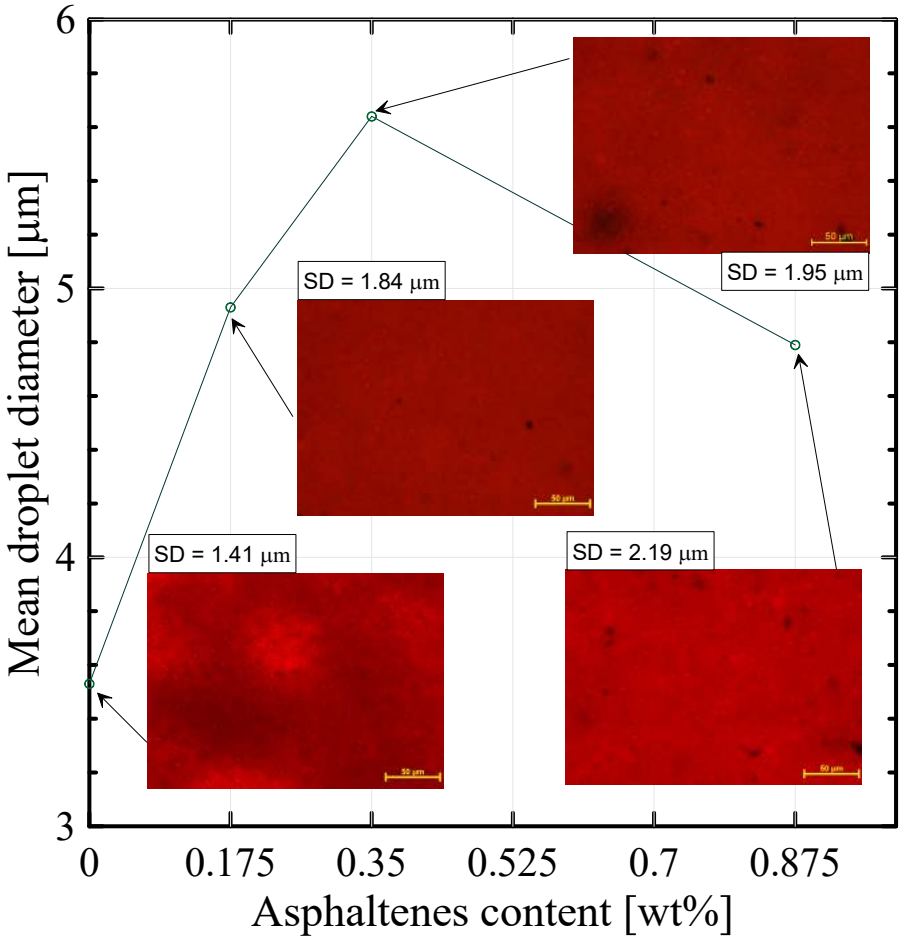

Figure 3.18: Mean droplet diameter as a function of the asphaltenes content added (in wt%) to the emulsion prepared with the oil C.

the experiments were the same as that utilized in section 3.1, with the same supercooling of 6 ^{0}C.

3.2.3 Influence of gas condensate on CO_2 gas hydrate formation

All the results are presented by means of viscosity curves as a function of time. Figure 3.19 shows a typical experiment of hydrate formation (blue curve). The first increment in viscosity is due to the temperature reduction until reach 4 ^{0}C, after that, the viscosity remains at a constant level for almost 18 h, and suddenly, just after crystallization occurs, a hydrate growth happens and, consequently, a viscosity jump is noted due to the agglomeration of crystals. This elapsed time of 18 h is known as *the induction period* and is characterized by the nucleation and crystallization of hydrates. The viscosity jump

is associated with hydrate formation and, as it can be observed, the viscosity increased almost 3 times with respect to its previous value. The spike in viscosity is kept for a time and starts to reduce slowly when the shear forces produced by the rheometric geometry are higher than the cohesion forces of hydrate crystals. In the experiments presented in this section is not possible to observe the pressure drop, because they are carried out at a constant pressure so that the CO_2 inlet valve is kept open throughout the test.

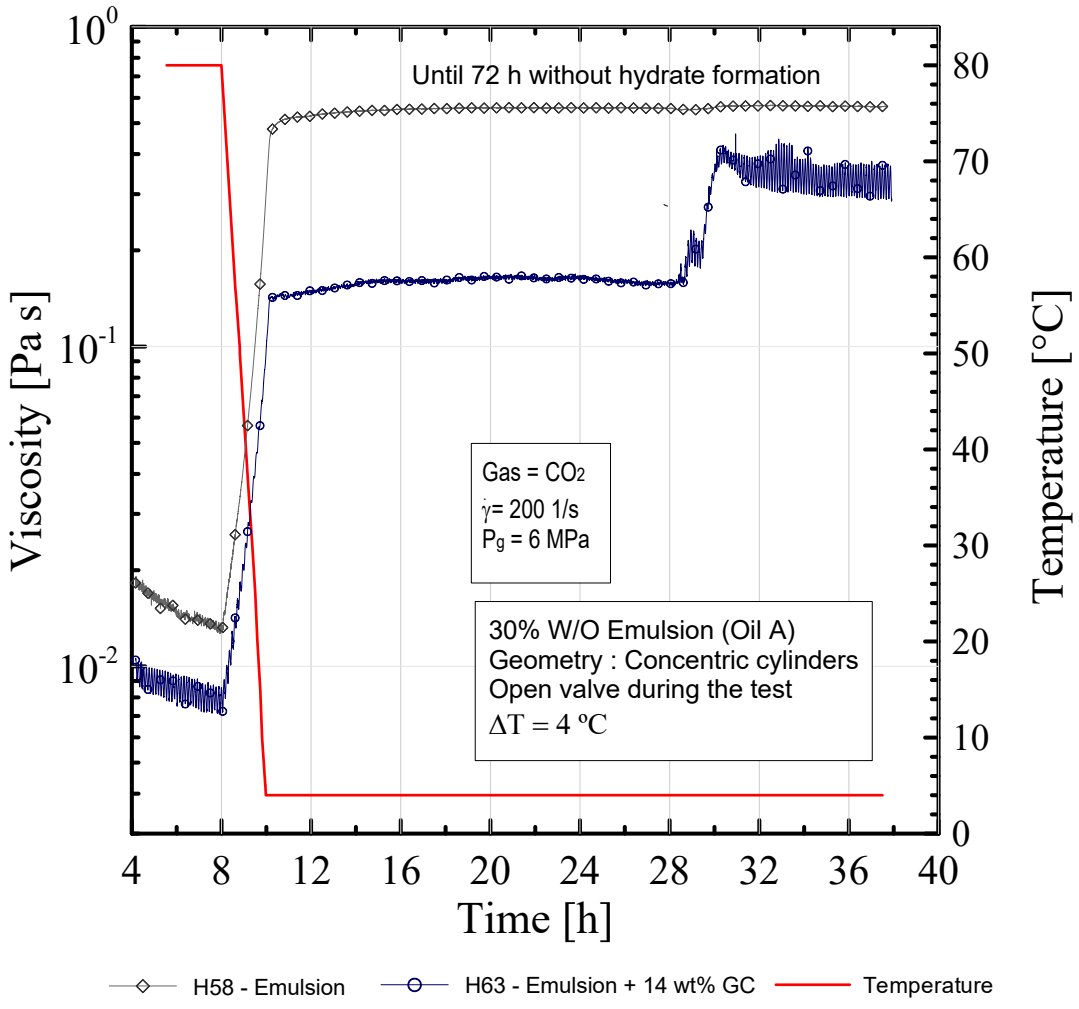

Figure 3.19: Two curves of viscosity over time for an emulsion with 30 wt% of water-in-Oil A. When a solution of 14 wt% of GC is added the viscosity at 4 ^{0}C decreases, but after approximately 20 h of induction time, hydrate formation is observed.

Figure 3.19 depicts two different curves with 30% water-in-oil A. The grey curve (rhombus symbol) shows the viscosity data obtained for the pure emulsion. As noted, the increase in viscosity is due to the temperature reduction, but after the temperature achieved 4 ^{0}C, the viscosity remained in the value of 0.55 Pa·s without showing another increment

after 72 h of the experiment, indicating that hydrates do not form during this period. In another experiment, the same emulsion was prepared again (with the same oil), but in this case, it was added a solution of 14 wt% of GC to the emulsion. It is observed that the viscosity was reduced both at 80 ^{0}C, as well as 4 ^{0}C (approximately 4 times at this temperature), but after approximately 20 h of induction time, the viscosity increased, indicating hydrate formation.

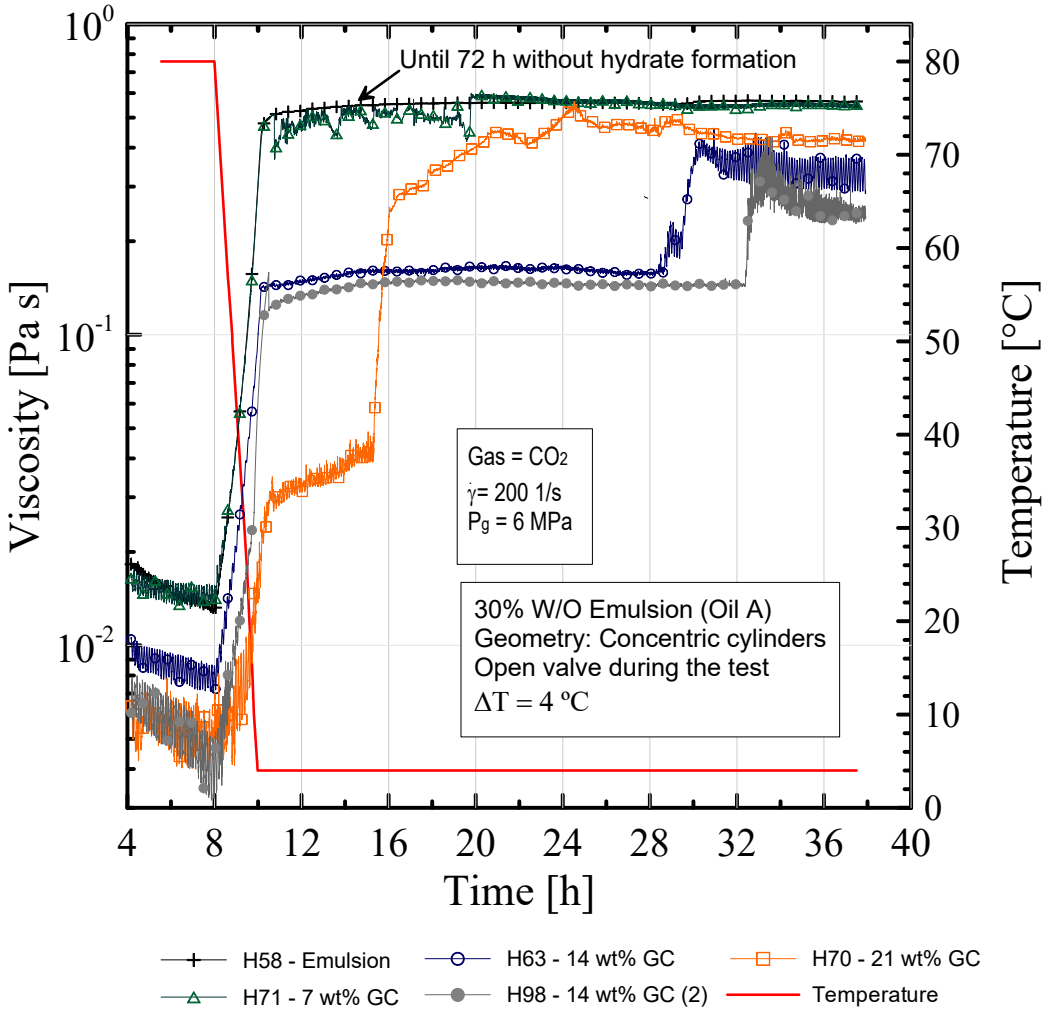

Figure 3.20: Effects of gas condensate for Oil A.

Figure 3.20 shows the viscosity behavior versus time for different amounts of gas condensate added to the oil A. When 7 wt% of GC is added to the emulsion, the viscosity is quite similar with that of the pure emulsion, indicating no effect of the GC quantity on the viscosity. On the other hand, when 21 wt% of GC is added to the emulsion, the viscosity at 4 ^{0}C is reduced by approximately 14 times in comparison with the pure emulsion, but the spike in viscosity arises after 5 h of induction time, and with an increment

about one order of magnitude. This indicates that the addition of gas condensate reduces considerably the viscosity, but also promotes hydrate formation. Figure 3.20 also shows another curve for 14 wt% of GC. It experiment was made with a different emulsion in another day of the year to obtain more confidence in the results. Look that the difference in the induction time between the experiments is roughly 4 h.

3.2.4 Effect caused by the pressure in the driving forces of CO_2 hydrates

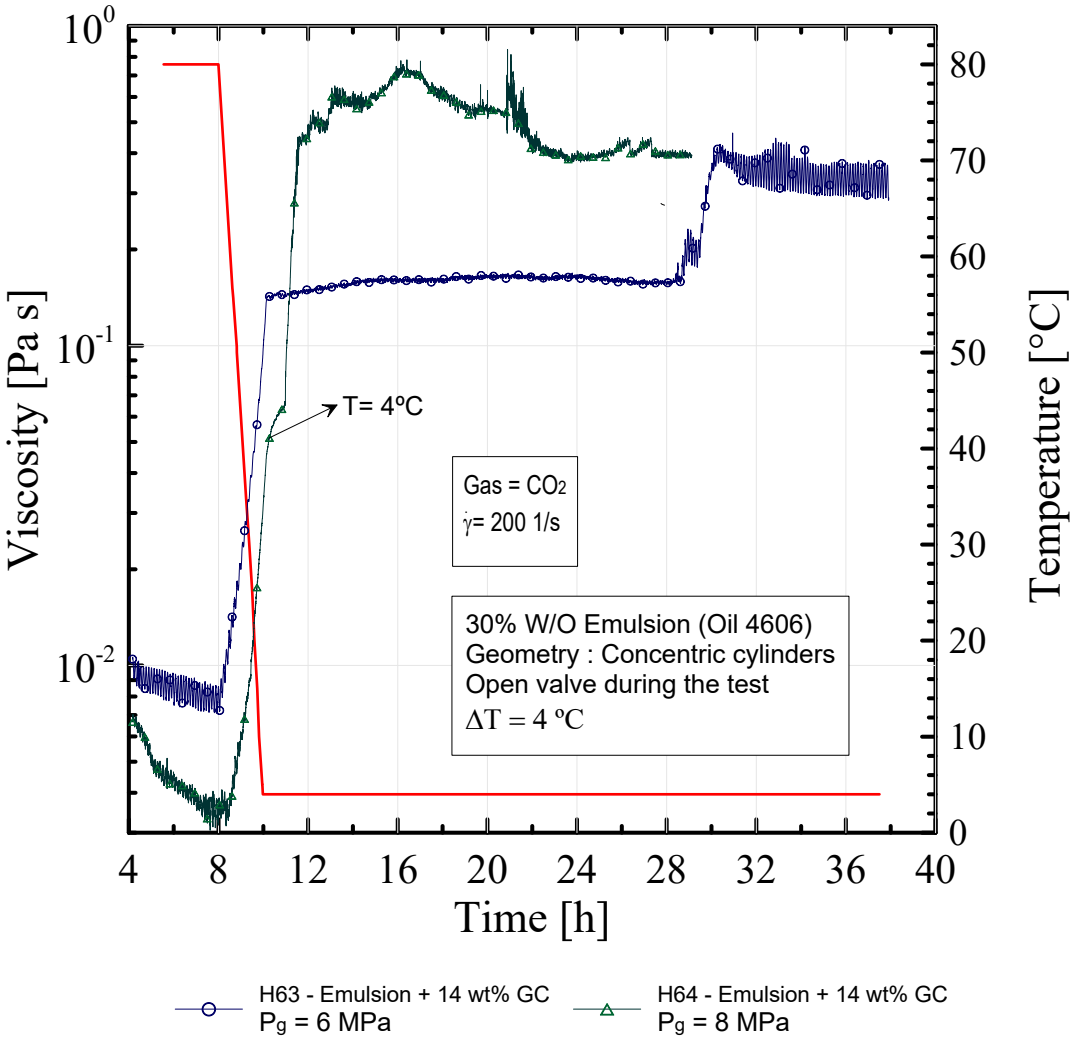

Figure 3.21: Analysis of two different pressures (6 and 8 MPa) for the Oil A.

Once having studied the effect of the gas condensate on oil A, the next step is to analyze the influence of the heaviest components of the oil, the asphaltenes. As observed in Fig. 3.19 the pure emulsion does not show hydrate formation. If more asphaltenes are

added to the emulsion, it becomes more stable and with a higher probability of not forming hydrates. Therefore, we selected the emulsion of 14 wt% of gas condensate to evaluate the effect caused by the asphaltenes added to oil A. Since the induction time of the sample with 14 wt% of gas condensate shows around 20 h to form hydrates, it was envisaged to increase the driving forces for hydrate formation in the system. Then, one idea was to raise the pressure cell to 8 MPa. The result obtained for the pure emulsion is shown in Fig. 3.21, (triangle symbol). As it is noticed, the viscosity growth starts very fast and remains only about half an hour after achieving the temperature of 4 ^{0}C, i.e. the induction time was reduced from 20 h to 0.5 h. That increase in pressure not only accelerated CO_2 hydrate formation but also influenced in the hydrate formation rate. While the viscosity increased about 3 times in the experiment with 6 MPa, when the pressure is raised to 8 MPa the viscosity increased around an order of magnitude. A qualitative response was obtained with the oil C (Fig. 3.22), that was studied at the same test parameters of the experiment showed in Fig. 3.21, except to the higher pressure of 10 MPa (square symbol). Notwithstanding, in such a case is not possible to note the reduction on the induction time at both pressures, since the hydrate growth begins as soon as the temperature reaches 4 ^{0}C. A slight difference is only noticed on the induction period between the curves. Once again, the hydrate formation rate is also larger for the pressure of 10 MPa, approximately twice the amount formed with the pressure of 6 MPa. For both pure emulsions A and C at 6 MPa show in Fig. 3.19 and Fig. 3.22 respectively, there is a dissimilarity on the induction time. The oil A did not show hydrate formation, while the oil C formed hydrate as soon as the temperature achieved 4 ^{0}C. That behavior is probably due to the chemical compounds present in each oil.

Some authors have investigated the effect of pressure in the driving potentials, see, for example, Christiansen and Sloan Jr (1995); Kashchiev and Firoozabadi (2002); Anklam and Firoozabadi (2004); Arjmandi et al. (2005). Arjmandi et al. (2005) indicated that for a single hydrate former, the driving force is proportional to the degree of subcooling at isothermal and isobaric conditions. In addition, at a constant degree of subcooling, the driving force decreases as pressure increases, mainly at pressures lower than 20 MPa, despite this decreasing is not significantly. The opposite trend was observed for double hydrates (two or more compounds take part in hydrate formation as natural gas) where the subcooling underestimates the real driving forces for pressures between 4 and 20

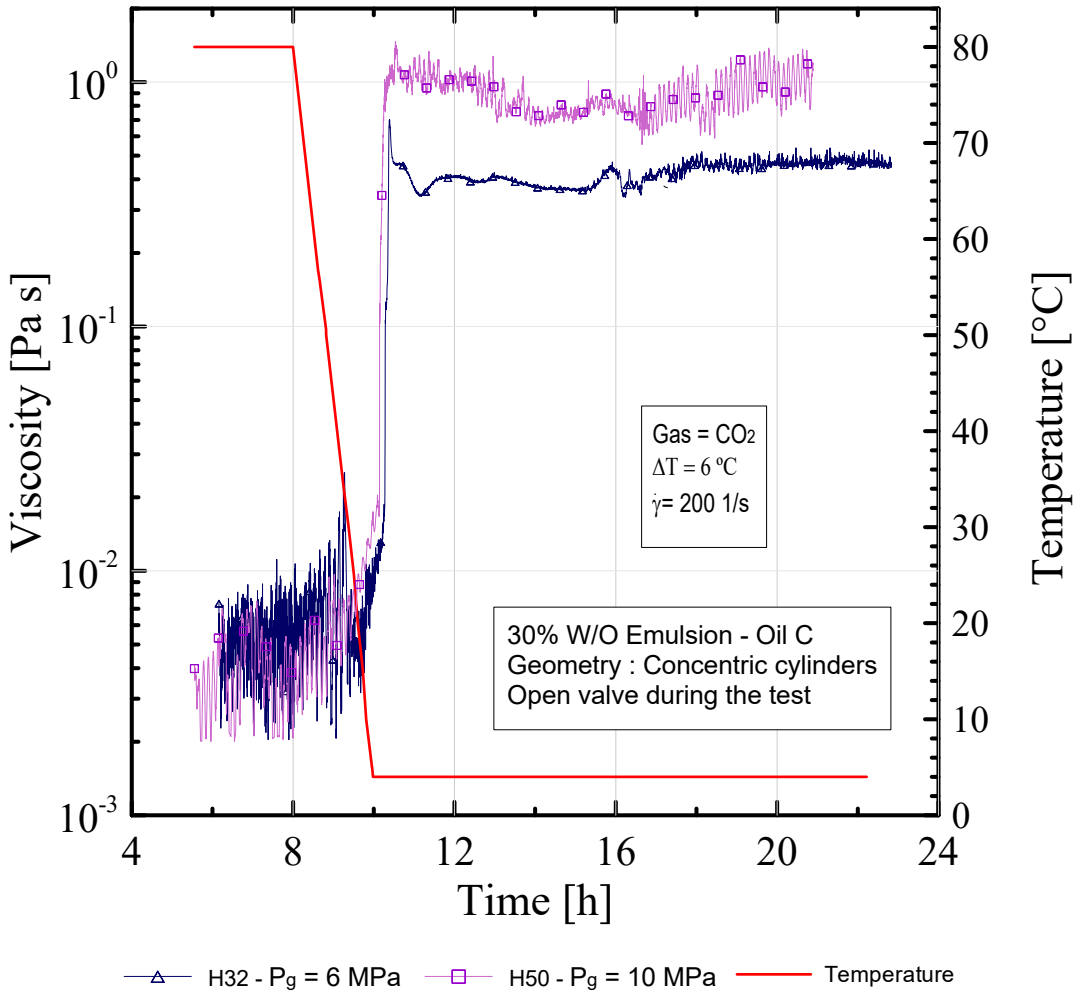

Figure 3.22: Analysis of two different pressures (6 and 8 MPa) for the Oil C.

MPa. Regarding induction periods, the authors reported through experimental data for a gas-natural-water system that the change in pressure had no significant effect on the induction time at a constant degree of subcooling. However, for systems in the presence of a kinetic inhibitor, it was observed shorter induction times when the pressure was increased, in spite of lower driving forces than those in the low-pressure test. Although the experiments shown here are conducted for a single hydrate former (CO_2), perhaps this guest molecule and the water-in-oil emulsion and its natural inhibitors could contribute to influence in the induction time as well as in the hydrate formation rate, as depicted in Fig. 3.21. However, in a recent study it has been shown that methane hydrate formation is insensitive to the addition of impurity particles, see Cox et al. (2018), but a different behaviour could be expected for more hydrophilic or water-soluble gas molecules as CO_2. This phenomenon deserves a deeper investigation.

3.2.5 Influence caused on CO_2 hydrates by the addition of powder asphaltenes

The results obtained when asphaltenes are added to the emulsions prepared with the oil A present a different effect in the induction time in comparison with the GC, as shown in Fig. 3.23. All the experiments were made with 14 wt% of gas condensate in the oil and with a pressure of 8 MPa. The curve of pure emulsion plotted in Fig. 3.21 was inserted again in Fig. 3.23 for comparison reasons. When 0.7 wt% of asphaltenes is added to the emulsion (square symbol in Fig. 3.23), the induction time augmented around 2 h regarding with the pure emulsion. When 1.4 wt% was added (gray curve) to the emulsion, the induction time increased 4.5 h, as well as the growth time. While the experiment with the pure emulsion spent about 2 h to attain the maximum viscosity value, the test with 1.4 wt% of asphaltenes took approximately 6 h. Since it was observed that the asphaltenes have a positive effect on the induction time, then we added 50% more of asphaltenes to observe if hydrate formation would be avoided for the conditions of these experiments. The result is represented by the orange curve (cross symbol). The viscosity was quite similar with that of the pure emulsion at 80 ^{0}C, as well as for 4 ^{0}C, but after 15 h of induction time the viscosity presented an increment and rapidly returned to the previous value. As expected, the increase in the amount of asphaltenes in the emulsion, also increased the viscosity value. However, we can identify a fast spike in viscosity after 14 h of induction time, that did not happen with the pure emulsion. A possible explanation for such behavior is the addition of the GC since the saturates/asphaltenes ratio is around 4.8 for both, the crude oil A and the blending oil-GC-asphaltenes. As it should be also noted, asphaltenes act delaying the induction time and the growth period but do not avoid hydrate formation, indicating a time-dependent behavior. A different case has been reported when asphaltenic crude oils were studied (see Camargo and Palermo (2002)). In that case, it is suggested that the natural compounds of the crude oils helped to transport the agglomerated hydrate particles as a suspension in the oil phase. Sinquin et al. (2001) also analyzed how the chemical compounds of the oil influence in hydrate formation. For that, two different asphaltenic crudes were studied, a paraffinic oil and one condensate. The results showed that the paraffinic oil and the gas condensate (despite form unstable emulsions) displayed a rapid hydrate formation, contrary to the asphaltenic oils that exhibited a delay in the order of 1.5 h on the induction time and, a smooth hydrate

formation regarding the condensate and paraffinic oil.

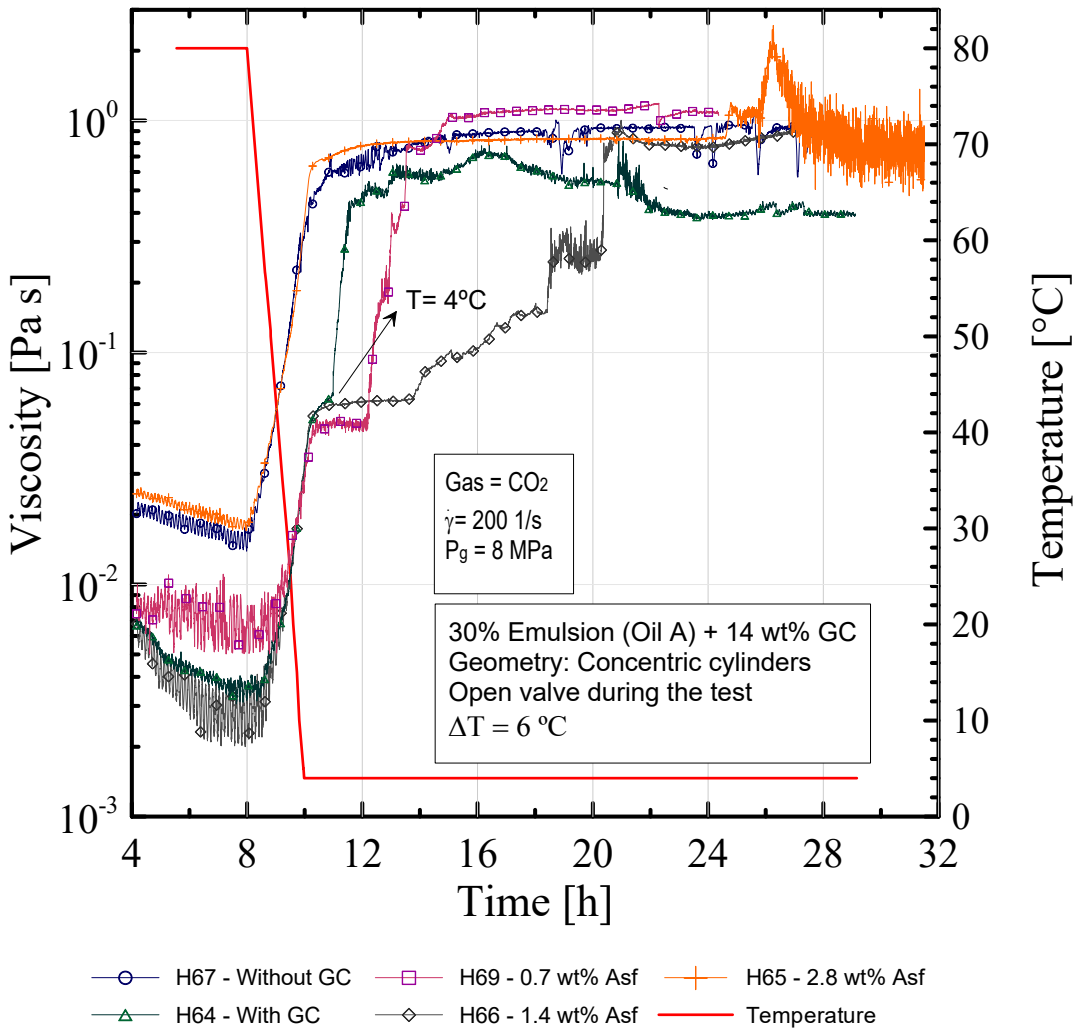

Figure 3.23: Effect caused by the addition of the asphaltenes to emulsions of 30% of water content and 14% of gas condensate for and Oil A.

To corroborate the asphaltenes effect on the induction time of gas hydrate formation, the oil C was used. As noticed in Table 3.1, the properties of the oil C are quite different from the oil A. The relation saturates/asphaltenes is around 90 times, and the quantity of asphaltenes in the oil C is almost unnoticeable by the measurement technique, less than 0.05 wt%. Figure 3.24 shows the viscosity behavior for a different asphaltene content as a function of time for oil C. The spike in viscosity of the pure emulsion (green curve) appears after half an hour of induction time, and after that, the viscosity increases almost 25 times. In that case, it was not necessary to add GC, since hydrate formed easily for the 30% water-in-oil emulsion at a pressure of 60 bar. After the test with the pure emulsion,

the next step was to prepare another emulsion adding 0.0875 wt% of asphaltenes, what made the viscosity to slightly increased (1.3 times) at 4 ^{0}C as shown in the grey curve in Fig. 3.24. A relevant change was again on the induction time, which increased roughly 7 h. The growth period also augmented, it was 4 h longer than the pure emulsion growth. Other two experiments were made with the same oil C increasing the concentration of asphaltenes: the 0.175 wt% represented by the blue curve with up triangles and the 0.35 wt% represented by the brown curve with down triangles. The induction time increased 14 h and 20 h respectively, compared with the pure emulsion. Once again, the growth period raised for the emulsion prepared with 0.35 wt% in around 6 h, but the same did not occur with the emulsion of 0.175 wt%, whose growth period was similar to that of the pure emulsion. The induction time for the first two concentrations of asphaltenes increased monotonically, but the same did not happen with the third quantity (0.35 wt%, 4 times the initial amount), where the performance was reduced in 7 h. On the other hand, the maximum increases in viscosity at 4 ^{0}C was obtained as expected by the emulsion with the larger quantity of asphaltenes. The value increased from 0.016 Pa·s for the pure emulsion until 0.05 Pa·s for the quantity of 0.35 wt% of asphaltenes, i.e. approximately 3 times. In practical applications, for this kind of oil, this increment in viscosity is more acceptable than having to deal with the large increase in viscosity caused by the formation of hydrates. It is important to note that the final value of viscosity is very similar for the different curves. This tendency can be associated with the fixed shear rate, that reduces the cohesion forces until a similar level.

To obtained more confidence in the results with the addition of asphaltenes, other repetitive experiments were made with different samples and in different days. The results are shown in Fig. 3.25 and Fig. 3.26, where are also displayed three curves for the pure emulsions with the same conditions (plotted in both Figs). Figure 3.25 shows the result for the samples with the addition of 0.175 wt% of asphaltenes. As observed, the maximum difference in the induction time is around 2 h, and the values of the asymptote viscosity are similar, approximately 0.35 Pa·s. For the addition of 0.35 wt% of asphaltenes (shown in Fig. 3.26), the discrepancy between the different tests is around 3 h, but after the growth period, the viscosity curves, although different, tend to the same final level.

From the results presented above, it can be concluded that the addition of small amounts of asphaltenes plays two main roles in CO_2 hydrates formation. The first effect is to

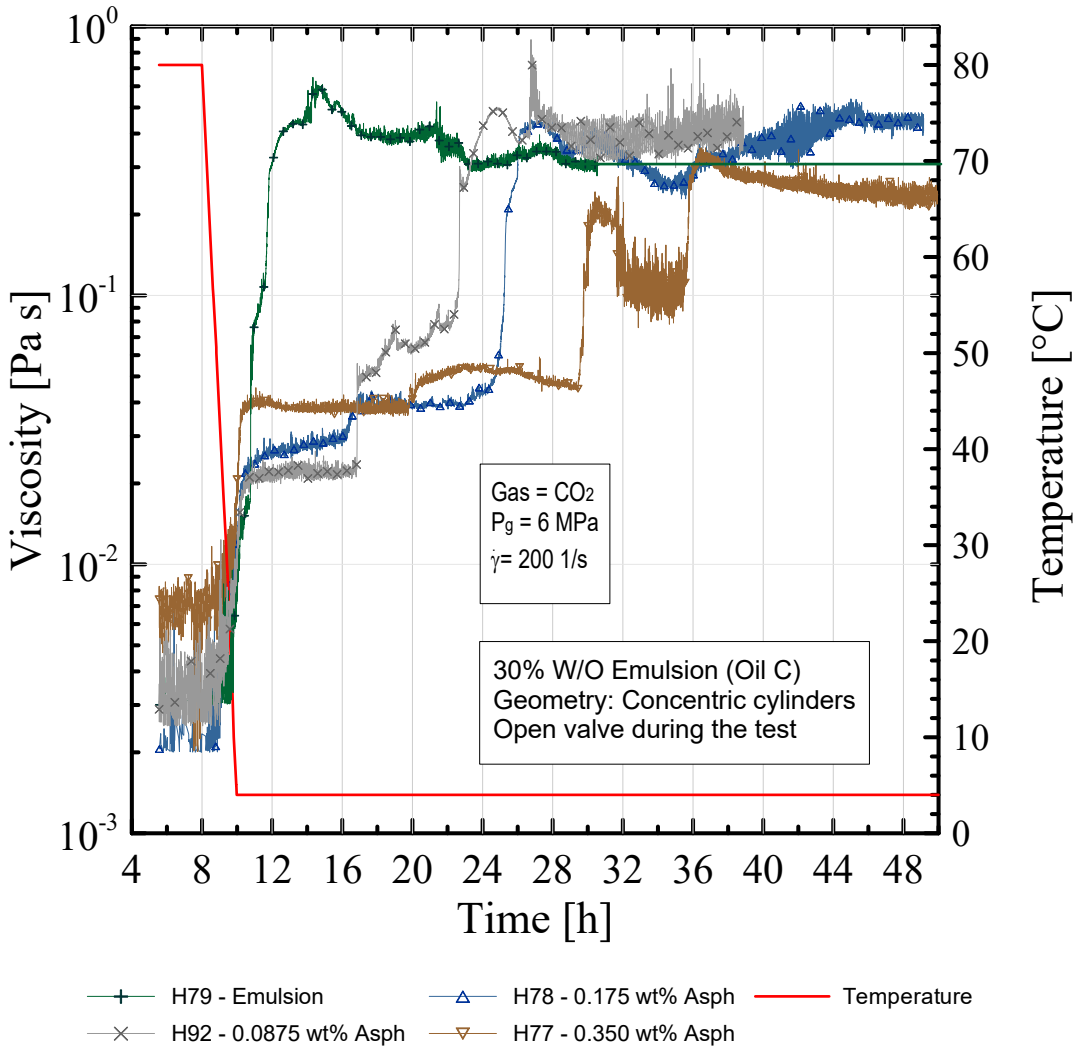

Figure 3.24: Effect caused by the addition of powder asphaltenes to emulsions of 30% of water content for and Oil C.

delay the induction time and the second one is to extend the growth period. Such a performance is a characteristic of a kinetic hydrate inhibitor that acts on the interface between the water and oil phases. Indeed, Sinquin et al. (2001) proposed that the delay on the induction time of asphaltenic crudes when compared with paraffinic ones is promoted by the arrangement and solubility of the polar compounds at the water-oil interface. That same causes are assumed to be the reason for the asphaltenes ability to stabilize emulsions, forming strong viscoelastic films and a strong adsorption to surface (Nordgård et al., 2008). It is suggested that the strong interaction among molecular π-electrons are produced when the asphaltenes are tilted in a way that its aromatic sheets are arranged face-to-face normal to the surface plane, instead of lying with the aromatic core flat on the surface (Lobato et al., 2007). Another mechanism to explain the asphaltenes effect on the kinetic

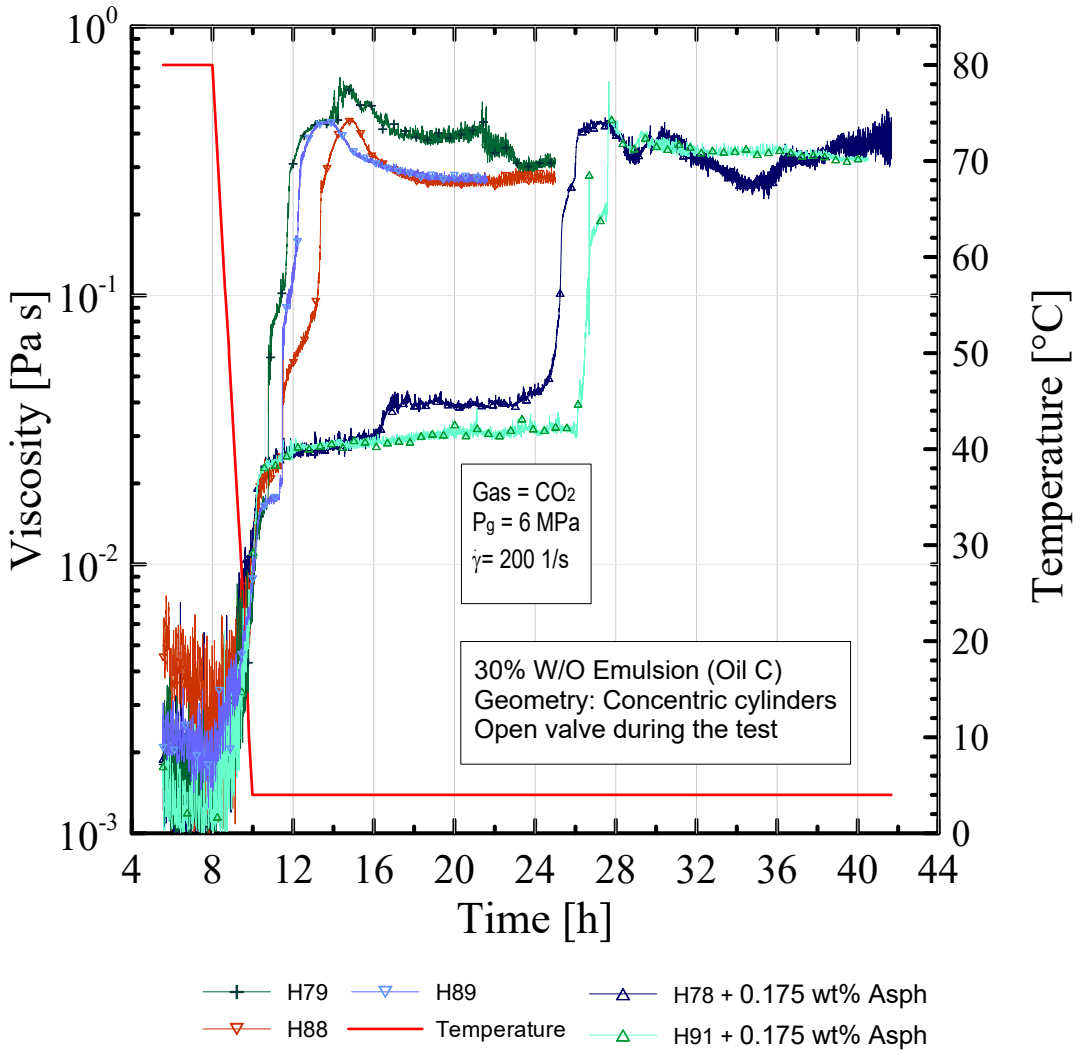

Figure 3.25: Addition of 0.175% of asphaltenes. Two independent experiments to assess repeatability between them.

hydrate formation could be accounted for by a theory of the particles effect on hydrate crystal growth (Cha et al., 2014; Baek et al., 2015, 2018). The authors have studied the effect of silica nanoparticles on the kinetics of hydrate crystal growth for cyclopentane and methane in water-in-oil emulsions. They proposed that the particles form a layer at the oil-water interface that restricts the hydrate conversion and crystallization. In other words, the particles create a physical barrier that interrupts the interaction between the water and the guest molecule. Baek et al. (2018) also argued that the silica nanoparticles interrupt the appearance of hydrate crystals by occupying the nucleation site and, in this manner the contact between the methane and water molecules is prevented due to the reduction of the hydrate growth region on the surface of the water droplets. These two

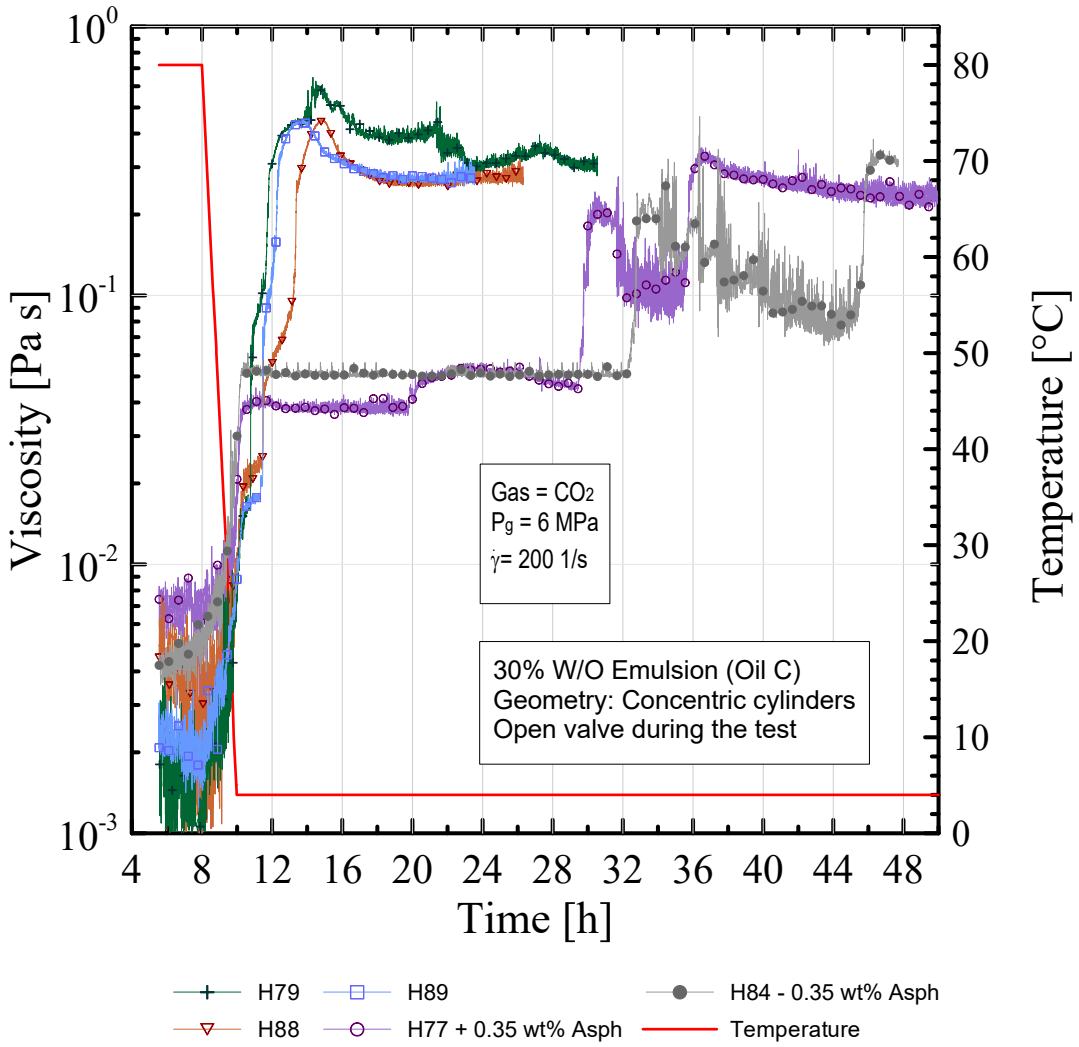

Figure 3.26: Addition of 0.35% of asphaltenes. Two independent experiments to assess repeatability between them.

mechanisms presented previously could be the grounds for the positive effect caused by the asphaltenes on the induction time for hydrate formation.

Chapter 4

Final remarks

The rheological analysis of CO_2 hydrates slurries was performed by means of a rheometric geometry in a rotational rheometer. The thermodynamic conditions (pressure and temperature) employed to form the hydrates are similar to those used in the industry. Before executing the main tests of hydrate analysis, preliminary experiments were realized with the objective to verify the accuracy of the pressure cell. This step is very important since such kind of apparatus is not widely used and the absence of a mechanical connection between the measuring device and the rotor imposes an extra challenge (see Fig. 2.3). Then, tests such as optimal gap, friction factor correction, and rotor stabilization were made to validate the geometry. Preliminary results for a Newtonian fluid were compared with a Cannon-Fenske viscometer (see Fig. 2.5) and with another geometry for a non-Newtonian fluid as illustrated in Fig. 2.7. Unfortunately, it was difficult to obtain a good measure for the yield stress presented in the CO_2 hydrates slurries (data not shown).

The main results show the behavior of the viscosity of the samples as a function of the experimental time and were presented in two separate sections. In the first section, the results were displayed to characterize CO_2 hydrates from water-in-oil emulsions, from the rheological point of view. It was noted that the viscosity increased abruptly when the hydrate was formed and subsequently it began to decrease due to the break down of the structures. Several variables were studied, and it was observed that increasing the water fraction and shear rate favors the hydrate formation. The induction time takes place earlier, and the amount of formed hydrates increase with the quantities. Some of the reported behaviors were also noticed by other authors using methane as the guest molecule. Another series of tests were conducted in order to investigate the ability of reconstruc-

tion of the CO_2 hydrates after a certain period of time at rest at the same pressure and temperature of the initial test. Indeed, CO_2 hydrates exhibited shear thinning behavior and time-dependency. At the end of the section, a sequence of tests was shown with the objective of studying the memory effect phenomenon. In those results, it is worth noting the anticipation of the induction time as well as the larger amount of formed hydrate during the second cycle of the experiment. In the second section, there were presented several results to assess the effect caused on the induction time of CO_2 hydrates by the addition of gas condensate and the addition of small quantities of powder asphaltenes in water-in-oil emulsions. The analysis was made in two different oils, including the one that was used in the first section. It was noticed that the addition of gas condensate to the emulsions promotes hydrate formation. Two main roles were observed regarding the influence of the powder asphaltenes, a delay on the induction time and an increase of the growth periods. Such behaviors are typical of kinetic hydrate inhibitors. Probably, this positive effect on the induction time is caused by both or one of the following mechanisms. One is the arrangement and solubility of the asphaltenes at the water-oil interface. The other is the construction of a physical barrier that interrupts the interaction between the water and the guest molecule. The main advantage of using powder asphaltenes as an inhibitor is that they are natural components of the same crude oil. However, this phenomenon deserves a deeper investigation.

Bibliography

12185, I., 1996. Iso 12185 – Petroleum products determination of density oscillating U tube method. International Organization for Standardization ISO 12185.

2549, A. S. D., 2012. Standard test method for separation of representative aromatic and nonaromatic fractions of high boiling oils by elution chromatography.

4377, A. S. D., 2011. Astm D4377 – Standard test method for water in crude oils by Potentiometric Karl Fischer Titration.

5854, A. S. D., 2005. Standard practice for mixing and handling of liquid of petroleum and petroleum products. ASTM International, West Conshohocken, PA (reapproved 2005).

6560, A. S. D., 2012. Standard test method for determination of asphaltenes (heptane insolubles) in crude petroleum and petroleum products. Annual Book of Standards.

Ahuja, A., Zylyftari, G., Morris, J. F., 2015. Yield stress measurements of cyclopentane hydrate slurry. Journal of Non-Newtonian Fluid Mechanics 220, 116–125.

Al-Adel, S., Dick, J. A., El-Ghafari, R., Servio, P., 2008. The effect of biological and polymeric inhibitors on methane gas hydrate growth kinetics. Fluid Phase Equilibria 267 (1), 92–98.

Andersson, V., Gudmundsson, J. S., 2000. Flow properties of hydrate-in-water slurries. Annals of the New York Academy of Sciences 912 (1), 322–329.

Anklam, M. R., Firoozabadi, A., 2004. Driving force and composition for multicomponent gas hydrate nucleation from supersaturated aqueous solutions. The Journal of chemical physics 121 (23), 11867–11875.

Arjmandi, M., Tohidi, B., Danesh, A., Todd, A. C., 2005. Is subcooling the right driving force for testing low-dosage hydrate inhibitors? Chemical engineering science 60 (5), 1313–1321.

Baek, S., Min, J., Ahn, Y.-H., Cha, M., Lee, J. W., 2018. Effect of hydrophobic silica nanoparticles on the kinetics of methane hydrate formation in water-in-oil emulsions. Energy & Fuels.

Baek, S., Min, J., Lee, J. W., 2015. Inhibition effects of activated carbon particles on gas hydrate formation at oil–water interfaces. RSC Advances 5 (72), 58813–58820.

Ballard, A., Sloan Jr, E., 2002. The next generation of hydrate prediction: I. hydrate standard states and incorporation of spectroscopy. Fluid Phase Equilibria 194, 371–383.

Barnes, H., Carnali, J., 1990. The vane-in-cup as a novel rheometer geometry for shear thinning and thixotropic materials. Journal of Rheology 34 (6), 841–866.

Barnes, H. A., 1994. Rheology of emulsions - a review. Colloids and surfaces A: physicochemical and engineering aspects 91, 89–95.

Barnes, H. A., 1997. Thixotropy - a review. Journal of Non-Newtonian fluid mechanics 70 (1-2), 1–33.

Bassane, J. F. P., Sad, C. M., Neto, D. M., Santos, F. D., Silva, M., Tozzi, F. C., Filgueiras, P. R., de Castro, E. V., Romão, W., Santos, M. F., et al., 2016. Study of the effect of temperature and gas condensate addition on the viscosity of heavy oils. Journal of Petroleum Science and Engineering 142, 163–169.

Bonnecaze, R., Brady, J., 1992. Yield stresses in electrorheological fluids. Journal of Rheology 36 (1), 73–115.

Boxall, J., Greaves, D., Mulligan, J., Koh, C., Sloan, E. D., 2008. Gas hydrate formation and dissociation from water-in-oil emulsions studied using pvm and fbrm particle size analysis. In: Proceedings of the 6th International Conference on Gas Hydrate, Vancouver, British Columbia, Canada.

Bozzo, A. T., Hsiao-Sheng, C., Kass, J. R., Barduhn, A. J., 1975. The properties of the hydrates of chlorine and carbon dioxide. Desalination 16 (3), 303–320.

Camargo, R., Gonçalves, M., Montesanti, J., Cardoso, C., Minami, K., et al., 2004. A perspective view of flow assurance in deepwater fields in brazil. In: Offshore Technology Conference. Offshore Technology Conference.

Camargo, R., Palermo, T., 2002. Rheological properties of hydrate suspensions in an asphaltenic crude oil. In: Proceedings of the 4th International Conference on Gas Hydrates. Vol. 1. pp. 880–885.

Camargo, R., Palermo, T., Sinquin, A., Glenat, P., 2000. Rheological characterization of hydrate suspensions in oil dominated systems. Annals of the New York Academy of Sciences 912 (1), 906–916.

Cardoso, C. B., Alves, I. N., Ribeiro, G. S., et al., 2003. Management of flow assurance constraints. In: Offshore Technology Conference. Offshore Technology Conference.

Cha, M., Baek, S., Morris, J., Lee, J. W., 2014. Hydrophobic particle effects on hydrate crystal growth at the water–oil interface. Chemistry–An Asian Journal 9 (1), 261–267.

Chen, J., Sun, C.-Y., Peng, B.-Z., Liu, B., Si, S., Jia, M.-L., Mu, L., Yan, K.-L., Chen, G.-J., 2013. Screening and compounding of gas hydrate anti-agglomerants from commercial additives through morphology observation. Energy & Fuels 27 (5), 2488–2496.

Chhabra, R. P., Richardson, J. F., 2011. Non-Newtonian flow and applied rheology: engineering applications. Butterworth-Heinemann.

Christiansen, R., Sloan Jr, E., 1995. A compact model for hydrate formation. Tech. rep., Gas Processors Association, Tulsa, OK (United States).

Chun, M.-K., Lee, H., 1996. Kinetics of formation of carbon dioxide clathrate hydrates. Korean Journal of Chemical Engineering 13 (6), 620–626.

Cox, S. J., Taylor, D. J., Youngs, T. G., Soper, A. K., Totton, T. S., Chapman, R. G., Arjmandi, M., Hodges, M. G., Skipper, N. T., Michaelides, A., 2018. Formation of methane hydrate in the presence of natural and synthetic nanoparticles. Journal of the American Chemical Society 140 (9), 3277–3284.

D664, A. S., 2011. Astm D664 – Standard test method for acid number of petroleum products by potentiometric titration.

da Silva, M., Sad, C. M., Pereira, L. B., Corona, R. R., Bassane, J. F., dos Santos, F. D., Neto, D. M., Silva, S. R., Castro, E. V., Filgueiras, P. R., 2018. Study of the stability and homogeneity of water in oil emulsions of heavy oil. Fuel 226, 278–285.

Daraboina, N., 2012. Understanding the action of gas hydrate kinetic inhibitors. Ph.D. thesis, University of British Columbia.

Darbouret, M., Cournil, M., Herri, J.-M., 2005. Rheological study of tbab hydrate slurries as secondary two-phase refrigerants. International Journal of Refrigeration 28 (5), 663–671.

Davies, S. R., Sloan, E. D., Sum, A. K., Koh, C. A., 2009. In situ studies of the mass transfer mechanism across a methane hydrate film using high-resolution confocal raman spectroscopy. The Journal of Physical Chemistry C 114 (2), 1173–1180.

de Oliveira, M. C. K., Carvalho, R. M., Carvalho, A. B., Couto, B. C., Faria, F. R., Cardoso, R. L., 2009. Waxy crude oil emulsion gel: impact on flow assurance. Energy & Fuels 24 (4), 2287–2293.

de Souza Mendes, P. R., Dutra, E. S., 2004. A viscosity function for viscoplastic liquids. An. Trans. Nordic Rheo. Soc 12, 183–188.

de Souza Mendes, P. R., Thompson, R. L., 2012. A critical overview of elasto-viscoplastic thixotropic modeling. Journal of Non-Newtonian Fluid Mechanics 187, 8–15.

Delahaye, A., Fournaison, L., Jerbi, S., Mayoufi, N., 2011. Rheological properties of co2 hydrate slurry flow in the presence of additives. Industrial & Engineering Chemistry Research 50 (13), 8344–8353.

Delahaye, A., Fournaison, L., Marinhas, S., Martínez, M. C., 2008. Rheological study of co2 hydrate slurry in a dynamic loop applied to secondary refrigeration. Chemical engineering science 63 (13), 3551–3559.

Derkach, S. R., 2009. Rheology of emulsions. Advances in colloid and interface science 151 (1), 1–23.

Di Lorenzo, M., Seo, Y., Soto, G. S., 2011. The csiro's hydrates flow loop as a tool to investigate hydrate behaviour in gas dominant flows. Korea 6 (7.8), 2–2.

Einstein, A., 1906. A new determination of molecular dimensions. Ann. Phys 19 (2), 289–306.

Englezos, P., Kalogerakis, N., Dholabhai, P., Bishnoi, P., 1987. Kinetics of formation of methane and ethane gas hydrates. Chemical Engineering Science 42 (11), 2647–2658.

Fingas, M. F., 2014. Water-in-oil emulsions: formation and prediction. Handbook of Oil Spill Science and Technology, 225.

Gudmundsson, J., Hveding, F., Børrehaug, A., 1995. Transport or natural gas as frozen hydrate. In: The Fifth International Offshore and Polar Engineering Conference. International Society of Offshore and Polar Engineers.

Jerbi, S., Delahaye, A., Oignet, J., Fournaison, L., Haberschill, P., 2013. Rheological properties of co 2 hydrate slurry produced in a stirred tank reactor and a secondary refrigeration loop. International Journal of Refrigeration 36 (4), 1294–1301.

Kashchiev, D., Firoozabadi, A., 2002. Driving force for crystallization of gas hydrates. Journal of crystal growth 241 (1-2), 220–230.

Kelland, M. A., 2006. History of the development of low dosage hydrate inhibitors. Energy & fuels 20 (3), 825–847.

Kelland, M. A., Svartås, T. M., Andersen, L. D., 2009. Gas hydrate anti-agglomerant properties of polypropoxylates and some other demulsifiers. Journal of Petroleum Science and Engineering 64 (1), 1–10.

Kennett, J. P., Cannariato, K. G., Hendy, I. L., Behl, R. J., 2003. Methane Hydrates in Quaternary Climate Change: The Clathrate Gun Hypothesi. Wiley Online Library.

Kvamme, B., Kuznetsova, T., Aasoldsen, K., 2005. Molecular dynamics simulations for selection of kinetic hydrate inhibitors. Journal of Molecular Graphics and Modelling 23 (6), 524–536.

Lambourne, R., Strivens, T., 1999. Paint and surface coatings: theory and practice. Elsevier.

Leopércio, B. C., de Souza Mendes, P. R., Fuller, G. G., 2016. Growth kinetics and mechanics of hydrate films by interfacial rheology. Langmuir 32 (17), 4203–4209.

Lobato, M., Pedrosa, J., Hortal, A., Martinez-Haya, B., Lebron-Aguilar, R., Lago, S., 2007. Characterization and langmuir film properties of asphaltenes extracted from arabian light crude oil. Colloids and Surfaces A: Physicochemical and Engineering Aspects 298 (1-2), 72–79.

Makogon, Y., 1965. A gas hydrate formation in the gas saturated layers under low temperature. Gas Industry 5, 14–15.

Makogon, Y. F., 2010. Natural gas hydrates–a promising source of energy. Journal of Natural Gas Science and Engineering 2 (1), 49–59.

Moore, J., Vers, L. V., Conrad, P., et al., 2009. Ss: Flow assurance: Understanding kinetic hydrate inhibitor and corrosion inhibitor interactions. In: Offshore Technology Conference. Offshore Technology Conference.

Neto, D. M., Sad, C. M., Silva, M., Santos, F. D., Pereira, L. B., Corona, R. R., Barbosa, L. R., Silva, S. R., Bassane, J. F., Castro, E. V., et al., 2018. Rheological study of the behavior of water-in-oil emulsions of heavy oils. Journal of Petroleum Science and Engineering.

Nordgård, E. L., Landsem, E., SjoÌˆblom, J., 2008. Langmuir films of asphaltene model compounds and their fluorescent properties. Langmuir 24 (16), 8742–8751.

Oignet, J., Delahaye, A., Torré, J.-P., Dicharry, C., Hoang, H. M., Clain, P., Osswald, V., Youssef, Z., Fournaison, L., 2017. Rheological study of co 2 hydrate slurry in the presence of sodium dodecyl sulfate in a secondary refrigeration loop. Chemical Engineering Science 158, 294–303.

'OReilly, R., Ieong, N. S., Chua, P. C., Kelland, M. A., 2011. Missing poly (n-vinyl lactam) kinetic hydrate inhibitor: high-pressure kinetic hydrate inhibition of structure ii gas hydrates with poly (n-vinyl piperidone) and other poly (n-vinyl lactam) homopolymers. Energy & Fuels 25 (10), 4595–4599.

Palermo, T., Mussumeci, A., Leporcher, E., et al., 2004. Could hydrate plugging be avoided because of surfactant properties of the crude and appropriate flow conditions? In: Offshore Technology Conference. Offshore Technology Conference.

Paso, K., Silset, A., Sørland, G., GoncÌ§alves, M. d. A., SjoÌˆblom, J., 2008. Characterization of the formation, flowability, and resolution of brazilian crude oil emulsions. Energy & Fuels 23 (1), 471–480.

Peixinho, J., Karanjkar, P. U., Lee, J. W., Morris, J. F., 2010. Rheology of hydrate forming emulsions. Langmuir 26 (14), 11699–11704.

Peytavy, J., Monfort, J., Gaillard, C., 1999. Investigation of methane hydrate formation in a recirculating flow loop: Modeling of the kinetics and tests of efficiency of chemical additives on hydrate inhibition. Oil & Gas Science and Technology 54 (3), 365–374.

Rensing, P. J., Liberatore, M. W., Koh, C. A., Sloan, E. D., 2008. Rheological investigation of hydrate slurries.

Rensing, P. J., Liberatore, M. W., Sum, A. K., Koh, C. A., Sloan, E. D., 2011. Viscosity and yield stresses of ice slurries formed in water-in-oil emulsions. Journal of Non-Newtonian Fluid Mechanics 166 (14), 859–866.

Saji, A., Yoshida, H., Sakai, M., Tanii, T., Kamata, T., Kitamura, H., 1992. Fixation of carbon dioxide by clathrate-hydrate. Energy Conversion and Management 33 (5), 643–649.

Sakai, H., Gamo, T., Kim, E., Tsutsumi, M., Tanaka, T., Ishibashi, J., Wakita, H., Yamano, M., Oomori, T., 1990. Venting of carbon dioxide-rich fluid and hydrate formation in mid-okinawa trough backarc basin. Science 248 (4959), 1093–1097.

Samaniuk, J. R., Hermans, E., Verwijlen, T., Pauchard, V., Vermant, J., 2015. Soft-glassy rheology of asphaltenes at liquid interfaces. Journal of Dispersion Science and Technology 36 (10), 1444–1451.

Sandoval, G. A., Soares, E. J., Thompson, R. L., Siqueira, R. d. N., de Andrade, R. M., Campos, F., Teixeira, A., 2018. Analysis of co2 hydrates in crude oils from a rheological point of view. Energy & Fuels 32 (3), 2733–2741.

Shigemoto, N., Al-Maamari, R. S., Jibril, B. Y., Hirayama, A., 2006. A study of the effect of gas condensate on the viscosity and storage stability of omani heavy crude oil. Energy & fuels 20 (6), 2504–2508.

Shindo, Y., Lund, P., Fujioka, Y., Komiyama, H., 1993. Kinetics of formation of of co 2 hydrate. Energy Conversion and Management 34 (9), 1073–1079.

Sinquin, A., Bredzinsky, X., Beunat, V., et al., 2001. Kinetic of hydrates formation: influence of crude oils. In: SPE annual technical conference and exhibition. Society of Petroleum Engineers.

Sinquin, A., Palermo, T., Peysson, Y., 2004. Rheological and flow properties of gas hydrate suspensions. Oil & gas science and technology 59 (1), 41–57.

Sloan, E. D., 2003. Fundamental principles and applications of natural gas hydrates. Nature 426 (6964), 353–363.

Sloan, E. D., Koh, C. A., Sum, A., 2011. Natural gas hydrates in flow assurance. Gulf Professional Publishing.

Sloan Jr, E. D., Koh, C., 2008. Clathrate hydrates of natural gases. CRC press.

Soares, E. J., Thompson, R. L., Machado, A., 2013. Measuring the yielding of waxy crude oils considering its time-dependency and apparent-yield-stress nature. Appl Rheol 23, 62798–1.

Speight, J., 2004. Petroleum asphaltenes-part 1: Asphaltenes, resins and the structure of petroleum. Oil & gas science and technology 59 (5), 467–477.

Sum, A. K., Koh, C. A., Sloan, E. D., 2009. Clathrate hydrates: from laboratory science to engineering practice. Industrial & Engineering Chemistry Research 48 (16), 7457–7465.

Sun, M., Firoozabadi, A., 2015. Gas hydrate powder formation–ultimate solution in natural gas flow assurance. Fuel 146, 1–5.

Tariq, M., Rooney, D., Othman, E., Aparicio, S., Atilhan, M., Khraisheh, M., 2014. Gas hydrate inhibition: a review of the role of ionic liquids. Industrial & Engineering Chemistry Research 53 (46), 17855–17868.

Taylor, C. J., 2006. Adhesion force between hydrate particles and macroscopic investigation of hydrate film growth at the hydrocarbon/water interface. Ph.D. thesis, Colorado School of Mines. Arthur Lakes Library.

Taylor, G. I., 1932. The viscosity of a fluid containing small drops of another fluid. Proceedings of the Royal Society of London. Series A, Containing Papers of a Mathematical and Physical Character 138 (834), 41–48.

Teng, H., Kinoshita, C., Masutani, S., 1995. Hydrate formation on the surface of a co2 droplet in high-pressure, low-temperature water. Chemical Engineering Science 50 (4), 559–564.

Tohidi, B., Anderson, R., Mozaffar, H., Tohidi, F., 2015. The return of kinetic hydrate inhibitors. Energy & Fuels 29 (12), 8254–8260.

Webb, E. B., 2014. Rheology of methane hydrate slurries formed from water-in-oil emulsions. Colorado School of Mines.

Webb, E. B., Rensing, P. J., Koh, C. A., Dendy Sloan, E., Sum, A. K., Liberatore, M. W., 2012a. High pressure rheometer for in situ formation and characterization of methane hydrates. Review of Scientific Instruments 83 (1), 015106.

Webb, E. B., Rensing, P. J., Koh, C. A., Sloan, E. D., Sum, A. K., Liberatore, M. W., 2012b. High-pressure rheology of hydrate slurries formed from water-in-oil emulsions. Energy & fuels 26 (6), 3504–3509.

Yoshimura, A. S., Prud'homme, R. K., Princen, H., Kiss, A., 1987. A comparison of techniques for measuring yield stresses. Journal of Rheology 31 (8), 699–710.

Zhang, L., Xie, L., Shi, C., Huang, J., Liu, Q., Zeng, H., 2016. Mechanistic understanding of asphaltene surface interactions in aqueous media. Energy & Fuels 31 (4), 3348–3357.